Disorder Effects on Electron Transport in Nanocrystal Assemblies and Topological Insulators

A DISSERTATION
SUBMITTED TO THE FACULTY OF THE GRADUATE SCHOOL
OF THE UNIVERSITY OF MINNESOTA
BY

Tianran Chen

IN PARTIAL FULFILLMENT OF THE REQUIREMENTS
FOR THE DEGREE OF
Doctor of Philosophy

Boris Shklovskii

August, 2014

Acknowledgements

I have been the beneficiary of great kindness and great support throughout my graduate studies. First and foremost I would like to thank my advisor, Boris Shklovskii, for providing tremendous and invaluable guidance to my research and for showing me the beauty of science. Without him this thesis would not have been possible. He has been an inspiration and an incredible life advisor, from whom I have learned not only just physics but also many things outside research. It has truly been a great pleasure and privilege to work with him.

I am grateful for the opportunity of working with Brian Skinner and Matt Loth. Much of the thesis is in collaboration with Brian Skinner, who is not only a wonderful colleague but also my mentor on research and graduate life. As an expert on computational physics, Matt Loth offered me a lot of help and guidance with the computation part of my research when I first joined the group.

I would like to thank Allen Goldman for having me work in his superconductivity lab in the beginning of the graduate school, and for the opportunity of collaborating with his group on the superconducting grain project later on. I also want to thank my collaborators Alexander Efros, Kostya Reich and Yeongbae Lee. It has been such a great experience to work with them.

I would like to extend my gratitude to my thesis committee members (Alex Kamenev, James Kakalios and Chris Leighton), my physics professors and my family and friends, for their enormous help and support throughout my graduate studies. Without them life would not have been nearly as enjoyable.

Chapters 2 – 5 represent a collaborative effort with Brian Skinner, and Chapter 4 is in part a collaboration with Allen Goldman group at the University of Minnesota.

Dedication

To my parents

Abstract

The continuing development of new energy technologies for electronic devices and medical applications necessitates the search for advanced nanomaterials. Among the more promising candidates are two novel materials: nanocrystal (NC) assemblies and three-dimensional (3D) topological insulators (TIs). The former have great promise for optoelectronic and photovoltaic devices, while the latter can be applied in spintronics and quantum computing. Thus far, however, the development of NC- and TI-based devices have been slowed by a lack of a solid theoretical understanding of many of their electronic properties, in particular, the influence of the presence of disorder on charge transport. In this thesis we propose to help address this need by performing a detailed, theoretical analysis of the disorder effects on electronic transport properties of NC arrays and TIs.

NC assemblies can be made from different materials. Specifically, we consider three types of systems: semiconductor NCs, metallic NCs and superconducting grains. As-grown semiconductor NCs are insulators, and in order for them to be useful in photovoltaic devices, their electrical conductivity must be tuned by doping. Recent experiments have shown that the resistivity of a dense crystalline array of semiconductor NCs depends in a sensitive way on the level of doping as well as on the NC size and spacing. We show that in sufficiently small NCs, the fluctuations in donor number from one NC to another provide disorder that helps to determine the conduction mechanism in the array. Using this model, we explain how the different regimes of resistivity observed in experiment arise based on the interplay between the charging spectrum of NCs, the long-ranged Coulomb interactions between charged NCs, and the discrete quantum energy levels of confined electrons. We supplement our theory with a computer simulation, which we use to calculate the single particle density of states (DOS) and the resistivity.

Compared to semiconductor NCs, the quantum gaps in metallic NCs become negligible and disorder is provided by donors and acceptors that are randomly situated in the interstitial spaces between grains. These changes may lead to different results for electron energy distribution and charge transport. Using a computer simulation we calculate the DOS and the conductivity in 2D and 3D arrays of metallic NCs. While the Coulomb gap in the DOS is a universal consequence of electron-electron interaction

in disordered systems with localized electron states, we show that for granular metals there is not one but three identical adjacent Coulomb gaps, which together form a structure that we call a "Coulomb gap triptych." Furthermore, unlike in the conventional Coulomb glass models, in metallic NC arrays the DOS has a fixed width in the limit of large disorder.

The third type of NC assemblies we consider are granular superconductors in the strongly insulating regime, in which the array as a whole is insulating while individual grains may still contain Cooper pairs. In such cases, coherent tunneling is absent. Instead, electronic states are localized and electron conduction proceeds primarily by hopping of electrons between grains through the insulating gaps which separate them. In principle, electronic conduction can occur either through tunneling of single electrons or through simultaneous tunneling of an electron pair (or both). Using a simple computer simulation, we numerically calculate the DOS and conductivity, and study the evolution of conduction mechanism as a function of temperature, charging energy and superconducting gap. The implications of our results for magnetoresistance and tunneling experiments are also discussed.

The rest of the thesis discusses another type of disorder system: 3D TI. The 3D TI has gapless surface states that are expected to exhibit a range of interesting quantum phenomena. However, as-grown TIs are typically heavily-doped n-type crystals. Compensation by acceptors is used to move the Fermi level to the middle of the band gap, but even then TIs have a frustratingly small bulk resistivity. We show that this small resistivity is the result of band bending by poorly screened fluctuations in the random Coulomb potential. Using numerical simulations of a completely compensated TI, we find that the bulk resistivity has an activation energy of just 0.15 times the band gap, in good agreement with experimental data. At lower temperatures activated transport crosses over to variable range hopping with a relatively large localization length. We also extend our theory to the more practical case of strongly compensated semiconductors, as in experiments the exact condition of complete compensation is difficult to meet. We calculate the DOS, conductivity and activation energy of a strongly compensated TI as a function of compensation degree. Historically known as good thermoelectric materials, the thermopower properties of compensated TIs are also discussed.

Contents

List of Tables

List of Figures

Chapter 1

Introduction

1.1 Nanocrystal assemblies

There has never been a greater need for efficient new energy technologies than at present. As the world's fossil fuel resources are increasingly depleted, and as the environmental consequences of their depletion accumulate, the need for clean and renewable energy technologies becomes more critical. Solar cell technologies, in particular, seem like an ideal candidate to replace fossil fuels, given their ability to directly convert sunlight into useful electrical power via the photovoltaic effect. However, the high cost and low efficiency of current photovoltaic devices has thus far prevented their widespread implementation.

These practical limitations have led researchers to examine alternate materials and methods of fabrication for solar cells. Among the more promising approaches is to make solar cells from arrays of semiconductor nanocrystals (NCs). NC arrays retain the broadband absorptive properties and superior transport properties of traditional bulk semiconductors while offering the advantages of cheap and scalable synthesis and an absorption spectrum that can be readily tuned by adjusting the NC size or shape.

A NC is an aggregate of between a few hundred and a few hundred thousand atoms that combine into a crystalline form of matter. Given the small size of NCs, which are typically between 3 and 10 nanometers in diameter, quantum mechanical effects strongly affect the energy of electrons confined within the NCs, and thus help to determine the optical and electronic properties of the NC array. As produced, because of various forces

such as the van der Waals internaction, individual NCs can self-assemble themselves into a superlattice, where the interplay between individual and collective properties may lead to many interesting phenomena in optics and electronic transport. Such dense, crystalline assemblies of NCs are the main objects of interest in this thesis.

One of the major technological challenges associated with NC-based photovoltaic devices is that, as produced, NC arrays are insulating, meaning that light-created electrons and holes are not easily converted into useful electrical current. Thus, in order for NC arrays to be useful in photovoltaic devices, their electrical conductivity must be tuned by the addition of donor electrons or acceptor holes ("doping"), either by chemical modification of the NC composition or by electrochemical gating.

In particular, we consider the case where each NC is made from a semiconductor that is heavily-doped, for example, by donor impurities. In this case all donor electrons reside in the conduction band of the NC. It is known that a heavily-doped bulk semiconductor is essentially a good conductor due to relatively large overlap between the wave functions of donor electrons. In NC assemblies, however, the condition of metallic conduction is usually difficult to meet even under heavily-doping for the following reasons.

Note that NCs do not touch each other but are separated by some insulator material such as the ligands shown in Fig. 1.1. In order to conduct across the array, donor electrons must tunnel between NCs under the high barrier associated with those insulating ligands. The tunneling integral t between neighboring NCs decays exponentially with the separation d and with the height of the tunneling barrier between them. For metallic conduction this means t being larger than the characteristic disorder energy in the system.

In fact, one can show that, even a small amount of disorder (such as the standard 5% size distribution) will cause relatively large fluctuations of the electron energy from one NC to another [1] so that donor electrons experience Anderson localization. In this situation conduction proceeds only by phonon-assisted tunneling, or "hopping", between localized electron states. This hopping is a thermally-activated process in which electron tunneling occurs simultaneously with the absorption or emission of a phonon whose energy accounts for the difference between the initial and final electron states.

Suppose in the global ground state of the array all NCs are neutral, then hopping

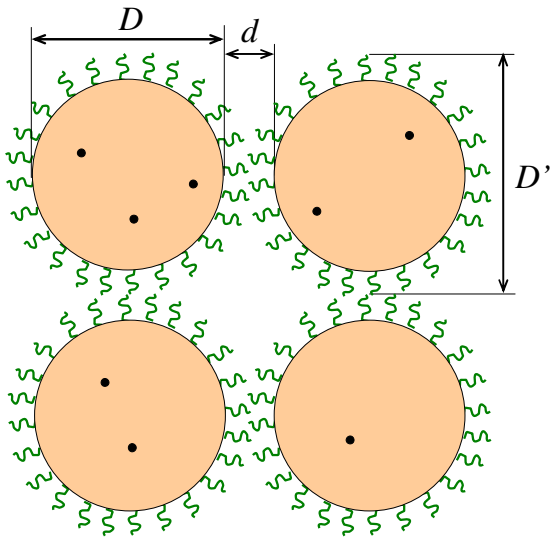

Figure 1.1: (Color online) Schematic drawing of spherical semiconductor NCs (large, light-colored circles) with diameter D arranged in a crystalline lattice with lattice constant D'. Each NC is coated in a thin layer of insulating ligands (curvy lines) that maintain a separation $d = D' - D$ between NCs and prevent them from sintering. Each NC has a random number of donors in its interior (small, black circles).

transport requires an electron to be thermally excited to jump from one neutral NC to another. This process produces two oppositely charged NCs, each of which has a corresponding Coulomb self-energy $E_c = e^2/\kappa D$, where κ is the effective dielectric constant of the NC array and D is the NC diameter. This charging energy plays the role of an activation energy for resistivity in the case where all NCs are neutral in the global ground state. Equivalently, one can say that the distribution of electron ground state energies, or the "density of ground states" (DOGS) of NCs, has a gap of width $2E_c$ centered at the electron Fermi level. As a result, the resistivity ρ follows the Arrhenius law: $\ln \rho \propto E_c/k_B T$, where $k_B T$ is the thermal energy.

In experiments, however, one often observes a temperature dependence of the resistivity that is different from simple activation: $\ln \rho \propto T^{-\gamma}$, with the temperature exponent $\gamma < 1$. Such "stretched exponential" behavior is believed to be possible only if the disorder is so strong that a substantial fraction of NCs is charged in the global ground state. Such charging creates a random Coulomb potential landscape that shifts up and down the electron energy spectra at different NCs. As a result of this shifting,

the gap in the DOGS is smeared and filled. This smearing means that some electron states have energies very close to the Fermi level, and as a result one can find a pair of empty and filled electron states separated by an energy ΔE that is much smaller than E_c. At small temperature $k_B T \ll E_c$, it is hopping between such pairs that are close in energy that dominates the conduction. For small ΔE the typical separation r between the corresponding NC pair is much larger than the spacing D' between neighboring NCs. Thus, at small temperature T electron conduction relies on tunneling between distant NCs.

If the temperature T is made increasingly small, the corresponding energy difference ΔE of electron hops becomes increasingly small due to the scarcity of available high-energy phonons, and as a result the typical hop length increases. Such behavior is known as variable range hopping (VRH), and is responsible for the stretched exponential behavior $\gamma < 1$ in the resistivity. When the DOGS is constant near the Fermi level, the resistivity follows the Mott law of VRH [2]: $\ln \rho \propto T^{-1/4}$. However, in systems where the long-ranged Coulomb potential is not screened, electron correlation effects produce a DOGS that vanishes quadratically with energy at the Fermi level [3]. Such a vanishing DOGS results in the Efros-Shklovskii (ES) law of VRH: $\ln \rho \propto T^{-1/2}$. In principle, all three of these conduction behaviors — Arrhenius ($\gamma = 1$), Mott VRH ($\gamma = 1/4$), and ES VRH ($\gamma = 1/2$) — are possible in arrays of semiconductor NCs, depending on the magnitude and type of disorder present.

A number of transport experiments on seminconductor NC arrays found that factors such as doping level, temperature and NC size can all affect the resistivity. For instance, as the average number ν of dopant electrons per NC is varied, the dependence of the resistivity ρ on the temperature T changes between Arrhenius-type activated conduction ($\gamma = 1$) and VRH ($\gamma < 1$); on the other hand, at some particular doping level (e.g., $\nu = 2$), as the temperature is decreased a transition from activated transport to VRH was observed [4]. Thus far, however, there is no general theory to explain how different types of conduction can coexist, especially how disorders affect conductivity. According to the above analysis, the presence of sufficiently strong disoder is essential for the non-vanishing DOGS at the Fermi level and thereby non-activated transport. While both doping level and NC size may have fluctuations in real experiments, understanding the role of disorders in NC charge transport is therefore crucial to the development and

applications of NC-based devices.

In this thesis, such a theory is presented to examine the disorder effects on resistivity of a dense, crystalline array of semiconductor NCs. Specifically, we study the temperature dependence of the resistivity on the level of doping as well as on the NC size and spacing. The choice of these parameters determines whether electron conduction through the array will be characterized by activated nearest-neighbor hopping or VRH.

Once understood, this model is adapted to explore hopping transport in two other types of NC assemblies: metallic NCs and superconducting grains. Similar to semiconductor NCs, conduction in metallic ones also proceeds by hopping between localized electron states. However, there are two different aspects that must be taken into account when studying metallic NCs. First, quantum confinement effects are negligible, for the spacing between quantum energy levels is now small compared to the charging energy of a dot. Second, disorder no longer comes from the random chemical doping process but has a different source. These features are shown below to lead to very different (and striking) results on DOGS and conductivity in metallic NCs.

Finally we turn our attention to periodic arrays of superconducting grains. Such systems combine the unique electronic spectrum of superconducting quantum dots with the strong Coulomb correlations that are ubiquitous in disordered systems [5]. Granular superconductors exhibit many interesting quantum phenomena such as a giant magnetoresistance peak [6, 7, 8] and a disorder-driven superconductor-insulator transition [9, 10]. So far, a comprehensive theory of the electron conductivity that can explain these features remains elusive.

Here, we focus on the strongly disordered limit, where the array of superconducting grains as a whole is insulating while individual grains may still retain prominent features of superconductivity [10, 11, 6]. In this case, electronic states are localized and electron conduction proceeds primarily by hopping of electrons between grains through the insulating gaps which separate them. In principle, electronic conduction can occur either through tunneling of single electrons or through simultaneous tunneling of an electron pair (or both). What determine the conduction mechanism are two important energy scales associated with the spectrum of electron energy states within each grain: charging energy E_c, and the superconducting gap Δ_0 that represents an activation energy for separating a Cooper pair. As the ratio of Δ_0/E_c is gradually increased, say,

by an applied magnetic field, the system goes from single-electron dominated regime to electron pair dominated regime. The evolution of DOGS and conductivity also provides a qualitative explanation for the giant magnetoresistance peak that has been observed in some of the superconducting ultra-thin films.

Although the above systems are made of different materials, they all share one important feature: the presence of disorders plays an important role in charge transport. In semiconductor NCs, the only disorder is assumed to be the fluctuations in donor numbers among NCs; in metallic NCs and superconducting grains, disorder is provided by random impurity charges embedded in the insulating gaps between grains. It will be explained below that, the interplay between disorder, Coulomb interactions and quantum effects can have significant influence on electron conduction and lead to peculiar results on DOGS and resistivity that are not seen in conventional bulk seminconductor and Coulomb glasses.

1.2 Topological insulators and strongly compensated semiconductors

The discovery and classification of distinctive electronic phases of matter has always been an important topic in condensed matter physics. As we know, the behavior of electrons in different materials varies dramatically. The electrical insulator, for instance, is one of the most basic electronic phases of matter, characterized by an energy gap for electronic excitations. Recent work has, however, now uncovered a new class of materials termed topological insulators (TIs) [12, 13, 14, 15, 16]. The most distinguishing feature of these insulators is that they can insulate on the inside but conduct on the outside - analogous to a block of wood covered with a layer of copper, except that the material is actually the same throughout. Due to strong spin-orbit coupling, electrons that move along the surface have their spin locked perpendicular to their momentum (spin-momentum locking) (see Fig. 1.2(a) for the band structure of a typical 3D TI [17]). Furthermore, these gapless surface states are topologically protected against disruptions such as defects, chemical passivation, and thermal fluctuations. First predicted and then discovered experimentally in semiconducting alloy $Bi_{1-x}S_x$, 3D TI has attracted enormous attention in the physics community for their potential applications ranging

from spintronics to quantum computation.

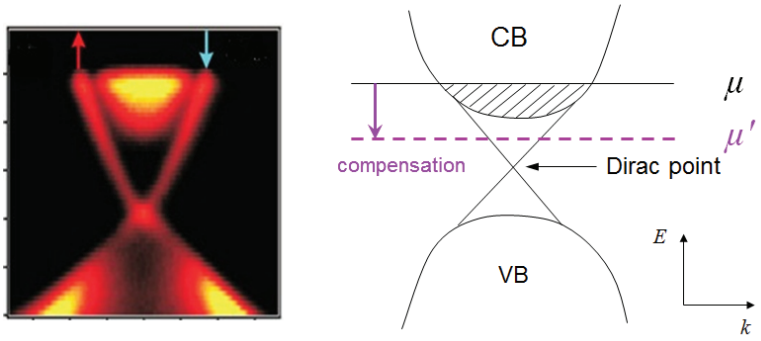

Figure 1.2: (a) Energy band structure of undoped Bi_2Se_3 measured by ARPES. The top and bottom are the conduction and valence band of the bulk, respectively; in the middle are the gapless surface states that have a dirac-cone like band structure. (b) Schematic drawing of energy band structure of 3D TI in momentum space. The large concentration of intrinsic dopants puts the Fermi level μ high in the conduction band. To achieve a bulk insulating state, the (shallow) intrinsic dopants must be compensated by (shallow) acceptors. As a result, the original Fermi level μ moves from the conduction band down into the band gap.

While a number of crystals have been identified to be 3D TIs, unfortunately, most of them are poor insulators and the bulk of TI crystals of substantial size (> 10 μm) shunts the surface conductivity. The current literature [18, 19, 20, 21, 22, 23, 24, 25, 26]broadly discusses how one can achieve a bulk-insulating state.

Typically as-grown TI crystals such as Bi_2Se_3 are heavily doped n-type semiconductors, so that the Fermi level resides in the bulk conduction band. (In as-grown Bi_2Se_3, Se vacancies are believed to play the role of intrinsic donor impurities.) To make them insulating, these TIs are compensated by acceptors such as Te. The compensation process is illustrated in Fig. 1.2(b). With increasing compensation $K = N_A/N_D$, where N_D and N_A are the concentrations of monovalent donors and acceptors, respectively, the Fermi level shifts from the conduction band to inside the gap and then into the valence band at $K > 1$. When compensation of donors is complete, $K = 1$, the Fermi level is in the middle of the gap and the most insulating state of TI is achieved. The hope is that for a TI with the gap $E_g \sim 0.3$ eV the resistivity should obey the activation law $\rho = \rho_0 \exp(\Delta/k_B T)$, with activation energy $\Delta = E_g/2 \sim 0.15$ eV, so that TI is well insulating at room temperatures and below.

However, the typical experimental situation near $K = 1$ is frustrating [25]. In the range of temperatures between 100 and 300 K, although the resistivity is activated, the activation energy $\Delta \sim 50$ meV, which is three times smaller than expected. At $T \sim 100$ K the activated transport is replaced by VRH and resistivity grows even more slowly with decreasing T. Finally, at even smaller $T < 50$ K resistivity saturates around $\rho(T) < 10$ Ωcm. This means that, in spite of complete compensation the conductance of TI samples thicker than 10 μm is dominated by the bulk even at helium temperatures.

The above theory is based on the assumption that the conduction and valence band edges are flat just like in undoped (or lightly doped) semiconductors. However, the bulk of 3D TI is essentially a heavily-doped, strongly-compensated semiconductor. As the semiconductor is fabricated, due to some high temperature process (explained below in more detail), a large amount of dopants are randomly situated in space. At $K = 1$, when almost all donors and acceptors are charged, random spatial fluctuations in the local concentration of impurities lead to large fluctuations of charge. The resulting potential is poorly screened because of the vanishing average concentration of screening electrons $n = N_D - N_A \ll N_D$, and therefore, has huge fluctuations.

Below we show that it is the disorder effect neglected in the conventional flat bands theory that leads to the unexpected bulk conductivity. Specifically, the anomalously large bulk conductivity of TI at $K = 1$ can be explained as a consequence of disorder potential created by randomly-distributed in space donor and acceptor impurities. The disorder potential significantly bend the conduction and valence bands and in some places bring them to the Fermi level, resulting in a reduced activation energy. Our theory is supplemented with a computer simulation, which we use to calculate the DOGS, conductivity and activation energy. A transition from thermally activated transport to VRH conduction at low temperatures is also found.

Our theory is then extended to the case of finite compensation. In experiments, tuning the compensation is tricky and it can be difficult to reach the exact $K = 1$ condition. Instead, one may end up with somewhere near the complete compensation. Thus, it is a very practical question that whether our model holds for $1 - K \ll 1$ as well, especially the validation of the relation between activation energy and compensation degree. Furthermore, Bismuth compounds are known historically as good thermoelectric materials. Using our theory based on disorder potential, we calculate the thermopower

of $Bi_{1-x}Se_x$ and compare our numerical results with the recent experimental data.

1.3 Main results of this thesis

As briefly explained in the previous section, in disordered systems where electrons are strongly localized, electron conduction primarily proceeds by hopping between localized states. This hopping transport is sensitive only to the *ground state* energies of electrons and holes that are added to the as-grown materials. In order to calculate conductivty of NC assembilies and TIs, a detailed description of the ground state energy distribution is needed. Each physical system has its own characteristic disorder source, and one of the main goals of this thesis is to examine disorder effects on the electron ground states and the corresponding conductivity.

In Ch. 2 we present such a theory, based on a first-principles description of the ground state arrangement of electrons within an array of doped semiconductor NCs. We focus on a simple model of identical spherical NCs that are covered by a thin layer of insulating ligand (or some other insulator) and arranged in an ideal crystalline lattice, as depicted in Fig. 1.1. We show that the presence of fluctuations in donor number between different NCs is sufficient to produce charging of NCs, which results in a disordered Coulomb landscape that encourages VRH. This charging is driven by the large gaps between shells of the electron quantum energy spectrum in NCs with large Bohr radius a_B. Specifically, these inter-shell gaps drive electrons to depart from NCs with a large number of donors, where maintaining electroneutrality would require placing electrons in higher quantum energy shells, and reside instead on nearby NCs with small donor number. In this way some NCs spontaneously acquire a positive or negative charge, and it is this charging that leads to VRH when the temperature is not too large.

Using this model, we explain how the different regimes of resistivity observed in experiment arise based on the interplay between the charging spectrum of NCs, the long-ranged Coulomb interactions between charged NCs, and the discrete quantum energy levels of confined electrons. We supplement our theory with a simple computer simulation to calculate the DOGS and the resistivity.

Our main result is that VRH appears when the average number ν of electrons per

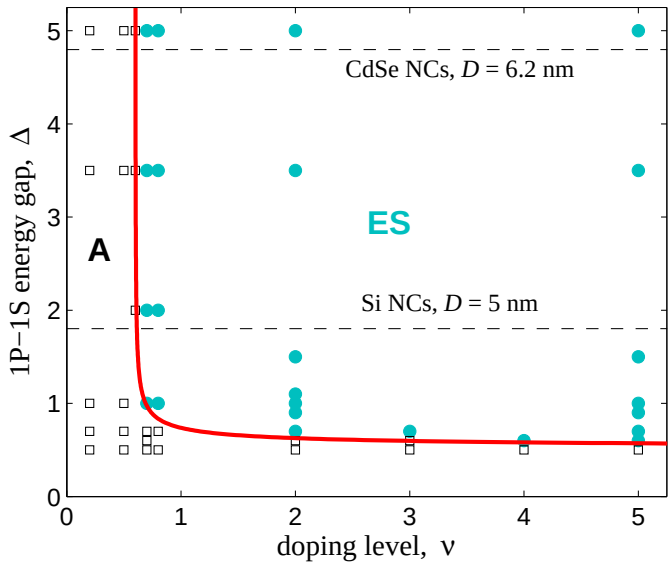

Figure 1.3: (Color online) Phase diagram indicating regimes of activated and ES resistivity as a function of doping level ν and the dimensionless quantum energy gap $\Delta \equiv 20.64\kappa a_B/\kappa_{\rm NC}D$ at low temperature $k_BT \ll e^2\xi/\kappa D^2$. Symbols correspond to simulated systems: filled (light blue) circles indicate systems that exhibited ES resistivity and open squares indicate systems that exhibited activated resistivity. The thick (red) curve is an approximate boundary between these two regimes, which are labeled "ES" and "A", respectively. Dashed, horizontal lines indicate the value of Δ corresponding to Si NCs with $D = 5$ nm (as in Ref. [27]) and to CdSe NCs with $D = 6.2$ nm (as in Ref. [4]). This phase diagram and the computer simulation methods are discussed more thoroughly in Ch. 2.

NC, the NC diameter D, and the temperature T satisfy the following three conditions:

(i) $\nu \gtrsim 0.6$,

(ii) $D \lesssim 34\kappa a_B/\kappa_{\rm NC}$, and

(iii) $k_BT \lesssim 0.5e^2\xi/\kappa D^2$.

Here, $\kappa_{\rm NC}$ is the internal dielectric constant of NCs. When these three conditions are satisfied, the resistivity follows the ES law. In situations where any of the three criteria is not met, the conduction is activated. This result is depicted at low temperature, $k_BT \ll e^2\xi/\kappa D^2$, in the phase diagram of Fig. 1.3.

In contrast to semiconductor NCs, where the spontaneous charging is driven by random doping and relatively large quantum gaps, metallic NCs are different in two ways. First, in metallic NCs the gap Δ between quantum energy levels becomes vanishingly small and spontaneous charging does not occur. Second, disorder now comes from a different source. Instead of fluctuations in donor number among dots, in such systems disorder is provided by donors and acceptors that are randomly situated in the interstitial spaces between grains—for example, in the metal oxide of the grains (more details about the disorder mechanism are discussed in Ch. 3). It is then an interesting question to see how the DOGS and conductivity of the system are going to be modified.

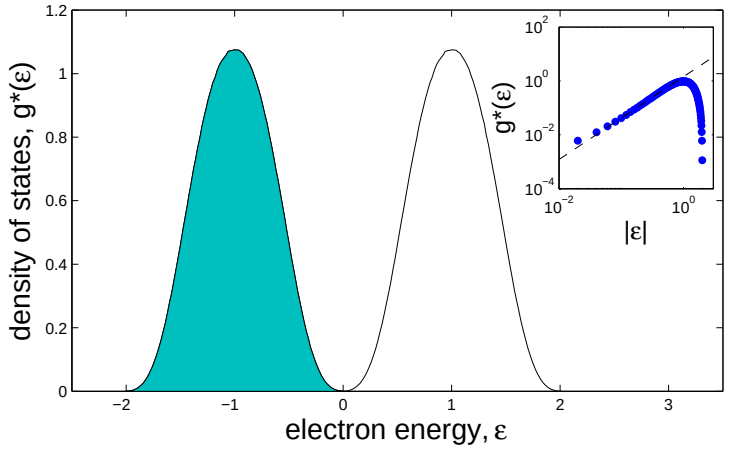

Figure 1.4: (Color online) The DOGS of a regular 3d array of monodisperse NCs, where $\varepsilon = E/(e^2/2C_0)$ is the dimensionless single-particle energy and $g^*(\varepsilon) = (e^2D^d/2C_0)g(\varepsilon)$ is the dimensionless DOGS, where D is the NC diameter. Here, the results are shown from a computer simulation of a 3d cubic lattice. The shaded area shows filled electron states, and the empty area indicates empty states. In addition to electron–hole symmetry, the two peaks of the DOGS have a mirror symmetry across $\varepsilon = \pm 1$, respectively (dotted lines). This symmetry creates from the central Coulomb gap two additional half-gaps at $\varepsilon = \pm 2$, resulting in a "Coulomb gap triptych." Insets show the DOGS near the Fermi level $\varepsilon = 0$ in log-log scale.

In Ch. 3, we explore hopping transport in two-dimensional (2D) and three-dimensional (3D) arrays of monodisperse normal metallic grains. The most striking result is the repeated Coulomb gap in the DOGS. We show that, as a result of the periodic charging spectrum of individual grains, there is not one but three identical adjacent Coulomb gaps

in the DOGS (one full gap at the Fermi level and two "half-gaps" on either side), which together form a structure that we termed a "Coulomb gap triptych." The Coulomb gap triptych represents a bridge between the concepts of the Coulomb gap and the Coulomb blockade. In addition, the DOGS in metallic granular arrays exhibits a rather surprising feature: unlike in conventional Coulomb glass models, it has a fixed width in the limit of large disorder. This result is shown in Fig. 1.4, which can be verified by tunneling experiments.

The final type of NC arrays to be discussed is periodic arrays of superconducting grains in the strongly disordered limit, where the array of superconducting grains as a whole is insulating while individual grains may still contain Cooper pairs. Coherent tunneling of Cooper pairs (the Josephson effect) is neglected. In such a system, electronic states are localized and electron conduction proceeds primarily by hopping of electrons between grains through the insulating gaps which separate them.

At a given temperature T, two important energy scales associated with the spectrum of electron energy states within each grain affect the magnitude of hopping conductivity . The first one is the charging energy $E_c = e^2/2C_0$, where C_0 is the self-capacitance of a single grain. The second energy scale is the superconducting gap Δ_0, which represents an activation energy for separating a Cooper pair. In the limit where $\Delta_0/E_c \to 0$, the array is equivalent to a granular metal [5, 28, 29, 30]; in the opposite limit, each grain has the properties of a bulk superconductor. Here, we are interested in the regime when E_c and Δ_0 are similar in magnitude. The previous study of metallic NCs can be considered as a model for a granular superconductor in the limit where $\Delta_0/E_c \to 0$.

In principle, electronic conduction can occur either through tunneling of single electrons or through simultaneous tunneling of an electron pair (or both). Using a simple computer simulation, we show that it is the ratio of superconducting gap to charging energy Δ_0/E_c that determines whether the hopping transport is governed by tunneling of single-electrons or electron pairs. Specifically, we study the DOGS and conductivity as a function of gap Δ_0 and temperature T. The result for the DOGS of single electrons, which is denoted $g_1(\varepsilon)$, is shown in Fig. 1.5(a) for different values of $\Delta^* = \Delta_0/E_c$. Fig. 1.5(b) shows the DOGS for electron pairs, $g_2(\varepsilon)$. As Δ^* grows, the system switches from single-electron dominated regime to electron pair dominated regime. The transition is also reflected in system's hopping conductivity, which is discussed thoroughly in Ch. 4.

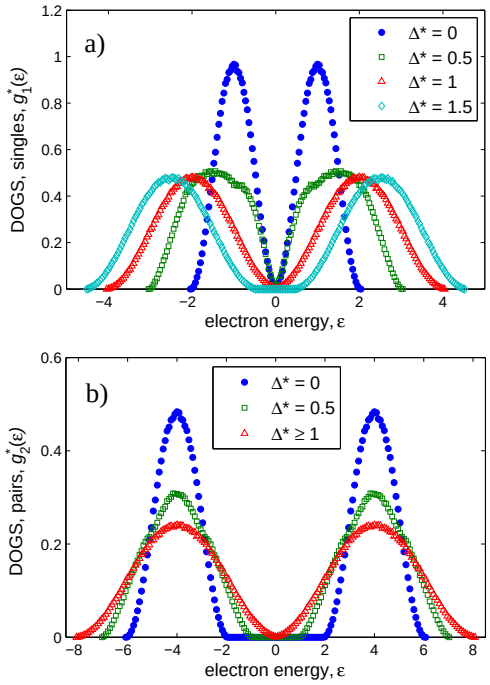

Figure 1.5: (Color online) Single electron and pair DOGS, $g_1^*(\varepsilon)$ and $g_2^*(\varepsilon)$, of a regular 2d array of monodisperse metallic grains as a function of the dimensionless electron energy $\varepsilon = E/E_c$ at different values of the superconducting gap $\Delta^* = \Delta_0/E_c$. At $\Delta^* < 1$, the single electron DOGS g_1^* has a soft Coulomb gap at $\varepsilon = 0$, while the pair DOGS g_2^* has a hard gap, and the situation is reversed for $\Delta^* > 1$. $\Delta^* = 1$ is a critical point at which both $g_{1,2}^*$ have a soft Coulomb gap. The three DOGS curves corresponding to $g_1^*(\varepsilon)$ at $\Delta^* = 0, 1$ and $g_2^*(\varepsilon)$ at $\Delta^* \geq 1$ constitute "Coulomb gap triptychs" and can be scaled onto each other by rescaling the electron charge.

The mechanism of the giant magnetoresistance peak observed in many superconducting thin films can also be qualitatively explained by the evolution of DOGS.

In the remainder of this thesis, we turn our attention from NC assemblies to another important type of disorder system: 3D topological insulators. As briefly discussed in the previous section, the bulk of a 3D TI is essentially a heavily-doped, strongly compensated semiconductor, with a large number of charged dopants present in the bulk. These impurities create enormously-fluctuating random Coulomb potential that bend the conduction and valence bands, and the bulk resistivity can be dramatically different from the one assumed in the flat bands picture of TI [31]. First, at relatively high

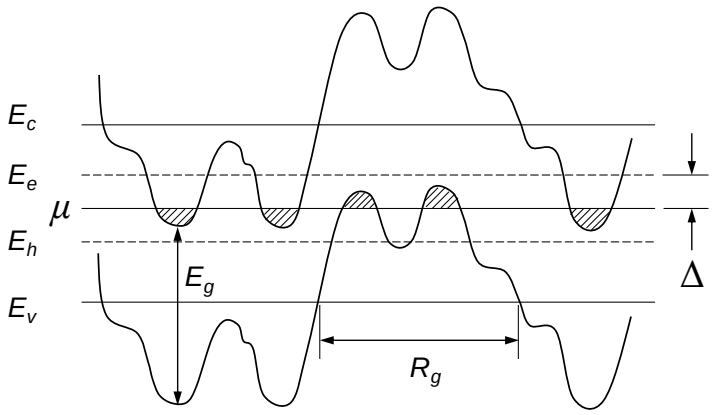

Figure 1.6: Energy diagram of a completely compensated TI with band gap E_g. The upper and the lower straight lines (E_c and E_v) indicate the unperturbed positions of the bottom of the conduction band and the ceiling of the valence band; the middle line (μ) corresponds to the Fermi level. Meandering lines represent the band edges, which are modulated by the fluctuating potential of charged impurities; R_g is the characteristic size of these potential fluctuations. The percolation levels for electrons, E_e, and holes, E_h, are shown by dashed lines; the activation energy Δ corresponds to the difference $E_e - \mu$ (or $\mu - E_h$). Puddles occupied by carriers are shaded. Shallow impurity levels are not shown because they merge with the band edges.

temperatures activated conduction is due to electrons and holes being activated from the Fermi level to their corresponding classical percolation levels (classical mobility edges), E_e and E_h, in the conduction and the valence bands. These may be substantially closer to the Fermi level μ than the unperturbed by random potential bottom of the conduction band E_c and ceiling of the valence band E_v (Fig. 1.6). [1] Thus, one can think of the universal small factor $\Delta/E_g \simeq 15$ as corresponding to a percolation threshold associated with percolation through the potential created by random impurities in 3D. Second, at low enough temperatures electrons and holes can hop (tunnel) between puddles, so that variable range hopping replaces activated transport. In the low temperature limit $\rho(T)$ should obey the ES law of VRH [3].

The above theory on the enhanced bulk conductivity in TI was confirmed by numerical simulations using percolation approach. We compute the resistivity as a function

[1] Note that E_c here represents the bottom of the conduction band, and should not be taken as the charging energy defined in the sections of NC assemblies.

of temperature, and find two activated regimes of hopping conductivity. At high temperatures we see the large activation energy $E_a \sim E_c - \mu$; in the range of intermediate temperatures, we see much smaller activation energy $\Delta \simeq 0.3(E_c - \mu) = 55$ meV, which is in good agreement with the experimental value. At low temperatures the resistivity is well described by ES law.

So far we have focused on the case of complete compensation $K = 1$. In the remainder of Chapter 5, we move on to a more practical situation: a strongly compensated semiconductor (SCS), namely $1 - K \ll 1$. This is because with existing methods of growth of TI samples one cannot reach $K = 1$ exactly. It is then important to know how stable the resistivity results at $K = 1$ are for the case of $1 - K \ll 1$.

We model numerically the ground state of such SCS and its resistivity using algorithms similar to Ref. [31]. We find that in agreement with the analytic theory [32], when $1 - K$ grows, the screening of the random potential improves and its correlation length R_g decreases. The amplitude of the random potential decreases as well. As a result, hole puddles shrink and eventually vanish and the chemical potential μ moves up, so that $E_c - \mu$ decreases. One can say that with increasing $1 - K$, the screening due to bending of the conduction band occurs only while all acceptors remain occupied by electrons and negatively charged.

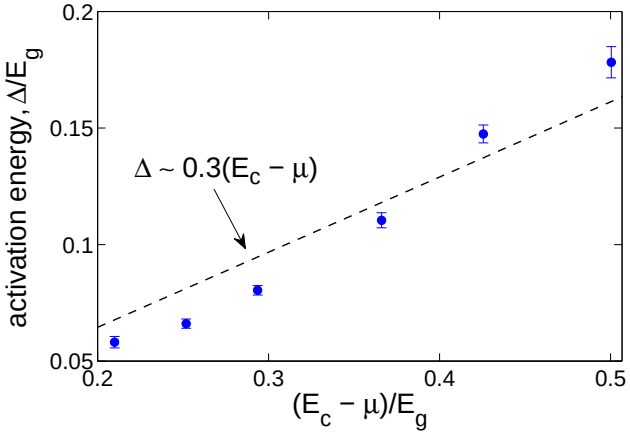

Figure 1.7: (Color online) The activation energy Δ at $K = 1, 0.99, 0.98, 0.97, 0.96$ and 0.95 (from right to left). The dashed line is the best linear fit $\Delta \simeq 0.3(E_c - \mu)$.

As a result of these changes, the activation energy Δ decreases with growing $1 - K$.

We find that the relation $\Delta = 0.3(E_c - \mu)$ obtained in Ref. [31] for $K = 1$ remains valid for $1 - K \ll 1$ (see Fig. 1.7) as well. [In p-type semiconductor where $K = N_D/N_A$, a similar relationship $\Delta = 0.3(\mu - E_v)$ takes place.] In principle, our prediction that $\Delta = 0.3(E_c - \mu)$ can be directly compared with experiments in TIs. Indeed, for each K, the position of the Fermi level can be found via measurements of the surface concentration of electrons in the gapless surface state using Shubnikov-de-Haas oscillations.

Chapter 2

Semiconductor Nanocrystals

2.1 Introduction

Arrays of semiconductor NCs have great promise for optoelectronic and photovoltaic devices, for both their optical and electronic properties can be readily tuned – the former by choosing the size or shape of NCs [27, 33], and the latter by the addition of dopants or surface ligands that control the spacing between NCs [34, 35]. Recent experiments have demonstrated that dense, crystalline arrays of spherical semiconductor NCs can be reliably produced with diameter in the range 4–10 nm and with less than 5% dispersion [27, 28]. Thus, optoelectronic or photovoltaic devices made from NCs can be designed to operate precisely in any chosen region of the optical spectrum.

In Fig. 2.1(a), for example, a high-resolution tunneling electron microscope image of a single CdSe NC is shown, where the dark spots are CdSe atoms aligned periodically just like in a bulk crystal. NCs made from PbSe or Si are also commonly studied. As produced, due to a variety of forces such as the van der Waals internaction, individual NCs can self-assemble themselves into a superlattice. Fig. 2.1(b) shows a face-center cubed superlattice of CdSe NCs. Such a superlattice combines both individual and collective properties of NCs and may give a range of interesting physical phenomena.

From a practical standpoint, however, the development of NC-based devices is slowed by the high resistivity of the NC arrays. In their undoped state, semiconductor NCs are insulators, and in order to reduce their large resistivity it is necessary to bring additional electrons (or holes) to the NCs either through chemical doping [36] or electrochemical

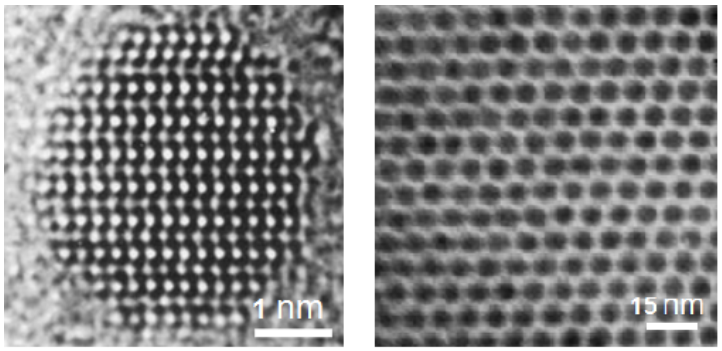

Figure 2.1: Transmission electron microscopy of (a) a single CdSe NC and (b) a face-center cubed superlattice of CdSe NCs.

gating [4]. In this chapter we focus primarily on the former, although we comment on electrochemical gating at the end of the chapter.

In particular, we consider the case where each NC is made from a semiconductor that is heavily-doped by donor impurities. In this case all donor electrons reside in the conduction band of the NC. In order to conduct across the array, these electrons must tunnel between NCs under the high barrier associated with the insulator (such as the ligands shown in Fig. 2.2) that fills the space between them.

In the presence of even a relatively small amount of disorder in the array, the large tunneling barriers imply that donor electrons experience Anderson localization due to fluctuations in the electron energy from one NC to another [1]. In this situation conduction proceeds only by phonon-assisted tunneling, or "hopping", between localized electron states. This hopping is a thermally-activated process in which electron tunneling occurs simultaneously with the absorption or emission of a phonon whose energy accounts for the difference between the initial and final electron states. (While metallic conduction through the array is in principle possible, and has been reported [37], it requires the characteristic disorder energy in the system to be smaller than the hopping integral t between neighboring NCs. Since t decays exponentially with the separation d between NCs and with the height of the tunneling barrier them, the condition for metallic conductivity is difficult to meet, and in this chapter we assume that electron conduction proceeds by hopping.)

If one assumes that in the global ground state of the array all NCs are neutral, then

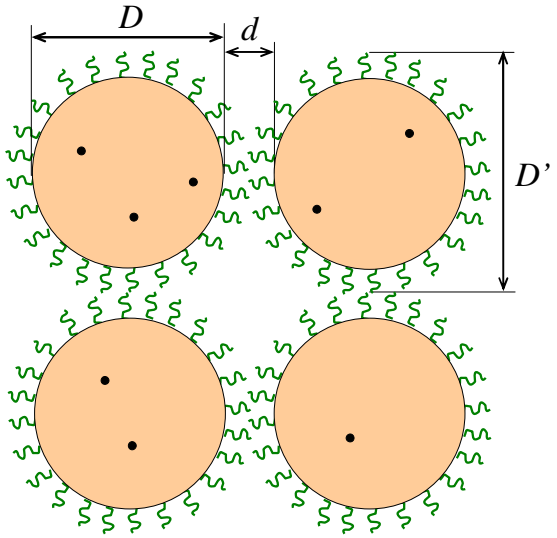

Figure 2.2: (Color online) Schematic drawing of spherical semiconductor NCs (large, light-colored circles) with diameter D arranged in a crystalline lattice with lattice constant D'. Each NC is coated in a thin layer of insulating ligands (curvy lines) that maintain a separation $d = D' - D$ between NCs and prevent them from sintering. Each NC has a random number of donors in its interior (small, black circles).

hopping transport requires an electron to be thermally excited to jump from one neutral NC to another. This process produces two oppositely charged NCs, each of which has a corresponding Coulomb self-energy $E_c = e^2/\kappa D$, where κ is the effective dielectric constant of the NC array and D is the NC diameter. This charging energy plays the role of an activation energy for resistivity in the case where all NCs are neutral in the global ground state. Equivalently, one can say that the distribution of electron ground state energies, or the "density of ground states" (DOGS) of NCs, has a gap of width $2E_c$ centered at the electron Fermi level, as shown in Fig. 2.3. As a result, the resistivity ρ follows the Arrhenius law: $\ln \rho \propto E_c/k_B T$, where $k_B T$ is the thermal energy. We emphasize that the activation energy for hopping conduction is sensitive only to the *ground state* energies of electrons and holes that are added to NCs. For this reason when calculating the resistivity it is sufficient to consider the DOGS, which does not include excited electron states with additional kinetic energy.

In experiments, however, one often observes a temperature dependence of the resistivity that is different from simple activation: $\ln \rho \propto T^{-\gamma}$, with the temperature

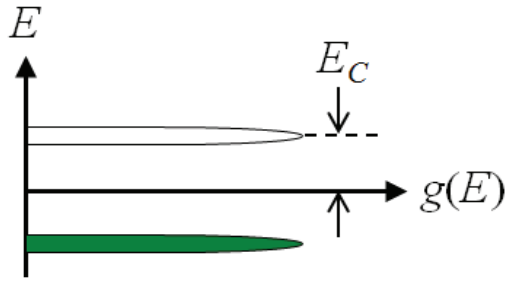

Figure 2.3: (Color online) Distribution of electron ground state energies in the absence of any disorder. The bottom shaded (green) peak corresponds to the filled states, while the top empty one corresponds to the excited states. The DOGS has a gap of width $2E_c$ centered at the electron Fermi level.

exponent $\gamma < 1$. Such "stretched exponential" behavior is believed to be possible only if the disorder is so strong that a substantial fraction of NCs is charged in the global ground state. Such charging creates a random Coulomb potential landscape that shifts up and down the electron energy spectra at different NCs. As a result of this shifting, the gap in the DOGS is smeared and filled. This smearing means that some electron states have energies very close to the Fermi level, and as a result one can find a pair of empty and filled electron states separated by an energy ΔE that is much smaller than E_c. At small temperature $k_B T \ll E_c$, it is hopping between such pairs that are close in energy that dominates the conduction.

Of course, for small ΔE the typical separation r between the corresponding NC pair is much larger than the spacing D' between neighboring NCs. Thus, at small temperature T electron conduction relies on tunneling between distant NCs. To understand how such long-range tunneling is possible, consider first the tunneling of an electron between nearest-neighboring NCs. When the electron tunnels through the insulating gap of thickness d between NCs, it accumulates an action $\hbar d/a$, where a is the decay length of the electron wavefunction outside of the NC. Thus, the tunneling amplitude between nearest neighbors is suppressed by a factor $\sim \exp[-d/a]$. On the other hand, when an electron tunnels to a NC at a distance $x \gg D'$, the path of least action for the electron is to travel primarily through nearest-neighboring NCs, making hops only through the small gaps between neighbors and thereby accumulating an action $\sim \hbar(d/a)(x/D')$, plus an additional much smaller term corresponding to action accumulated across the

interior of each NC. Thus, the tunneling amplitude to the distance x is suppressed by a factor $\sim \exp[-xd/D'a]$. The exponential decay of the tunneling amplitude is described by defining the localization length ξ, such that tunneling between NCs with separation r is suppressed by the factor $\exp[-2r/\xi]$. By the argument above, one cannot simply equate ξ with a, but rather $\xi \sim aD'/d \gg a$ [29]. It is this enhanced localization length, made possible by tunneling through intermediate NCs, that allows for long-range hopping. In the remainder of this chapter, we consider the limit where d and a are both very small compared to the NC diameter, so that $D' \simeq D$ while ξ remains finite.

If the temperature T is made increasingly small, the corresponding energy difference ΔE of electron hops becomes increasingly small due to the scarcity of available high-energy phonons, and as a result the typical hop length increases. Such behavior is known as variable range hopping (VRH), and is responsible for the stretched exponential behavior $\gamma < 1$ in the resistivity. When the DOGS is constant near the Fermi level, the resistivity follows the Mott law of VRH [2]: $\ln \rho \propto T^{-1/4}$. However, in systems where the long-ranged Coulomb potential is not screened, electron correlation effects produce a DOGS that vanishes quadratically with energy at the Fermi level [3]. Such a vanishing DOGS results in the Efros-Shklovskii (ES) law of VRH: $\ln \rho \propto T^{-1/2}$. In principle, all three of these conduction behaviors — Arrhenius ($\gamma = 1$), Mott VRH ($\gamma = 1/4$), and ES VRH ($\gamma = 1/2$) — are possible in arrays of semiconductor NCs, depending on the magnitude and type of disorder present. In this chapter we focus our description on the fundamental role played by inherent fluctuations in donor number among doped NCs.

Experiments probing the resistivity of NC arrays have reported that the resistivity depends in a sensitive and qualitative way on the level of doping [4]. Specifically, as the average number ν of dopant electrons per NC is varied, the dependence of the resistivity ρ on the temperature T changes between Arrhenius-type activated conduction ($\gamma = 1$) and VRH ($\gamma < 1$). VRH has been reported in a variety of granular semiconductor systems [4, 33, 38, 39], but thus far there is no general theory to explain how these different types of conduction can coexist and why they appear in particular ranges of the electron "filling factor" ν.

In this Chapter we present such a theory, based on a first-principles description of the ground state arrangement of electrons within an array of doped NCs. We focus on a simple model of identical spherical NCs that are covered by a thin layer of insulating

ligand (or some other insulator) and arranged in an ideal crystalline lattice, as depicted in Fig. 2.2. We show that the presence of fluctuations in donor number between different NCs is sufficient to produce charging of NCs, which results in a disordered Coulomb landscape that encourages VRH. This charging is driven by the large gaps between shells of the electron quantum energy spectrum in NCs with large Bohr radius a_B. Specifically, these inter-shell gaps drive electrons to depart from NCs with a large number of donors, where maintaining electroneutrality would require placing electrons in higher quantum energy shells, and reside instead on nearby NCs with small donor number. In this way some NCs spontaneously acquire a positive or negative charge, and it is this charging that leads to VRH when the temperature is not too large.

Using this model, we explain how the different regimes of resistivity observed in experiment arise based on the interplay between the charging spectrum of NCs, the long-ranged Coulomb interactions between charged NCs, and the discrete quantum energy levels of confined electrons. We supplement our theory with a simple computer simulation, which we use to calculate the DOGS and the resistivity.

Ch. 2 is organized as follows. In Sec. 2.2 the theoretical model for semiconductor NCs is defined. Sec. 2.3 describes our computer simulation, including our methods for numerically calculating the DOGS and resistivity. Results are presented in Sec. 2.4, along with a discussion of why Arrhenius and VRH resistivity appear in particular regimes of ν, D, and T. We also discuss interesting features of the DOGS in this model, including the appearance of "reflected Coulomb gaps" at either side of the Fermi level. Sec. 2.5 presents some speculation on how our results can be applied to electrochemical gating of NC arrays using ionic liquids followed by concluding remarks in Sec. 2.6.

2.2 Model of NC arrays with random number of dopants

In order to describe the resistivity of a dense array of semiconductor NCs and capture its dependence on doping level, temperature, and NC diameter, we adopt the following simplified theoretical model. We consider NCs to be identical spheres of diameter D with large internal dielectric constant $\kappa_{\rm NC} \gg \kappa$. These spheres are arranged in a regular, three-dimensional (3D) lattice, with each lattice site i located at the center of a NC. For simplicity, we consider a cubic lattice with lattice constant D' just barely larger than

D, so that $d \ll D$ (see Fig. 2.2). Our choice of a cubic lattice does not qualitatively affect any of the results we present below.

We further assume that the radius $D/2$ of the NCs is comparable to or smaller than the effective electron Bohr radius $a_B = \hbar^2 \kappa_{\rm NC}/me^2$ of the semiconductor, where e is the electron charge and m is the effective electron mass. As an example, NCs made from Si have $a_B \approx 2.4$ nm; for CdSe NCs, $a_B \approx 5$ nm. Under this condition the wavefunction of a donor electron is extended across the entire volume of a NC, rather than localized around a donor impurity, and the energy of the electron is strongly affected by quantum confinement within the NC. As an example, a single donor in the center of a NC has a delocalized electron state when $D < 6a_B$ [40, 41]. This condition can be used as a somewhat conservative estimate for how small the diameter should be to produce electron states that are extended across the NC.

In order to obtain the quantum energy spectrum in NCs, one can make the approximation that each NC is an infinite 3D square well. Such an approximation is valid because of the NCs' relatively large work function. The resulting energy spectrum can be described by defining the energy $E_Q(n)$ of the nth lowest electron, which gives for the first few energy levels

$$E_Q(n) = \frac{\hbar^2}{mD^2} \times \begin{cases} 0, & n = 0 \\ 19.74, & n = 1, 2 \\ 40.38, & 3 \leq n \leq 8 \\ 66.43, & 9 \leq n \leq 18 \end{cases} . \tag{2.1}$$

These first three nonzero energy levels can be labeled 1S, 1P, and 1D, respectively. Higher electron shells have thus far not been examined by experiment, since they correspond to very large doping, and will not be discussed in this work. We focus primarily on the case where the spacing between quantum energy levels $\approx 20\hbar^2/mD^2$ is larger than the characteristic scale of Coulomb energies, $e^2/\kappa D$. The expression of Eq. (2.1) ignores the weak perturbation of quantum energy levels resulting from electron-electron interactions. This approximation is justified because of the large internal dielectric constant $\kappa_{\rm NC}$, as explained below.

During the doping process, each NC i acquires some number N_i of positively-charged donors that it contains within its interior. These are assumed to be fixed, while the number of electrons n_i within the NC can change due to electron tunneling between

NCs. We assume that donors are added randomly to each NC by some high-temperature process, so that if the average number of donors per NC is ν, then the probability that a given NC will have exactly N donors is given by the Poisson distribution:

$$P(N) = \frac{\nu^N}{N!} e^{-\nu}. \tag{2.2}$$

This randomness in the number of donors is the only form of disorder that we include in our model. We show in Sec. 2.4 that this disorder is sufficient to produce random charging of NCs, which leads to VRH. As mentioned in the introduction, the spontaneous charging of NCs is the result of the large gaps between quantum kinetic energy shells, which drive electrons away from NCs with many donors (emptying higher shells) and into NCs with few donors (filling lower shells), so that the number of electrons in a given NC is not generally equal to the number of donors. Additional disorder arising from fluctuations in the NC size is not considered explicitly in this chapter. The possible effect of such size fluctuations is discussed at the end of Sec. 2.4, but we note here that fluctuation of NC size alone cannot produce spontaneous charging of NCs in the global ground state, which, as we show below, plays a crucial role for VRH.

In addition to the quantum kinetic energy of the system, transport through the array is also greatly affected by long-ranged Coulomb interactions, which must be taken into account. In general, one could expect that calculating the total Coulomb energy of the system is a difficult problem, since the positions of negative electrons within each NC are described by their corresponding quantum wavefunctions and the positions of positive donors are random within the NC's volume. For our problem, however, a significant simplification is available because the internal dielectric constant κ_{NC} is much larger than both the external dielectric constant κ_{i} of the insulator in which the NCs are embedded and the overall effective dielectric constant κ of the assembly. Specifically, the large internal dielectric constant κ_{NC} implies that any internal charge e is essentially completely compensated by the dielectric response, with the great majority of that charge, $e(\kappa_{\mathrm{NC}} - \kappa)/\kappa_{\mathrm{NC}}$, becoming distributing across the surface of the NC. In this way each NC can be thought of as metallic in terms of its Coulomb interactions. This allows us to write that the Coulomb self-energy of a NC with net charge q is given approximately by $q^2/\kappa D$, irrespective of how its constituent internal charges

are arranged. The interaction between two NCs i, j at a distance r_{ij} can also be approximated as $q_i q_j/\kappa r_{ij}$. These approximations are equivalent to the so-called constant interaction model, which is commonly used for individual quantum dots [42].

It should be noted that the effective dielectric constant κ of the NC array is not simply equal to the dielectric constant $\kappa_{\rm i}$ of the insulating medium between NCs, but also includes the effect of polarization of NCs in response to an applied field. This polarization effectively decreases both the Coulomb self-energy of a single NC and the interaction between neighboring NCs. Generally speaking, the renormalization of the dielectric constant is not very strong, so that κ is not very different from $\kappa_{\rm i}$ even when $\kappa_{\rm NC} \gg \kappa_{\rm i}$. The canonical Maxwell-Garnett formula gives the approximate relation [43]

$$\kappa \simeq \kappa_{\rm i} \frac{\kappa_{\rm NC} + 2\kappa_{\rm i} + 2f(\kappa_{\rm NC} - \kappa_{\rm i})}{\kappa_{\rm NC} + 2\kappa_{\rm i} - f(\kappa_{\rm NC} - \kappa_{\rm i})}, \tag{2.3}$$

where $f = \pi D^3/[6(D')^3]$ is the volume fraction occupied by the NCs; for $f < 0.4$, this expression is accurate to within 8% [44]. As an example, for the case of a cubic lattice with $D = 5$ nm and $D' = 6$ nm (so that $f = 0.3$) and for $\kappa_{\rm NC}/\kappa_{\rm i} = 5$, one has $\kappa \approx 1.6\kappa_{\rm i}$.

Given this model, we can write down the Hamiltonian for our system as

$$\begin{aligned} H &= \sum_i \left[\frac{e^2(N_i - n_i)^2}{\kappa D} + \sum_{k=0}^{n_i} E_Q(k) \right] \\ &\quad + \sum_{\langle i,j \rangle} \frac{e^2(N_i - n_i)(N_j - n_j)}{\kappa r_{ij}}. \end{aligned} \tag{2.4}$$

Here, the first term describes the electrostatic self-energy of NC i, which has charge $q_i = e(N_i - n_i)$, the second term describes the total quantum energy of the n_i electrons on NC i, and the last term indicates the Coulomb interaction between different NCs.

The ground state for a particular system (a set of donor numbers $\{N_i\}$) is defined by the set of electron occupation numbers $\{n_i\}$ that minimizes the Hamiltonian H. Given the ground state configuration, one can determine the energy of the highest filled electron level, $\varepsilon_i^{(f)}$, and the lowest empty electron level, $\varepsilon_i^{(e)}$, at each NC i. Specifically,

$$\begin{aligned} \varepsilon_i^{(f)} &= E_Q(n_i) + \frac{e^2[(N_i - n_i)^2 - (N_i - n_i + 1)^2]}{\kappa D} \\ &\quad - \sum_{j \neq i} \frac{e(N_j - n_j)}{\kappa r_{ij}} \end{aligned} \tag{2.5}$$

and

$$\begin{aligned}\varepsilon_i^{(e)} &= E_Q(n_i+1) + \frac{e^2[(N_i-n_i-1)^2-(N_i-n_i)^2]}{\kappa D} \\ &\quad -\sum_{j\neq i}\frac{e(N_j-n_j)}{\kappa r_{ij}}.\end{aligned} \tag{2.6}$$

For the global ground state configuration, $\varepsilon_i^{(f)} < \varepsilon_j^{(e)}$ for all i, j. As alluded to in the introduction, the definitions of $\varepsilon_i^{(f)}$ and $\varepsilon_i^{(e)}$ describe only the lowest energy state of an electron or hole added to the site i. For this reason we refer to the density of states of these energy states $\varepsilon_i^{(e,f)}$ as the DOGS.

The resistivity of the NC array is largely determined by the set of these ground state single-particle energies $\{\varepsilon_i^{(f)}\}$ and $\{\varepsilon_i^{(e)}\}$. In the following section we show how these energy states can be used to calculate both the ground state electron DOGS $g(\varepsilon)$ and the resistivity ρ as a function of temperature and doping level. Note that in this problem every site is represented by two energies, in contrast to the canonical impurity band of lightly-doped semiconductors [32], where every donor has only one relevant excitation energy.

It is also important to note that in our model these donor electrons are assumed to be responsible for all conduction. In other words, we assume that the temperature T is low enough (and the doping level ν is high enough) that donor electrons are much more abundant than electrons activated from the valence band. In practical cases, this assumption is easily met: it requires only that the thermal energy k_BT be much smaller than the band gap energy E_g. More exactly, it requires that $k_BT \ll E_g/\ln[\kappa_{\rm NC}D^2E_g/e^2a_B\nu^{2/3}]$.

2.3 Computer modeling

In this section we describe our computational method for calculating the density of states and the resistivity at a given value of ν, T, and D. These calculations are based on a computer simulation of a finite, cubic array of $L\times L\times L$ NCs, which proceeds as follows. First, we specify the doping level ν. The simulation then assigns the donor number N_i for each NC i according to Eq. (2.2). The initial values of the electron numbers $\{n_i\}$ are then assigned randomly in such a way that the system is overall electro-neutral, i.e., $\sum_i n_i = \sum_j N_j$. The simulation then searches for the ground state by looping over all

NC pairs $\langle ij \rangle$ and attempting to move one electron from i to j. If the move lowers the Hamiltonian H, then it is accepted, otherwise it is rejected. Equivalently, one can say that for each pair i, j we check that two ES ground state criteria are satisfied:

$$\varepsilon_j^{(e)} - \varepsilon_i^{(f)} - \frac{e^2}{\kappa r_{ij}} > 0 \tag{2.7}$$

and

$$\varepsilon_i^{(e)} - \varepsilon_j^{(f)} - \frac{e^2}{\kappa r_{ij}} > 0. \tag{2.8}$$

If either one of these criteria is violated, then an electron is transferred. This process continues until all sites i, j satisfy Eqs. (2.7) and (2.8).

It should be noted that this procedure does not in general find the exact ground state, but only a "pseudo-ground state" that is stable with respect to single-electron transfers. In principle, the system energy can be lowered further by some multi-electron transfers. The effect of these higher-order relaxation processes on the properties of the pseudo-ground state has been examined for similar models [45, 46], and they are generally beyond our intended accuracy in this chapter, so we do not consider them here.

Once the pseudo-ground state occupation numbers $\{n_i\}$ have been found, one can define the single-particle energies $\varepsilon_i^{(f)}$ and $\varepsilon_i^{(e)}$ for each NC i using Eqs. (2.5) and (2.6). These energies are tabulated and then histogrammed in order to calculate the single-particle DOGS $g(\varepsilon)$. In the results presented below we define electron energies ε relative to the Fermi level μ, which is calculated for each realization of the simulation as $\mu = [\min\{\varepsilon_i^{(e)}\} - \max\{\varepsilon_i^{(f)}\}]/2$. In this way $\varepsilon < 0$ corresponds to filled electron states $\varepsilon^{(f)}$ while $\varepsilon > 0$ corresponds to empty states $\varepsilon^{(e)}$. (See, for example, Fig. 2.5 below.)

Once the pseudo-ground state energies $\{\varepsilon_i^{(f)}\}$ and $\{\varepsilon_i^{(e)}\}$ are determined, we calculate the resistivity of the system by mapping the simulated NC array to an effective resistor network. The equivalent resistance R_{ij} between NCs i and j can be determined by writing down the time-averaged rate of electron transfer between sites i and j in the presence of an electric field and expanding in the limit of small field, as in the canonical Miller-Abrahams resistor network [32, 47]. In calculating R_{ij} we consider only electron transfer among the highest filled states, $\varepsilon^{(f)}$, and the lowest empty states, $\varepsilon^{(e)}$, which is appropriate when the temperature is small enough that $T < e^2/\kappa D$, so that thermal excitation of multi-electron transitions is exponentially unlikely.

Since each NC has two energy levels that can participate in conduction, $\varepsilon^{(f)}$ and $\varepsilon^{(e)}$, one can say that there are four parallel conduction processes that contribute to the resistivity between two NCs i and j: one for each combination of the initial energy level at site i (either $\varepsilon_i^{(f)}$ or $\varepsilon_i^{(e)}$) and the final energy level at site j (either $\varepsilon_j^{(f)}$ or $\varepsilon_j^{(e)}$). Each of these four processes has a corresponding effective resistance $R_{ij}^{(\alpha\beta)}$, where $\alpha, \beta = (f), (e)$. These four resistances can be said to be connected in parallel between NCs i and j, and their value can be written compactly as

$$R_{ij}^{(\alpha\beta)} = R_0 \exp\left[\frac{2r_{ij}}{\xi} + \frac{\varepsilon_{ij}^{(\alpha,\beta)}}{k_B T}\right], \tag{2.9}$$

where R_0 is a prefactor that has only a relatively weak power-law dependence on temperature. The first term in the exponential of Eq. (2.9) describes the exponential suppression of the tunneling rate with distance r, as explained in the introduction, and the second term describes thermal activation by exponentially-rare phonons of energy $\varepsilon_{ij}^{(\alpha,\beta)}$. Since we are interested only in identifying the exponential component of the dependence of resistivity on temperature, we take R_0 to be a constant. The energy $\varepsilon_{ij}^{(\alpha,\beta)}$ in Eq. (2.9) is defined as follows [32]:

$$\varepsilon_{ij}^{(\alpha,\beta)} = \begin{cases} |\varepsilon_j^{(\beta)} - \varepsilon_i^{(\alpha)}| - \frac{e^2}{\kappa r_{ij}}, & \varepsilon_j^{(\beta)}\varepsilon_i^{(\alpha)} < 0 \\ \max\left[\left|\varepsilon_i^{(\alpha)}\right|, \left|\varepsilon_j^{(\beta)}\right|\right], & \varepsilon_j^{(\beta)}\varepsilon_i^{(\alpha)} > 0 \end{cases}. \tag{2.10}$$

The net resistance R_{ij} between NCs i and j is the parallel sum of the four resistances $R_{ij}^{(\alpha\beta)}$. Since the exponential factor in Eq. (2.9) provides a sharp differentiation between these four parallel resistances, at relatively low temperatures and to within the accuracy of our calculations we can equate R_{ij} with the minimum of the four parallel resistances. That is,

$$R_{ij} \simeq \min\left\{R_{ij}^{(\alpha\beta)}\right\}. \tag{2.11}$$

After calculating all resistances R_{ij} for a given simulated array, we find the dimensionless resistivity of the network ρ/ρ_0, where $\rho_0 = R_0 D'$, using a percolation approach [32]. Specifically, we find the minimum value R_c such that if all resistances R_{ij} with $R_{ij} < R_c$ are left intact while others are eliminated (replaced by $R_{ij} = \infty$), then there exists a pathway connecting the left and right faces of the simulation volume (the "infinite" percolation cluster). The resistivity ρ/ρ_0 is approximated as R_c/R_0.

In our analysis below we make use of the following dimensionless units, which reduce the number of free variables in the problem. We introduce the dimensionless distance between the centers of NCs i and j,

$$r_{ij}^* = \frac{r_{ij}}{D}, \tag{2.12}$$

the dimensionless temperature

$$T^* = \frac{2D^2\kappa k_B T}{e^2\xi}, \tag{2.13}$$

the dimensionless electron energy

$$\varepsilon^* = \frac{\varepsilon}{e^2/\kappa D}, \tag{2.14}$$

the dimensionless electron DOGS

$$g^*(\varepsilon^*) = \frac{e^2D^2}{\kappa} g(\varepsilon^*), \tag{2.15}$$

and the dimensionless resistivity

$$\ln \rho^* = \frac{\xi}{2D} \ln(\rho/\rho_0). \tag{2.16}$$

In these units, Eq. (2.9) can be written more simply as

$$\ln \rho_{ij}^* = r_{ij}^* + \varepsilon_{ij}^*/T^*, \tag{2.17}$$

and the problem loses any explicit dependence on the diameter or the localization length. It is also convenient to discuss the energy gap between the 1S and 1P shells in terms of the dimensionless parameter

$$\Delta \equiv \frac{E_Q(3) - E_Q(2)}{e^2/\kappa D} = 20.64\frac{\kappa\hbar^2}{me^2D} = 20.64\frac{\kappa a_B}{\kappa_{\rm NC} D}. \tag{2.18}$$

We use our simulation to examine the resistivity at various values of ν, T^*, and Δ.

Results below correspond to a simulated system of size $L = 25$ with open boundaries, averaged over 100 realizations. Simulations at smaller system size, $15 \leq L < 25$, do not produce noticeably different results for either the DOGS or the resistivity, which allows us to avoid having to extrapolate our results to infinite system size.

2.4 Results and discussion

Our goal is to determine which conditions produce VRH in the NC array. To this end we calculated the resistivity ρ and the electron density of ground states $g(\varepsilon)$ for a range of values of the doping level ν, the temperature T^*, and the quantum energy scale Δ. (Varying Δ is equivalent to considering different values of the NC diameter.) Before proceeding to present general results, however, we first illustrate the most important features of the problem by discussing the hypothetical case where all NCs have the same number of donors, so that there is absolutely no disorder in the system. Say, for example, that $\nu = 5$ and that $N_i = 5$ for all i. In this situation, the ground state arrangement of the system is for electrons to uniformly neutralize all donors: $n_i = N_i = 5$. The result, by Eqs. (2.5) and (2.6), is that every NC has the same two energy levels, $\varepsilon^{(f)} = E_Q(5) - e^2/\kappa D$ and $\varepsilon^{(e)} = E_Q(5) + e^2/\kappa D$, and the system's Fermi level $\mu = E_Q(5)$. Equivalently, one can say that the single-particle DOGS for this hypothetical system corresponds to two δ-function peaks at $\varepsilon = \pm e^2/\kappa D$.

As explained in the introduction, conduction in this uniformly neutral system requires the excitation of a positive/negative NC pair. Specifically, such an excitation produces one positive NC containing 4 electrons and one negative NC containing 6, and as such it has an excitation energy equal to the sum of the two Coulomb self-energies. Equivalently, one can say that conduction requires the production of a hole in the filled δ-function DOGS peak at $\varepsilon = -e^2/\kappa D$ and an electron in the empty DOGS peak at $\varepsilon = e^2/\kappa D$, and so the conduction has an activation energy $\varepsilon_A = E_c = e^2/\kappa D$. Thus, this hypothetical system without disorder has activated conduction: $\rho = \rho_0 \exp[\varepsilon_A/k_B T]$.

On the other hand, once the randomness in donor number is taken into account, one can no longer say in general that the ground state arrangement of electrons is uniformly neutral, $n_i = N_i$. Indeed, when N_i can take a wide range of values, then those NCs with very large N may become ionized so that their electrons can occupy lower-energy shells on other NCs with small N. In this way, the presence of a discrete quantum energy spectrum instigates the production of positively- and negatively-charged NCs. It is this spontaneous charging that allows for VRH, as we will show below.

Still, it is straightforward to see that the system remains nearly uniformly electroneutral in the ground state under either of two conditions: (i) very small quantum energy gap, $\Delta \ll 1$, or (ii) very small doping level, $\nu \ll 1$. In the former case, the difference between quantum energy levels becomes negligibly small compared to the energy required to produce charging of NCs. Thus, the NCs remain neutral and the conduction is activated, as explained above. In the limit of very small doping, $\nu \ll 1$, the system also remains nearly uniformly neutral due to an extreme scarcity of donors with $N_i > 2$. Indeed, by Eq. (2.2), at small ν the fraction of donors with $N_i > 2$ is $\simeq \nu^3/6$. Thus, neutrality of the system can be maintained without requiring any significant number of electrons to occupy the 1P shell, and there is essentially no charging of NCs. Therefore in the limit of very small ν the conduction is also activated.

In situations where either Δ or ν is not small, one can expect spontaneous charging of NCs in the ground state, and it is not trivial to predict the DOGS or the temperature dependence of the resistivity. We explore these situations using our simulation method, outlined in Sec. 2.3. Before proceeding to present results for a wide range of ν and Δ, we first focus on the illustrative cases of $\nu = 5$ and $\nu = 2$, taking for the quantum energy gap $\Delta = 5$.

At $\nu = 5$, the Fermi level resides in the middle of the 1P shell. Thus, since the gap between quantum energy levels is relatively large, in the ground state essentially all NCs satisfy $2 \leq n_i \leq 8$. By Eq. (2.2), however, roughly 11% of NCs have a donor number satisfying $N_i < 2$ or $N_i > 8$. Such NCs become charged in the ground state, driven by the large gaps in the quantum energy spectrum that induce electrons to leave the 1D shell and to fill the 1S shell. Thus, the ground state configuration of the system consists of randomly-distributed fixed charges, which correspond to those NCs with $N_i < 2$ (which become negatively-charged) or $N_i > 8$ (positively-charged), and mobile electrons and holes in the partially-filled 1P shell. The mobile electrons and holes arrange themselves in such a way that the ES criteria of Eqs. (2.7) and (2.8) are satisfied. It is these criteria that give rise to the vanishing DOGS near the Fermi level [3, 32].

This process of charging of NCs is illustrated schematically in Fig. 2.4, which shows the energy levels of isolated NCs with donor numbers $0 \leq N \leq 10$. In the neutral state, a NC with N donors has N filled electron energy levels (Fig. 2.4a). When the system

contains a mixture of NCs with different N, however, electrons abandon high energy levels in NCs with large N and fill empty states in NCs with small N. This process is shown for the case $\nu = 5$ in Fig. 2.4b. The resulting charged NCs produce a random Coulomb potential throughout the system that smears the single electron energy levels and produces a finite density of states near the Fermi level.

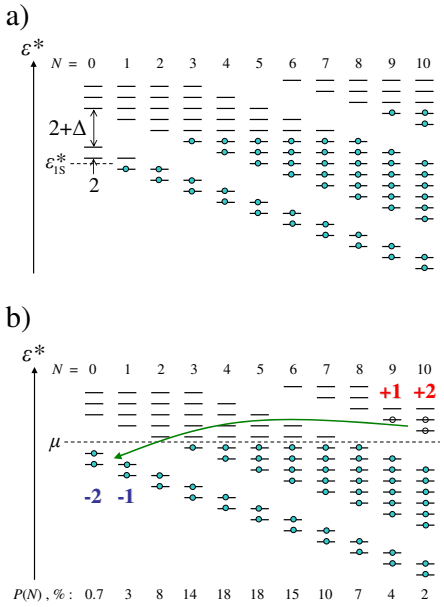

Figure 2.4: (Color online) Schematic depiction of the charging process in a system with NCs with varying donor number N. (a) The single-electron energy levels (horizontal line segments) are shown for isolated NCs. The Coulomb self-energy of charged NCs produces a spectrum where different charge states have a separation $2e^2/\kappa D$. The quantum confinement energy provides a gap between subsequent shells, e.g. 1S and 1P states or 1P and 1D states. In the neutral state, a NC with N donors has N filled energy levels (indicated by filled blue dots). ε^*_{1S} indicates the quantum kinetic energy of the 1S shell, $\varepsilon^*_{1S} = E_Q(1)/(e^2/\kappa D)$. (b) A depiction of the charging process at $\nu = 5$. Electrons in the 1D shell of NCs with $N > 8$ abandon these NCs and instead fill empty energy levels in the 1S shell of NCs with $N < 2$. In this way NCs with $N > 8$ become positively charged and NCs with $N < 2$ become negatively charged. The resulting Fermi level μ is shown by the dashed line. For NCs with $N = 5$, it resides in the center of the 1P shell. The relative abundance of different donor numbers at $\nu = 5$ is shown at the bottom of the figure as a percentage.

The DOGS for $\nu = 5$ and $\Delta = 5$, as calculated by our numerical simulation, is

plotted in Fig. 2.5a. One can see the quadratic Coulomb gap near the Fermi level, as proscribed by the ES theory. As compared to the conventional Coulomb gap problem in lightly-doped semiconductors [32], this Coulomb gap is remarkably well preserved, with the DOGS remaining quadratic until $\varepsilon^* \approx 1$. This strong Coulomb gap suggests that the resistivity should follow the ES law for all temperatures $T^* \ll 1$. Specifically, at these small temperatures the resistivity is described by

$$\rho(T) = \rho_0 \exp\left[\left(\frac{T_{ES}}{T}\right)^{1/2}\right], \tag{2.19}$$

where

$$T_{ES} = \frac{Ce^2}{k_B \kappa \xi} \tag{2.20}$$

and C is a numerical coefficient of order unity.

This behavior can indeed be seen in Fig. 2.5b, where $\ln \rho^*$ is plotted as a function of $(T^*)^{-1/2}$. The linear relationship at large $(T^*)^{-1/2}$ suggests that, as expected, the resistance follows the ES law at small temperatures. We find that the numerical coefficient $C \approx 8.1$, as compared to the typical value $C \approx 2.8$ in lightly-doped bulk semiconductors [32]. At larger temperatures $T^* > 1$ [or $(T^*)^{-1/2} < 1$], the resistivity saturates at $\ln \rho^* = 1$. At such large temperatures the factor ε^*_{ij}/T^* in Eq. (2.17) typically becomes smaller than unity, which indicates that electrons tunnel relatively easily between nearest neighbors, and VRH is abandoned in favor of nearest-neighbor hopping. At these large temperatures the resistivity can be expected to have only a relatively weak power-law dependence on temperature, which is beyond the accuracy of our numerical calculations.

In addition to the parabolic Coulomb gap near the Fermi level, another salient feature of the DOGS in Fig. 2.5a is that it has strong maxima at $\varepsilon^* = \pm 1$ and collapses nearly to zero at $\varepsilon^* = \pm 2$, as if there were additional Coulomb gaps that constrain the density of states around $\varepsilon^* = \pm 2$. These "reflected Coulomb gaps" are in fact the product of an approximate symmetry in the system, which can be seen by examining Eqs. (2.5) and (2.6). At $\nu = 5$, the great majority of NCs have $2 < n_i < 8$. For such NCs, $E_Q(n_i) = E_Q(n_i + 1)$; both the highest filled and lowest empty electron states are in the 1P shell. In this case, one can subtract Eqs. (2.5) and (2.6) to show that $\varepsilon_i^{*(e)} = \varepsilon_i^{*(f)} + 2$. Thus, the great majority of NCs contribute to the density of states two

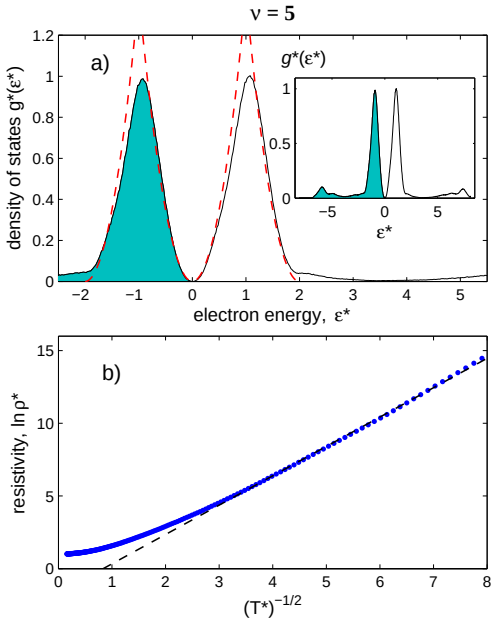

Figure 2.5: (Color online) Density of ground states and resistivity at $\nu = 5$ and $\Delta = 5$, as measured by computer simulation. (a) Density of states as a function of electron energy. Filled electron states are shaded. Dashed red lines show, schematically, the quadratic Coulomb gap near the Fermi level, $\varepsilon^* = 0$, and the "reflected Coulomb gaps" at $\varepsilon^* = \pm 2$. Note that that the total shaded and unshaded areas under the $g^*(\varepsilon^*)$ curve are both normalized to unity, since each NC has one electron and one hole excitation. The inset shows the DOGS over a wider energy range, with small, distant peaks indicating rare NCs whose highest filled electron state is in the 1S shell or whose first empty state is in the 1D shell. (b) The dimensionless logarithm of the resistance, $\ln \rho^*$, as a function of $(T^*)^{-1/2}$, which illustrates the existence of ES resistivity at small temperature.

energy levels – one filled, one empty – separated by $2e^2/\kappa D$. This creates an approximate discrete translational symmetry in the density of states, so that $g^*(\varepsilon^*) \approx g^*(\varepsilon^* - 2)$ for $0 < \varepsilon^* < 2$. As a consequence, the Coulomb gap at the Fermi level implies the existence of reflected Coulomb gaps at $\varepsilon^* = \pm 2$. In other words, one can say that because of the discrete charging spectrum of NCs the conventional quadratic bound on the DOGS near the Fermi level also produces (approximate) quadratic bounds on the DOGS near $\varepsilon^* = \pm 2$. The contribution of rare NCs with $n_i = 2$ or $n_i = 8$ to the DOGS can be seen in the small peaks at $\varepsilon^* = -6$ and $\varepsilon^* = 7$, as shown in the inset of Fig. 2.5a.

The presence of reflected Coulomb gaps is not unique to the doping level $\nu = 5$.

Indeed, for all ν that are sufficiently removed from the quantum energy gaps at $\nu = 2$, $\nu = 8$, etc., the relation $\varepsilon_i^{*(e)} = \varepsilon_i^{*(f)} + 2$ is valid for most NCs in the system and the resulting DOGS is essentially identical to that of Fig. 2.5a. Consequently, the resistivity plot shown in Fig. 2.5b accurately describes the resistivity at most values of $\nu > 1$. The reflected Coulomb gaps in Fig. 2.5a appear even more dramatically for large NCs with external impurity charges, as will be shown in Ch. 3.

On the other hand, one could expect qualitatively different behavior at $\nu = 2$, where there are precisely enough electrons to fill the 1S shell of every NC, and the Fermi level sits in between the 1S and 1P shells. In this case there is no "discrete translational symmetry" in the density of states, since the empty and filled energy levels for most NCs, $\varepsilon_i^{(e)}$ and $\varepsilon_i^{(f)}$, sit on opposite sides of the quantum energy gap, as shown schematically in Fig. 2.6. This produces a DOGS that is qualitatively different from what is shown in Fig. 2.5a. One could therefore expect that the dependence of the resistivity on temperature is also qualitatively different. Such thinking is supported by a recent experiment on electrochemically gated NCs [4], which reported that when ν is very close to 2 there appears an appreciable temperature window over which the resistivity follows the Mott law. Given these differences, it is worth giving some special consideration to the case $\nu = 2$.

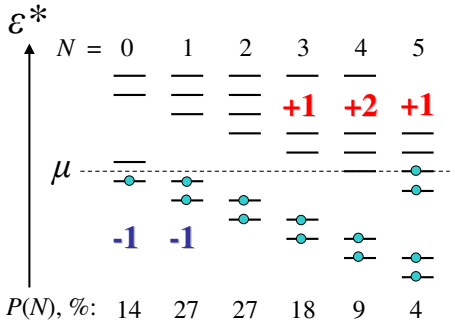

Figure 2.6: (Color online) Schematic depiction of the filled and empty energy levels at $\nu = 2$. Energy levels are shown for NCs in the absence of any Coulomb potential, similar to Fig. 2.4. At $\nu = 2$, some electrons leave the 1P shell of NCs with $N > 2$ and fill empty states in the 1S shell of NCs with $N < 2$. The resulting Fermi level μ is aligned with the first(second) energy level of the 1P shell in NCs with $N = 4(5)$, which is partially filled.

The DOGS for $\nu = 2$ is shown in Fig. 2.7a. Unlike at $\nu = 5$, where the DOGS

collapses at $\varepsilon^* = \pm 2$, the DOGS at $\nu = 2$ is much broader, with a width $\Delta + 2$. This broad DOGS can be seen as a consequence of the large gap between 1S and 1P energy shells, which implies that the energy of electron or hole excitations, $\varepsilon_i^{(f)}$ and $\varepsilon_i^{(e)}$, can take a wide range of values, depending on the donor number N_i. Alternatively, one can say that since both 1S and 1P electron states contribute to the DOGS near the Fermi level, the density of states has a characteristic width similar to that of the gap Δ.

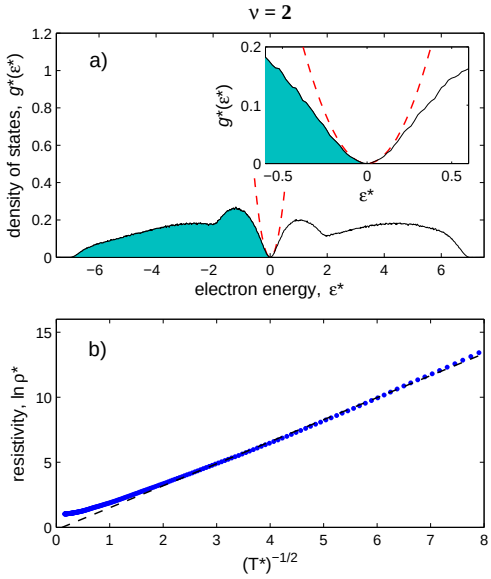

Figure 2.7: (Color online) Density of states and resistivity at $\nu = 2$ and $\Delta = 5$, as measured by computer simulation. (a) DOGS as a function of electron energy. Filled electron states are shaded. The dashed red curve is the same parabolic curve shown in Fig. 2.5a. The inset shows the DOGS very close to the Fermi level. (b) The dimensionless logarithm of the resistance, $\ln \rho^*$, as a function of $(T^*)^{-1/2}$, which shows ES resistivity at $T^* \ll 1$.

As at $\nu = 5$, the DOGS vanishes at the Fermi level (see the inset of Fig. 2.7a), but in this case it can only be described as parabolic over the fairly narrow range of energies $|\varepsilon^*| < 0.2$. In the intermediate range of energies $0.2 < |\varepsilon^*| < 1$, the DOGS grows roughly linearly with energy. At larger energies $1 < \varepsilon^* < \Delta$ the DOGS becomes roughly constant.

In spite of this relatively complicated DOGS, Fig. 2.7b shows that the resistivity is in excellent agreement with the ES law, with a coefficient $C \approx 5.7$ [see Eq. (2.20)],

at all but very large temperatures. This is somewhat surprising, since it suggests that the system exhibits ES resistivity even when the temperature is large enough that the band of energies over which VRH occurs is much larger than the width of the parabolic Coulomb gap. This behavior would be impossible if states were randomly distributed in space. Our observation of ES resistivity suggests that at $\nu = 2$ spatial correlations emerge which somehow preserve ES resistivity even in the absence of a parabolic DOGS.

To illustrate how this might be possible, let us first recall that in a disordered two-dimensional (2D) system, the DOGS is linear in energy near the Fermi level rather than parabolic, but the ES law of VRH is still obeyed [3]. One can now imagine a 3D system in which sites with energies close to the Fermi level are arranged in a 2D fractal subspace embedded in the system volume. In such a system, one would still have a linear DOGS near the Fermi level accompanied by ES resistivity, even though the system as a whole is three-dimensional. Using this reasoning, one can speculate that the results shown in Fig. 2.7 are indicative of such a fractal arrangement of sites near the Fermi level, driven in some way by the long-ranged Coulomb potential. More broadly, these results hint at the idea that in a disordered system of localized states dominated by Coulomb interactions, one should be able to derive the ES law without explicit reference to the DOGS or the system's dimensionality. Such an argument was in fact first put forward by Larkin and Khmelnitskii [48]. Our system at $\nu = 2$ may be a good application of this argument. It remains unclear, however, in which situations this argument is applicable *a priori*. This general question and its application to the case $\nu = 2$ will be the subject of a future publication.

By conventional thinking, the relatively constant DOGS at $|\varepsilon^*| > 1$ would seem to suggest a regime of temperature in which the resistivity follows the Mott law, which describes VRH in the presence of a constant DOGS. However, unlike the experiments of Ref. [4], we see no noticeable region of Mott VRH. The Mott resistivity observed in Ref. [4] at $\nu = 2$ is likely the result of some additional disorder that is outside the model considered in this section, and is discussed further in Sec. 2.5.

Having considered the specific cases of $\nu = 5$ and $\nu = 2$, we now turn our attention to a general description of VRH at different values of ν and Δ. In order to identify more precisely which conditions produce VRH, we used our simulation to measure the resistivity as a function of T^*, ν, and Δ over the range $0.01 \leq T^* \leq 10$,

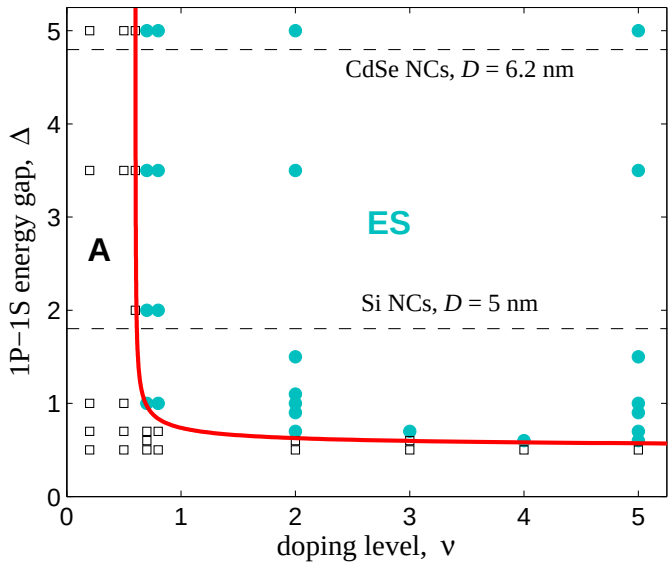

Figure 2.8: (Color online) Phase diagram indicating regimes of activated and ES resistivity as a function of doping level ν and the dimensionless quantum energy gap $\Delta \equiv 20.64\kappa a_B/\kappa_{\rm NC}D$ at low temperature $k_BT \ll e^2\xi/\kappa D^2$. Symbols correspond to simulated systems: filled (light blue) circles indicate systems that exhibited ES resistivity and open squares indicate systems that exhibited activated resistivity. The thick (red) curve is an approximate boundary between these two regimes, which are labeled "ES" and "A", respectively. Dashed, horizontal lines indicate the value of Δ corresponding to Si NCs with $D = 5$ nm (as in Ref. [27]) and to CdSe NCs with $D = 6.2$ nm (as in Ref. [4]).

$0.2 \leq \nu \leq 2$, and $0.5 \leq \Delta \leq 5$. For each case we measured the exponent γ of the temperature dependence of resistivity by calculating the "reduced activation energy" $w(T^*) = -d(\ln\rho^*)/d(\ln T^*) \propto T^{-\gamma}$ [49]. The exponent γ was identified by making a power law best fit to $w(T^*)$. Those values of T^*, ν, and Δ that produce $\gamma = 0.5 \pm 0.1$ were identified with ES resistivity; domains where $\gamma > 0.6$ were identified with activated resistivity. As discussed above, no significant regimes were identified that showed Mott behavior. We use this data to construct an approximate phase diagram in the space of T^*, ν, and Δ that identifies which behavior can be expected.

Our result is plotted in Fig. 2.8 for $T^* \ll 1$. Generally speaking, the results indicate that for $\nu > 0.6$ and $\Delta > 0.5$ one can expect ES resistivity, while for other conditions

the resistivity is activated. These conditions are equivalent to the conditions (i) and (ii) that were announced in the introduction. Dashed horizontal lines indicate, as an example, the values of Δ corresponding to CdSe NCs with $D = 6.2$ nm, as in Ref. [4], and Si NCs with $D = 5$ nm, as in Ref. [27]. Both of these dashed lines assume that $\kappa_{\rm NC}/\kappa_{\rm i} = 5$. At temperatures $T^* > 1$ VRH is gradually replaced by nearest-neighbor hopping. The condition $T^* < 1$ is equivalent to the condition (iii) from the introduction.

As mentioned above, the model considered in this section does not account explicitly for any sources of disorder other than fluctuations in donor number. For example, in real NC arrays the diameter D varies from one NC to another, which introduces variations in the quantum spectrum between NCs [see Eq. (2.1)]. Nonetheless, the presence of these size fluctuations in addition to fluctuations in donor number does not destroy ES VRH, since the Coulomb gap near the Fermi level is a universal result of the ES stability criteria [Eqs. (2.7) and (2.8)] and is independent of the source of disorder in the system. Whether size fluctuations or other sources of disorder enhance the role of VRH or significantly affect the magnitude of the resistivity remains yet to be studied. Generally speaking, however, one can expect that the phase diagram of Fig. 2.8 is accurate whenever the typical magnitude of size fluctuations δD satisfies $(\delta D)/D \ll 1/\Delta$. We further expect that even larger size fluctuations do not greatly affect VRH in regimes where the ES law applies, since in such cases the DOGS is already saturated by the disorder in donor number. In regimes where the resistivity is activated, the presence of a large additional disorder should generally promote the existence of VRH, which decreases the resistivity at small T^*.

2.5 Gating of a NC array by an ionic liquid

In Secs. 2.1 – 2.4 we discussed systems of NCs doped by random impurities, and we explored the dependence of the resistivity on the doping level. In such systems, the doping level is established during the fabrication of NCs. In many cases, however, it is desirable to have a doping level that can be continuously tuned, so that the resistivity of a single device can be set to a wide range of values. For this purpose, electrochemically gated arrays of semiconductor NCs are actively being studied [4, 35].

In such systems, conduction electrons are introduced into the system via a voltage

source, which drives electrons from a top gate to a bottom gate that is in electrical contact with the NC array. Generally, in between the top gate and the NC array is a room temperature ionic liquid that provides large capacitance and therefore allows for a high density of electrons to be introduced to the NC array at a relatively small voltage [50]. The cations from this ionic liquid intercalate into the spaces between NCs, penetrating deep into the array through the percolating network of pores between NCs, and thus provide a neutralizing charge for the conduction electrons. A schematic picture of this system is given in Fig. 2.9.

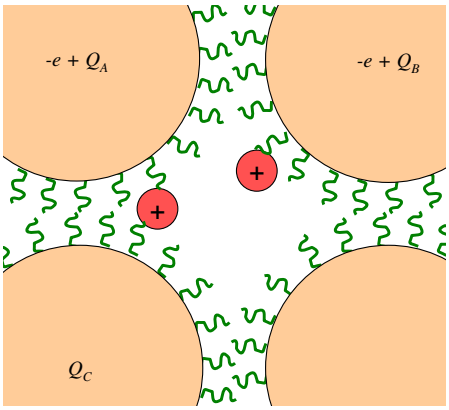

Figure 2.9: (Color online) A schematic picture of an array of semiconductor NCs (large circles) gated by an ionic liquid. Cations (small circles with +'s) are driven by a voltage source to intercalate between NCs. Because of the large NC dielectric constant $\kappa_{\rm NC}$, the net effect of positive ions is to provide a fractional donor charge Q_i at a given NC i. Neutralizing electrons occupy NCs in order to neutralize ionic charges. Ligands separating NCs are shown as curvy lines.

The large internal dielectric constant of NCs and the relatively small diameter of cations suggests the presence of strong image charge forces that bind cations electrostatically to their image charges in the NC surface. In this way, one can expect that cationic charges are located primarily on the surface of each NC. If one assumes that the position of cations on the NC surfaces is random, then one again arrives at a model of fractionalized cation image charges, similar to what is suggested in Sec. 3.2 (see below Ch. 3 for more details).

For this model one can use a Hamiltonian that includes both a prominent quantum kinetic energy spectrum, as in Sec. 2.2, and a fluctuating, fractionalized donor charge,

as in [29]:

$$H = \sum_i \left[\frac{(Q_i - en_i)^2}{\kappa D} + \sum_{k=0}^{n_i} E_Q(k) \right] + \sum_{\langle i,j \rangle} \frac{(Q_i - en_i)(Q_j - en_j)}{\kappa r_{ij}} \tag{2.21}$$

Here, the fractional charge Q_i/e can be chosen uniformly from the interval $[\nu - 1/2, \nu + 1/2]$.

Using our computer simulation method, we have briefly investigated the DOGS and resistivity of the system described by this Hamiltonian at various values of $\nu \geq 1$. We find that ES VRH appears at low temperature for all values of $\nu > 1$. In fact, when $|\nu - 2| > 1$ and $|\nu - 8| > 1$, the DOGS is exactly the same as in Fig. 3.2a, and the resistivity is also identical (see below Ch. 3 for more details).

We note that the model defined by Eq. (2.21), where the fractional donor charge is completely random, is unlikely to be accurate when ν is at the boundary between two quantum energy shells. At $\nu = 2$, for example, random fractional charges lead to a fluctuating Coulomb potential with characteristic amplitude much larger than $k_B T/e$ at room temperature. However, such a large Coulomb potential induces cations, which are mobile during the gating process, to rearrange in order to screen the potential. In this way the cation positions become correlated and the typical amplitude of the Coulomb potential is reduced to $k_B T/e$, which is not large enough to produce charging of NCs. As a result, the typical amplitude of fluctuations in Q_i is likely much smaller than e, so that one should not expect a finite DOGS near the Fermi level. Rather, in the absence of any other disorder, the resistivity should be large and activated.

Experiments with ionic liquid gating confirm that, as expected, the resistivity is much larger at $\nu = 2$ than at other filling factors [4]. However, the resistivity is generally shown to correspond to VRH rather than activated behavior, with ES resistivity seen at very small temperature and Mott resistivity at larger temperatures. This VRH is likely the result of some other source of disorder, unrelated to the positions of cations, which produces finite DOGS near the Fermi level even at $\nu = 2$. For example, if the NC diameters are not uniform, but are drawn from some distribution with finite width, then the energy levels corresponding to the 1S and 1P states are smeared. If the distribution of NC diameters has wide tails, then the 1S and 1P energy levels can be smeared as far

as the Fermi level, producing a finite DOGS near the Fermi level, as shown schematically in Fig. 2.10.

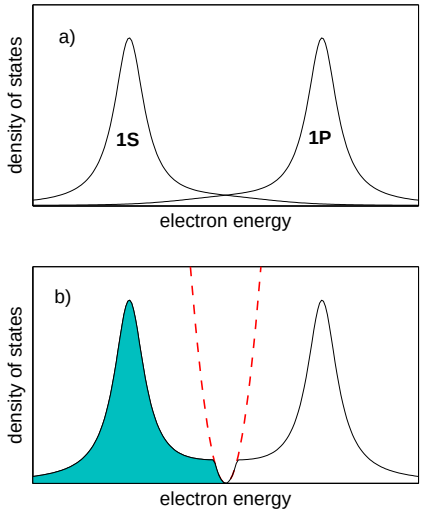

Figure 2.10: (Color online) Schematic picture of the density of states at $\nu = 2$ in the presence of fluctuations in the NC diameter D. (a) If D has some wide-tailed distribution, then the 1S and 1P energy levels are broadened and have a finite overlap. (b) Spatial correlations between rare 1S and 1P energy states near the Fermi level produce a Coulomb gap, so that ES resistivity is seen at very small temperatures and Mott resistivity is seen at larger temperatures.

The overlap between some 1S and 1P energy levels produces rare NCs with $n = 3$ or $n = 1$ whose energy is very close to the Fermi level. Such rare, mobile electrons are free to rearrange themselves in order to satisfy the ES stability criteria, and in doing so they produce a small Coulomb gap at the Fermi level (see Fig. 2.10). As a result, the resistivity follows the ES law at very small T, and the Mott law at larger T, where the DOGS sampled by electron hops is essentially constant. This is precisely what is seen in experiment [4].

It is worth mentioning that ionic liquid gating of NC arrays allows one to measure the total electronic charge Q as a function of applied gate voltage, or, in other words, the differential capacitance of the array $C = dQ/dV$. In arrays of small spherical NCs, where the quantum gaps Δ dominate over Coulomb energies, most electrons enter the array when the voltage coincides with the energies of a quantum energy shell (1S or

1P, for example). At such voltages the differential capacitance should have prominent peaks. Between these voltages the capacitance should be small, reflecting the small electron DOGS. We are not aware of any such experimental data [1] .

2.6 Conclusion

In this Chapter we have used a simple theoretical model and a computer simulation to show how both activated transport and VRH arise in arrays of doped semiconductor NCs. Our primary result is illustrated in the phase diagram of Fig. 2.8: when the doping level ν and the quantum confinement energy Δ are sufficiently large, and when the temperature T^* is sufficiently small, the resistivity of the array is characterized by ES VRH. Such VRH is driven by the fluctuations in donor number from one NC to another, which lead to spontaneous charging of NCs as electrons depopulate higher quantum energy shells and fill lower ones.

We have also identified a striking feature of the DOGS in NC arrays: the presence of "reflected Coulomb gaps" at electron energies $\pm 2e^2/\kappa D$, which are a consequence of the ES stability criteria and the discrete charging spectrum of NCs (see Fig. 2.5). This feature is even more prominent in large, metallic NCs with external impurity charges that is discussed in the following chapter.

The effect of additional disorder, such as fluctuations in NC size, remains yet to be explored quantitatively. We conjecture, however, that for chemically doped NCs our results will be largely unaltered by the addition of such disorder. For the case of NCs gated by ionic liquid, this external disorder seems crucial only for explaining the presence of Mott VRH at particular values of ν (see Fig. 2.10).

[1] In our recent paper [50], we studied the hypothetical case where cations are large enough that only one cation can enter a pore in the NC array. In this case, due to the Coulomb interaction, the cations form a crystal structure within the pores of the crystalline NC array. This situation is different from the model where ions are small and are introduced at relatively large temperature. In Ref. [50] we argued that in the former case the peak in capacitance corresponding to the 1S shell splits into two delta-function-like peaks, such that one electron enters every NC at two particular values of the voltage.

Chapter 3

Metallic nanocrystals

3.1 Introduction

Granular metals and arrays of metallic nanocrystals (NCs) represent interesting composite systems, wherein the unique properties of individual NCs are combined with collective, correlation-driven effects between NCs to produce novel material properties [34, 28]. One of the most important properties is the electron conductivity, which proceeds by electron tunneling, or "hopping", between NCs through the insulating gaps which separate them. In relatively dense NC arrays, electron conduction can occur both through nearest-neighbor hopping and through VRH. As already discussed in Ch. 2, in the presence of some disorder, the latter mechanism dominates at low temperatures, where the length of hops grows to optimize the conductivity. When the Coulomb interaction between localized electrons is taken into account, it can be shown that at sufficiently low temperature VRH conductivity obeys the Efros-Shklovskii (ES) law [3]:

$$\sigma = \sigma_0 \exp\left[-\left(T_{ES}/T\right)^{1/2}\right], \tag{3.1}$$

where σ_0 is a constant (or a weak, power-law function of temperature) and T_{ES} is a characteristic temperature (see Eq. (2.20)). (Eq. (3.1) can be viewed as the inverse of Eq. (2.19).) Eq. (3.1) has been observed in a number of granular metal systems at low temperature (see Refs. [5] and references therein). In these systems, as in lightly-doped semiconductors and other "Coulomb glasses", ES conductivity can be seen as the result of a vanishing single-particle density of states (DOS) at the Fermi level μ. This vanishing

DOS is the consequence of a very general stability criterion of the ground state [32], and it implies that in a system of d dimensions the DOS $g(\varepsilon)$ satisfies

$$g(\varepsilon) < \frac{A_d}{e^{2d}} |\varepsilon|^{d-1}. \tag{3.2}$$

Here, A_d is some numerical constant of order unity, ε is the electron energy relative to the Fermi level, and e is the electron charge. Eq. (3.2) is called the "Coulomb gap."

In this chapter we report an additional striking feature of the DOS in periodic arrays of monodisperse metal NCs surrounded by random impurity charges. Namely, we show that the Coulomb gap at $\varepsilon = 0$ necessarily implies the existence of additional, identical Coulomb gaps at energies $\varepsilon = \pm e^2/C_0$, where C_0 is the self-capacitance of each NC. This result is shown in Fig. 3.2.

The remainder of this chapter is organized as follows. In Sec. 3.2 I define the system being studied and outline our simulation technique. In Sec. 3.3 I describe our main results for the DOS and conductivity on both 2d and 3d arrays. We close in Sec. 3.4 with concluding remarks.

3.2 Model

Experimentally, regular arrays of metal NCs can now be reliably synthesized with diameter D in the range 3–7 nm and with size dispersion less than 5% [5, 28, 34]. For such small NCs, the self-capacitance C_0 is also small: $C_0 = \kappa D/2$, where κ is the effective dielectric constant of the array, given approximately by the Maxwell-Garnett formula [43, 50]. Correspondingly, the Coulomb self-energy $q^2/2C_0$ of an NC with charge q plays a large and important role in electron transport. To see this, one can imagine a hypothetical NC array with no disorder. In such an array, in the ground state all NCs are neutral and electron conduction requires the thermal excitation of positive-negative NC pairs. Thus, the conductivity is activated with an activation energy $e^2/2C_0$. For nanometer-sized NCs, this activation energy can easily exceed the thermal energy k_BT.

In the presence of some finite charge disorder, however, the fluctuating Coulomb potential can produce charging of NCs in the ground state and thus lead to a Coulomb gap in the DOS and to ES conductivity. To show how this happens, I adopt the following simplified model. I assume that identical, spherical, metallic NCs reside in a regular

d-dimensional square lattice with lattice constant D', and that impurity charges $\pm e$ are embedded in the insulator (oxide) between NCs. Such impurity charges can be thought to effectively create a fractional donor charge Q_i that resides on each NC i, for reasons that are explained below. The net charge of the NC can then be written as $q_i = Q_i - en_i$, where n_i is the integer number of electrons that reside on the NC relative to its neutral state (n_i can be positive or negative). Given this model, the Hamiltonian for the system is

$$H = \sum_i \frac{(Q_i - en_i)^2}{2C_0} + \sum_{\langle i,j \rangle} C_{ij}^{-1}(Q_i - en_i)(Q_j - en_j). \tag{3.3}$$

Here, the first term describes the Coulomb self-energy of each NC and the second term describes the interaction between charged NCs. The coefficient C_{ij}^{-1} is the inverse of the matrix of electrostatic induction C_{ij}. This Hamiltonian has been also been proposed as a model for arrays of large semiconductor NCs [51].

Because of the presence of the impurity charges, electrons become redistributed among NCs from their neutral state in order to screen the disorder Coulomb potential. In order to calculate the DOS and conductivity I first attempt to find numerically the set of electron occupation numbers $\{n_i\}$ that minimizes the Hamiltonian. In the numerical simulations that we describe below, we make the approximations that $C_0 = \kappa D/2$ and $C_{ij}^{-1} = 1/\kappa r_{ij}$. These approximations do not effect our main conclusions, as we explain below.

The model of fractional donor charges Q_i was first put forward in Ref. [29]; here its justification is briefly repeated. When an impurity charge, say with charge $+e$, is located close to the point of contact between two NCs, labeled A and B, it induces negative image charges $-q_A$ and $-q_B$ in the surfaces of NCs A and B, respectively. This is shown schematically in Fig. 3.1. In order to maintain overall neutrality of the NCs, an equal and opposite image charge appears at the center of each NC: $+q_A$ and $+q_B$. (These "image charges at the center" represent a uniform electronic charge at the NC surface.) The values of q_A and q_B are such that together the image charges $-q_A$ and $-q_B$ neutralize the donor charge: $q_A + q_B = e$. Their respective magnitudes are determined by the distance between the impurity and each NC surface. For example, if the impurity sits exactly along the line connecting the centers of NCs A and B and if the gap $w = D' - D$ between NCs satisfies $w \ll D$, then $q_A x_B = q_B x_A$, where x_A and x_B

are the distances between the impurity and the surface of NCs A and B, respectively. Since the impurity charges and the image charges $-q_A$, $-q_B$ together form a compact, neutral arrangement, the net effect of the impurity charge is to produce "fractionalized" donor charges, such that $+q_A$ is relayed to the center of NC A and $+q_B$ is relayed to the center of B.

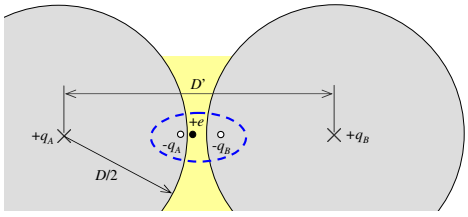

Figure 3.1: (Color online) A schematic depiction of the fractionalization of a charged impurity (small black circle) between NCs (large gray circles). The positive impurity induces negative image charges (white circles) in nearby metal surfaces and is effectively neutralized, while equal and opposite positive images are conveyed to the center of the NC ($\times$'s).

In this way, each NC i can be said to have a fractional donor charge Q_i, which is equal to the sum total of the fractionalized charges donated by individual impurities around it. In the limit where there are very many impurity charges surrounding each NC, one can think that the random variable Q_i is Gaussian-distributed with some standard deviation larger than e. In fact, however, in such cases one can effectively adopt a much simpler model, in which the value of Q_i is chosen randomly from the uniform distribution $Q_i \in [-e/2, +e/2]$. To see why this model is valid, consider that each NC minimizes its Coulomb self-energy by minimizing the magnitude of its net charge, $|Q_i - en_i|$. Since n_i can take any integer value, it is generally true that in the ground state $-e/2 \leq Q_i - en_i \leq e/2$. In other words, each NC can effectively adjust to the presence of an arbitrarily strong charge disorder by changing its electron number n_i (say, by drawing electrons from the voltage source) so that its net charge acquires a magnitude smaller than $e/2$. This has important implications for the disorder-dependence of conductivity, as I show below.

Given the ground state configuration for a particular system, defined by the set of electron occupation numbers $\{n_i\}$, one can determine the energy of the highest filled

electron level, $\varepsilon_i^{(f)}$, and the lowest empty electron level, $\varepsilon_i^{(e)}$, at each NC i. Specifically:

$$\varepsilon_i^{(f)} = \frac{2e^2 n_i - 2Q_i e - e^2}{2C_0} - e\sum_{j\neq i} C_{ij}^{-1}(Q_j - en_j), \tag{3.4}$$

$$\varepsilon_i^{(e)} = \frac{2e^2 n_i - 2Q_i e + e^2}{2C_0} - e\sum_{j\neq i} C_{ij}^{-1}(Q_j - en_j). \tag{3.5}$$

These energies are defined so that the Fermi level $\mu = 0$, and in the ground state $\varepsilon_i^{(f)} < 0$ and $\varepsilon_i^{(e)} > 0$ for all i. The single particle DOS $g(\varepsilon)$ is defined by making a histogram of the energy values $\varepsilon_i^{(f)}$ and $\varepsilon_i^{(e)}$. Higher and lower electron energy states are ignored in this work, as they play no role in conductivity at $k_B T \ll e^2/C_0$.

In order to evaluate numerically the DOS, I use a computer simulation to search for the ground state arrangement of electrons, $\{n_i\}$, in a finite array of NCs. For simplicity, we set the lattice constant $D' = D$; this corresponds to the limit where the gap w between NCs is very thin while the tunneling transparency of the barrier between them remains much smaller than unity. In our simulation we search for the ground state by looping over all NC pairs i, j and attempting to move one electron from i to j. If the move lowers the Hamiltonian H, then it is accepted, otherwise it is rejected. Equivalently, one can say that for all i, j we check that the ES ground state criterion is satisfied:

$$\varepsilon_j^{(e)} - \varepsilon_i^{(f)} - e^2 C_{ij}^{-1} > 0. \tag{3.6}$$

It should be noted that this procedure does not in general find the exact ground state, but only a "pseudo-ground state" that is stable with respect to single-electron transfers. In principle, the system energy can be lowered further by some simultaneous multi-electron transfers. Such processes are generally seen to have only a relatively weak effect on the DOS [45, 46] that slightly deepens the Coulomb gap near the Fermi level.

3.3 Results and discussion

The resulting DOS is shown in Fig. 3.2a for a two-dimensional (2d) simulated system of size 100×100 lattice sites and in Fig. 3.2b for a three-dimensional (3d) system of size $25 \times 25 \times 25$. Electron energies are plotted in the dimensionless form $\varepsilon^* = \varepsilon/(e^2/2C_0)$ and the DOS is plotted in the dimensionless form $g^*(\varepsilon^*) = (e^2 D^d/2C_0)g(\varepsilon^*)$. The insets

to these figures show a log-log plot of the DOS near $\varepsilon = 0$, which suggests that in 2d the DOS follows $g_{2\mathrm{d}}(\varepsilon) \propto \varepsilon^{1.5}$ at small energies and in 3d $g_{3\mathrm{d}}(\varepsilon) \propto \varepsilon^{2.4}$. These exponents are somewhat larger than the theoretical ones given in Eq. (3.1), so that apparently the ES bound is not saturated. This is similar to what happens in the Efros model of the Coulomb glass [52] at disorder strength $A = 1$ [45]. The results of Fig. 3.2 are generated using a uniform distribution $Q_i \in [-e/2, e/2]$ for the fractional charge. If one instead takes Q_i to be Gaussian-distributed with a standard deviation $< 3e$, the resulting DOS is everywhere equal to that of Fig. 3.2 to within 0.6%.

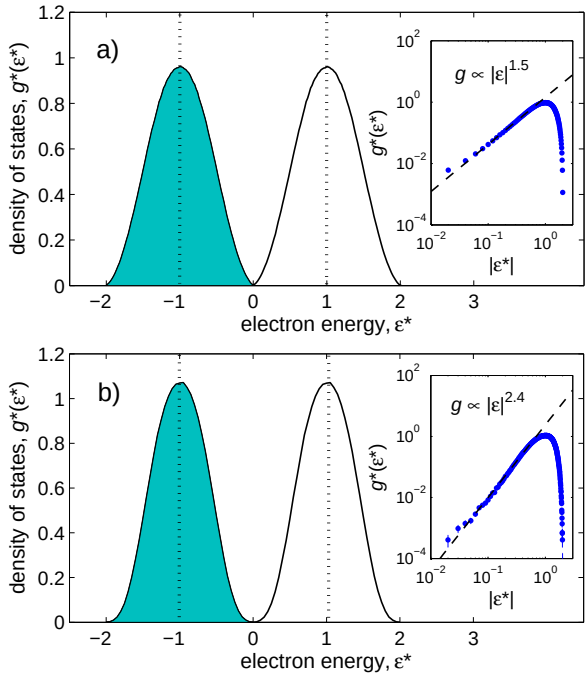

Figure 3.2: (Color online) The DOS of a regular array of monodisperse NCs, where $\varepsilon^* = E/(e^2/2C_0)$ is the dimensionless single-particle energy and $g^*(\varepsilon^*) = (e^2 D^d/2C_0)g(\varepsilon^*)$ is the dimensionless DOS, where D is the NC diameter. Here, the results are shown from a computer simulation of a) a 2d square lattice and b) a 3d cubic lattice. The shaded area shows filled electron states, and the empty area indicates empty states. In addition to electron–hole symmetry, the two peaks of the DOS have a mirror symmetry across $\varepsilon^* = \pm 1$, respectively (dotted lines). This symmetry creates from the central Coulomb gap two additional half-gaps at $\varepsilon^* = \pm 2$, resulting in a "Coulomb gap triptych." Insets show the DOS near the Fermi level $\varepsilon^* = 0$ in log-log scale.

Fig. 3.2 also highlights the striking additional symmetry in the DOS in both 2d and 3d, as compared to the DOS in the conventional Coulomb glass problem [32, 45]. Namely, each peak in the DOS is symmetric with respect to reflections about $\varepsilon^* = \pm 1$, so that the DOS has identical, repeated Coulomb gaps at $\varepsilon^* = \pm 2$. The origin of these additional Coulomb gaps can be understood by noting a particular symmetry in the Hamiltonian that is reflected in the filled and empty state energies, $\varepsilon_i^{(f)}$ and $\varepsilon_i^{(e)}$. Namely, by subtracting Eqs. (3.4) and (3.5) one can show that

$$\varepsilon_i^{*(e)} = \varepsilon_i^{*(f)} + 2 \tag{3.7}$$

for all i. Thus, all NCs contribute to the DOS two energy levels – one filled, one empty – separated by e^2/C_0. This implies that as the density of states collapses at ε very close to zero (the Coulomb gap), the density of states must also collapse as ε^* approaches ± 2 in identical fashion. That is, the ES stability criterion of Eq. (3.6) places constraints both on the DOS near $\varepsilon = 0$ and on the DOS near $\varepsilon = \pm e^2/C_0$.

One can also note that states with $\varepsilon_i^{*(f)} < -2$ or $\varepsilon_i^{*(e)} > 2$ are prohibited, since by Eq. (3.7) these would imply that some NC has $\varepsilon_i^{(e)} < 0$ or $\varepsilon_i^{(f)} > 0$. Thus, $g(\varepsilon)$ is strictly zero at $|\varepsilon^*| > 2$. This is a markedly different situation than in the conventional Efros model [52], where the width of the DOS reflects the characteristic strength of the disorder. In the present problem, for large enough disorder the DOS has a saturated width e^2/C_0. This saturation occurs because the number of electrons n at each site can adjust to screen an arbitrarily large Coulomb disorder. Thus, one can expect that at large disorder the conductivity also becomes independent of disorder strength.

In order to evaluate the conductivity directly, we employ the approach of the Miller-Abrahams network [47], similar to what is explained in the previous sections. Our results for the conductivity are shown in Fig. 3.3, plotted as a function of the dimensionless temperature $T^* = 4DC_0k_BT/(e^2\xi)$ raised to the power $-1/2$. The results indicate that the conductivity is well-described by the ES law of Eq. (3.1) at relatively small temperatures $T^* \lesssim 1$, both in 2d and 3d [1] .

This behavior is consistent with the prominent Coulomb gaps seen in Fig. 3.2. In

[1] In fact, if one repeats the original ES derivation [3] using the DOS shown in Fig. 3.2, one arrives at a slightly different temperature dependence $\ln\sigma \propto T^{-\gamma}$ at low temperature, with $\gamma \approx 0.56$ in 2d and $\gamma \approx 0.53$ in 3d. Due to finite size limitations, our conductivity data (Fig. 3.3) cannot discriminate between these exponents and $\gamma = 1/2$.

both 2d and 3d, replacing the uniform distribution of Q_i with a distribution with larger variance — for example, by taking Q_i as the sum of three or more independent fractional charges — did not affect the conductivity to within our numerical accuracy. This insensitivity to the disorder strength stands in contrast to the Efros model [52], where large disorder widens the DOS, so that ES conductivity exists only when the temperature is sufficiently small that electron hops are confined to within the parametrically narrow window of energies in which $g(\varepsilon)$ is constrained by the Coulomb gap [32]. On the contrary, in arrays of monodisperse metallic NCs the DOS becomes essentially independent of disorder strength, so that even at large disorder the Coulomb gap plays a prominent role and the conductivity follows the ES law.

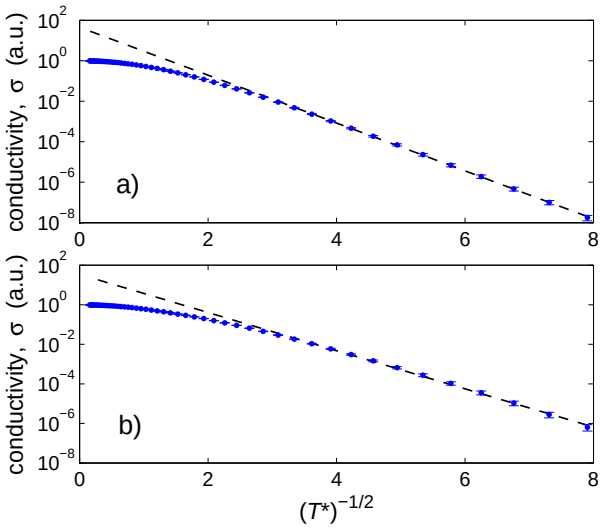

Figure 3.3: (Color online) The temperature dependence of the conductivity in (a) 2d and (b) 3d. In both cases, the conductivity follows the ES law [Eq. (3.1)] at small temperatures, $T^* \ll 1$, as shown by the dashed lines.

3.4 Conclusion

The triptych structure of the DOS should have observable consequences for a number of experiments on metal NC arrays. It is possible, for example, that the DOS can be probed directly by tunneling experiments, similar to the ones that have directly observed the Coulomb gap in doped semiconductors [53]. For systems with a finite dispersion δC

in the NC self-capacitance, the repeated Coulomb gaps will be smeared over some finite energy interval rather than collapsing to zero exactly at $\varepsilon^* = \pm 2$. One can simulate this behavior numerically by adding a stochastic spatial variation to C_0. Our simulations suggest that for root mean square deviation $\delta C \ll C_0$, $g(\varepsilon^* = \pm 2)/g(\varepsilon^* = \pm 1) \approx 3(\delta C/C_0)^2$. This implies that for a system with 5% dispersion in the NC diameter, the collapse of the DOS at $\varepsilon^* = \pm 2$ is complete to within 1%, and the resulting $g^*(\varepsilon^*)$ curve would not be distinguishable from that of Fig. 3.2 if added to the plot.

Chapter 4

Superconducting grains

4.1 Introduction

Granular superconductors are arrays of superconducting granules that are connected by electron tunneling. As such, these systems combine the unique electronic spectrum of superconducting quantum dots with the strong Coulomb correlations that are ubiquitous in disordered systems [5]. Among the more celebrated properties of granular superconductors are a giant magnetoresistance peak [6, 7, 8] and a superconductor-insulator transition that can be tuned by disorder or magnetic field [9, 10]. So far, a comprehensive theory of the electron conductivity that can explain these features remains elusive.

In the present chapter, we focus on the strongly disordered limit, where the array of superconducting grains as a whole is insulating while individual grains may still retain prominent features of superconductivity [6, 10, 11]. In this case, electronic states are localized and electron conduction proceeds by phonon-assisted tunneling, or "hopping," of electrons between grains through the insulating gaps which separate them. In principle, electronic conduction can occur either through tunneling of single electrons or through simultaneous tunneling of an electron pair. Here we note only that coherent tunneling of Cooper pairs (the Josephson effect) is neglected throughout this chapter, since it is not relevant in the strongly disordered limit that we are considering.

Since hopping conductivity is a thermally activated process, its magnitude at a given temperature T depends on two important energy scales associated with the spectrum of

electron energy states within each grain. The first is the charging energy $E_c = e^2/2C_0$, where e is the electron charge and C_0 is the self-capacitance of a single grain. The importance of the charging energy can be seen by considering that, in a neutral system, conduction requires an electron to hop from one neutral grain to another, thereby producing two charged grains, each with Coulomb self-energy E_c. The second important energy scale is the superconducting gap Δ, which represents an activation energy for separating a Cooper pair. In the limit where $\Delta/E_c \to 0$, the array is equivalent to a granular metal [28, 29, 5, 30]. In the opposite limit, where $\Delta/E_c \to \infty$, each grain has the properties of a bulk superconductor. In the present chapter our focus is on exploring the novel physics that results when E_c and Δ are similar in magnitude.

Since the superconducting gap Δ is typically on the order of 1 meV or smaller [10, 54], $E_c \sim \Delta$ implies that the self-capacitance $C_0 \gtrsim 80$ aF. This relatively large self-capacitance can be achieved either by fabricating large grains or by surrounding the grains by an environment with a high effective dielectric constant κ, so that the product of κ and the grain diameter D satisfies $\kappa D \gtrsim 400$ nm. For 3d arrays, large C_0 can also be achieved by making an array of very densely-packed grains, for example, cubic grains separated by a thin insulating layer [29]. In this chapter we assume that the Josephson coupling energy J between grains satisfies $J \ll E_c$, so that the array is indeed insulating [5] regardless of the value of Δ, and coherent tunneling of Cooper pairs is absent. Since we are considering the case of relatively large grains, we also assume that the spacing δ between discrete electron energy eigenstates within the grain satisfies $\delta \ll E_c$.

In relatively dense arrays, electron conduction can occur both through hopping of electrons between nearest-neighboring grains and through VRH between distant grains [34, 5, 29]. In systems with localized electron states, the latter transport mechanism dominates at low temperature. As previously shown, for systems with unscreened Coulomb interactions, due to a very general stability criterion of the global ground state the DOGS must vanish [3] at the Fermi level μ. This vanishing DOGS is called the Coulomb gap, and in the canonical Coulomb glass model of disordered systems it leads to a conductivity σ that obeys the Efros-Shklovskii (ES) law:

$$\sigma \propto \exp[-(T_{\rm ES}/T)^{1/2}], \tag{4.1}$$

where

$$T_{\rm ES} = \frac{Ce^2}{\kappa\xi} \tag{4.2}$$

is a characteristic temperature, C is a numerical coefficient, and ξ is the electron localization length of the array. Eq. (4.1) has been observed in a number of granular metals and superconductors at low temperature (see Ref. [5] and references therein).

In the previous chapter, we used a computer simulation to explore VRH in 2d and 3d arrays of monodisperse normal metallic grains. In such systems disorder is provided by donors and acceptors randomly situated in the interstitial spaces between grains—for example, in the metal oxide of the grains. We showed that as a consequence of the periodic charging spectrum of individual grains there is not one but three identical adjacent Coulomb gaps in the DOGS (one full gap at the Fermi level and two "half-gaps" on either side), which together form a structure that we termed a "Coulomb gap triptych." Unlike in conventional Coulomb glass models, in metallic granular arrays the DOGS has a fixed width in the limit of large disorder.

This previous study can be considered as a model for a granular superconductor in the limit where $\Delta/E_c \to 0$. In the present chapter, we generalize the theory of Ref. [30] to the case of finite $\Delta^* \equiv \Delta/E_c$. Specifically, we assume that within each grain electrons can form Cooper pairs, thereby lowering the system energy by -2Δ per pair. We use this model to study the DOGS and conductivity as a function of the gap Δ and the temperature T.

For energies close to the Fermi level our results for DOGS and conductivity are similar to those of an earlier seminal work [55], which aimed to capture the effect of pairwise attraction of electrons on the Coulomb gap and VRH conductivity. The authors of Ref. [55] started from the canonical Efros model of the Coulomb glass [52] with strong disorder and added the possibility of occupation of a site by two electrons with a finite (positive or negative) interaction energy U. They used this model to study how varying the on-site energy U affects DOGS, and the hopping conductivity σ in the presence of large external disorder. In this chapter we examine a model that is more realistic for granular superconductors, and we confirm a number of interesting observations made in Ref. [55].

Ch. 4 is organized as follows. In Sec. 4.2 we define the system being studied and outline our simulation technique. In Sec. 4.3 we describe our main results for the DOGS

and conductivity, focusing primarily on 2d arrays, and we present their implications for magnetoresistance. In Sec. 4.4 we show that our results generalize to the 3d case as well. Sec. 4.5 is devoted to translating our results for the DOGS into a prediction for tunneling experiments. We close in Sec. 4.7 with concluding remarks.

4.2 Model

In this chapter we consider an array of identical, spherical grains with diameter D arranged in a regular, d-dimensional square lattice with lattice constant $D' > D$. For simplicity of discussion, during the majority of this chapter we focus on case $d = 2$; results for $d = 3$ are presented in Sec. 4.4. Disorder in this system is assumed to be provided by impurity charges $\pm e$ that are embedded in the insulating interstitial spaces between grains. Such impurity charges can be thought to effectively create a random fractional donor charge Q_i that resides on each grain i, for reasons that are explained more fully in Ref. [30]. The net charge of the grain can then be written as $q_i = Q_i - en_i$, where n_i is the integer number of electrons that reside on the grain relative to its neutral state. We emphasize that n_i can be a positive or negative integer, and can be defined as $n_i = N_i - I_i$, where I_i is the number of positive ions and N_i the number of electrons at grain i. Within each grain, the N_i electrons can form bound pairs through the local attraction energy Δ. In general, Δ can be tuned by an applied magnetic field B, as discussed below.

Given this model, the Hamiltonian for the system can be written

$$\begin{aligned} H &= \sum_i \frac{(Q_i - en_i)^2}{2C_0} + \sum_{\langle i,j \rangle} C_{ij}^{-1}(Q_i - en_i)(Q_j - en_j) \\ &\quad -2\Delta \sum_i \left\lfloor \frac{N_i}{2} \right\rfloor . \end{aligned} \tag{4.3}$$

Here, the first term describes the Coulomb self-energy of each grain and the second term describes the Coulomb interaction between charged grains. The coefficient C_{ij}^{-1} is the inverse of the matrix of electrostatic induction C_{ij}. In the numerical simulations that we describe below, we make the approximations $C_0 = \kappa D/2$ and $C_{ij}^{-1} = 1/\kappa r_{ij}$. The third term in the Hamiltonian describes the total pairing energy of electrons; N_i is the number of electrons and $\lfloor N_i/2 \rfloor$ is the number of electron pairs within grain i. In Ref. [55], the

authors proposed a similar Hamiltonian as a model for disordered superconducting films such as InO_x. Unlike in Eq. (2.4), the model considered in Ref. [55] assumes that the electron occupation numbers are restricted to $N_i = 0, 1, 2$ and that disorder is provided by random, uncorrelated site energies rather than by the random charges Q_i. While we consider our model more realistic for granular superconductors, we will show that it reproduces many of the features reported in Ref. [55].

Because of the presence of the impurity charges, electrons become redistributed among grains from their neutral state in order to screen the disorder Coulomb potential. The corresponding ground state arrangement of electrons among grains plays an essential role in the conductivity, since it determines the lowest empty and highest filled electron energy levels at each grain. In our numerical simulation described below, we search for the set $\{n_i\}$ that minimizes the Hamiltonian and use it to calculate the DOGS and the conductivity.

In conventional Coulomb glass models, the characteristic strength of the disorder is a free parameter that determines the width of the DOGS [52, 32]. One can expect that in our problem a similar role is played by the typical magnitude of the disorder charge Q_i, which reflects the average number of impurity charges surrounding each grain. In fact, however, in the limit where there are many such charges one can effectively adopt a simple model in which the value of Q_i is chosen randomly from the uniform distribution $Q_i \in [-e, +e]$. To see why this model is valid, consider that each grain minimizes its Coulomb self-energy by minimizing the magnitude of its net charge, $|q_i| = |Q_i - en_i|$. In the absence of any Cooper pairing, n_i may freely take any integer value in order to arrive at a state for which $-e/2 \leq q_i \leq e/2$. If one assumes, on the other hand, that Cooper pairing is so strong that all electrons are paired in the ground state ($\Delta^* \gg 1$) , then $N_i = n_i + I_i$ may still freely take any even-integered value, so that in the ground state $-e \leq q_i \leq e$. In other words, regardless of the value of Δ, each grain can effectively adjust to the presence of an arbitrarily strong charge disorder by changing its electron number n_i so that its net charge acquires a magnitude smaller than e. For this reason, in the limit of large disorder the DOGS has a fixed width, as first explained in Ref. [30]. For the results presented below, we take Q_i to be randomly chosen from the uniform distribution $Q_i \in [-e, e]$. The ion number I_i is assumed to be very large, so that electrons are never completely depleted from any given grain. I_i is also taken to

be even or odd with equal probability; the relevance of this choice is explained below.

In our analysis below it is convenient to introduce the following dimensionless units, which reduce the number of free variables in the problem. We introduce the dimensionless distance between the centers of grains i and j,

$$r_{ij}^* = \frac{r_{ij}}{D}, \tag{4.4}$$

the dimensionless charge

$$q_i^* = \frac{Q_i - en_i}{e}, \tag{4.5}$$

the dimensionless electron energy

$$\varepsilon = E/E_c, \tag{4.6}$$

the dimensionless DOGS for single electrons and electron pairs

$$g_{1,2}^*(\varepsilon) = E_c D^d g_{1,2}(\varepsilon), \tag{4.7}$$

the dimensionless temperature

$$T^* = \frac{2Dk_BT}{E_c\xi}, \tag{4.8}$$

and the dimensionless resistivity

$$\ln \rho^* = \frac{\xi}{2D} \ln(\rho/\rho_0), \tag{4.9}$$

where ρ_0 is a prefactor for the resistivity with a weak, power-law dependence on temperature. We also assume that the gap between neighboring grains $D' - D \ll D$, so that $D' \simeq D$. The problem then loses any explicit dependence on the diameter or the localization length. With these definitions, one can write the Hamiltonian of Eq. (4.4) in dimensionless units as

$$H^* = \sum_i q_i^{*2} + \sum_{\langle i,j \rangle} \frac{q_i^* q_j^*}{r_{ij}^*} - 2\Delta^* \sum_i \left\lfloor \frac{N_i}{2} \right\rfloor. \tag{4.10}$$

If one is given the ground state electron occupation numbers $\{n_i\}$, then one can determine the highest occupied electron energy state, ε_i^{1-}, and the lowest empty state, ε_i^{1+}, at a given grain i. These energies determine the contribution of the grain i to the single-electron conductivity, and are given by:

$$\varepsilon_i^{1-} = -2q_i^* - 1 - \sum_{j \neq i} \frac{q_j^*}{r_{ij}^*} - \begin{cases} 0 & , N_i \text{ odd} \\ 2\Delta^* & , N_i \text{ even} \end{cases}, \tag{4.11}$$

$$\varepsilon_i^{1+} = -2q_i^* + 1 - \sum_{j\neq i} \frac{q_j^*}{r_{ij}^*} - \begin{cases} 2\Delta^* & , N_i \text{ odd} \\ 0 & , N_i \text{ even} \end{cases} . \tag{4.12}$$

From Eqs. (4.11) and (4.12) one can see that the spectrum of single-electron energy levels at a given grain i depends on the "parity" of the grain: whether the number of electrons in the neutral state, I_i, is odd or even. To understand why this is the case, consider first the spectrum of a single grain with $\Delta = 0$. In such a grain, $\varepsilon_i^{1+} - \varepsilon_i^{1-} = 2$ regardless of the number of electrons in the grain. This implies a ladder of electron energy levels, spaced by $2E_c$, corresponding to different charge states of the grain. These energy levels are shown schematically in the left side of Fig. 4.1. When Δ^* is finite, on the other hand, those energy states corresponding to an even total number of electrons in the grain become shifted by $-2\Delta^*$ as a consequence of the attractive interaction between electron pairs. As a result, $\varepsilon_i^{1+} - \varepsilon_i^{1-} = 2 - 2\Delta^*$ for grains with odd N_i and $\varepsilon_i^{1+} - \varepsilon_i^{1-} = 2 + 2\Delta^*$ for grains with even N_i. This suggests that the energy to add or remove one electron from the grain's neutral state depends on the parity of the grain, as shown in the center of Fig. 4.1. (The importance of the grain parity for its electronic spectrum has been well established by previous theoretical [56, 57] and experimental [58, 59] studies.) At $\Delta^* = 1$, pairs of electron energy states become two-fold degenerate, as shown on the right side of Fig. 4.1. As a consequence, at $\Delta^* \geq 1$ in the ground state all grains have an even total number of electrons, regardless of the disorder strength. This uniform pairing has an important consequence for the DOGS, as discussed below.

The diagram of Fig. 4.1 shows that the spacing between energy levels at $\Delta^* = 1$ is doubled relative to that of $\Delta^* = 0$. One can observe that this same increased spacing could be achieved if the electron charge e were replaced with an effective charge $\sqrt{2}e$, so that the charging energy $E_c \propto e^2$ is doubled. In fact, this effective charge $\sqrt{2}e$ plays a prominent role for the DOGS and conductivity at $\Delta^* = 1$, as will be shown in Sec. 4.3.

In the presence of some disorder, the ladder of energy states depicted in Fig. 4.1 becomes shifted randomly up or down from one grain to the next by the disorder potential. The values of ε_i^{1-} and ε_i^{1+} for each grain—those energy states just above and just below the constant global Fermi level—contribute to the DOGS $g_1^*(\varepsilon)$.

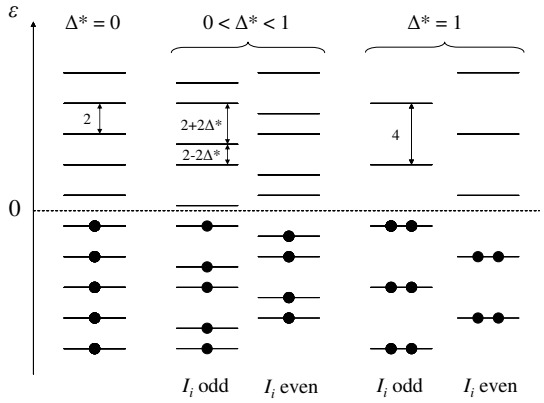

Figure 4.1: Single-electron energy levels of an isolated neutral grain. At $\Delta^* = 0$ (left), the Coulomb self-energy produces a spectrum where different charge states ε are separated in energy by 2. At $0 < \Delta^* < 1$ (center), those energy levels corresponding to the addition of an electron to a grain with an odd total number of electrons are shifted by $-2\Delta^*$. At $\Delta^* = 1$ (right), the difference in self-energy $2E_c$ between two successive charge states is compensated by the pairing energy -2Δ, so that pairs of subsequent electron levels merge. The Fermi level at $\varepsilon = 0$ is indicated schematically by a dashed line.

Thus far we have focused our discussion on hopping by single electrons, which is characterized by a localization length $\xi = \xi_1$. In principle, conduction may occur through simultaneous hopping of an electron pair as well, with a distinct localization length $\xi = \xi_2$. For example, one can expect pair tunneling to become dominant in the limit $\Delta^* \to \infty$, where thermally activated breaking of bound Cooper pairs is completely suppressed. In order to discuss conduction by electron pairs, one can similarly define the energy associated with pair excitations, in analogy with Eqs. (4.12) and (4.11). Specifically:

$$\varepsilon_i^{2-} = -4q_i^* - 4 - 2\sum_{j\neq i} \frac{q_j^*}{r_{ij}^*} - 2\Delta^*, \tag{4.13}$$

$$\varepsilon_i^{2+} = -4q_i^* + 4 - 2\sum_{j\neq i} \frac{q_j^*}{r_{ij}^*} - 2\Delta^*. \tag{4.14}$$

Note that, unlike for single electron excitations, for pairs we have $\varepsilon_i^{2+} - \varepsilon_i^{2-} = 8$ regardless of the parity of the grain. This suggests that the ladder of energy states corresponding to pair excitations has a uniform spacing $8E_c$, and thus all pair excitation energies

are independent of Δ. This is as expected, since the total number of bound pairs in the system is unchanged by the simultaneous tunneling of a pair. As with the single electron energy levels, the disorder potential produces a random shifting of the two-electron energy levels from one grain to another. The energies ε_i^{2-} and ε_i^{2+} in the ground state are histogrammed to produce the pair DOGS, $g_2^*(\varepsilon)$.

In order to evaluate numerically the DOGS, we use a computer simulation to search for the ground state arrangement of electrons, $\{n_i\}$, in a finite array of grains. This is done by looping over all pairs ij and attempting to move either one or two electrons from i to j. If the proposed move lowers the total system energy H^*, then it is accepted, otherwise it is rejected. This process is continued until no single-electron or pair transfers are possible that lower H^*. Equivalently, one can say that for all i, j we check that two sets of ES ground state criteria are satisfied:

$$\varepsilon_j^{1+} - \varepsilon_i^{1-} - 1/r_{ij}^* > 0. \tag{4.15}$$

and

$$\varepsilon_j^{2+} - \varepsilon_i^{2-} - 4/r_{ij}^* > 0. \tag{4.16}$$

The final arrangement of electrons can be called a "pseudo-ground state," which is not strictly equal to the true ground state of the system but which generally provides an identical DOGS up to very small energies [32, 45, 46].

Once the energies $\{\varepsilon_i^{1\pm,2\pm}\}$ are known, we evaluate the resistivity using the approach of the Miller-Abrahams resistor network [47]. This approach is described in detail in Refs. [30, 51], but here we give a brief conceptual overview. In the Miller-Abrahams description, each pair of grains ij is said to be connected by some equivalent resistance R_{ij}. The value of R_{ij} increases exponentially with the distance r_{ij} between the grains and with the activation energy E_{ij} required for hopping between them according to $R_{ij} \propto \exp[2r_{ij}/\xi + E_{ij}/k_BT]$. Note that, using the dimensionless units of Eqs. (4.4) – (4.9), one can define the dimensionless logarithm of the resistance $\ln R_{ij}^* = r_{ij}^* + \varepsilon_{ij}/T^*$, which has no explicit dependence on ξ. The resistivity of the system as a whole is found using a percolation approach. Specifically, we find the minimum value R_c such that if all resistances R_{ij} with $R_{ij} < R_c$ are left intact while others are eliminated (replaced with $R = \infty$), then there exists a percolation pathway connecting opposite faces of the simulation volume. The system resistivity is equated with $R_c D^{d-2}$.

In principle, single-electron hopping and pair hopping provide parallel mechanisms for charge transport between a given pair of grains ij, and so they can be represented as parallel resistors connecting the two grains. In most situations, however, one of the two mechanisms dominates the conductivity while the other can be neglected, as we show below. We therefore focus primarily on the case where single and pair excitations can be treated as independent, non-connected resistor networks with resistivities ρ_1 and ρ_2, respectively. Some limited results for mixed conduction are provided at the end of the following section.

All numerical results for 2d systems presented in the following section correspond to simulations of 100×100 lattice sites with open boundary conditions, averaged over 1000 independent, random realizations of the disorder. Energies are defined relative to the Fermi level μ, so that in the ground state $\varepsilon_i^{1-} < 0$, $\varepsilon_i^{2-} < 0$ and $\varepsilon_i^{1+} > 0$, $\varepsilon_i^{2+} > 0$ for all i.

4.3 Results and discussion

The DOGS is shown in Fig. 4.2 for single electron excitations, $g_1^*(\varepsilon)$, and for pair excitations, $g_2^*(\varepsilon)$, at different values of the gap Δ^*. For each curve, the DOGS vanishes at the Fermi level ($\varepsilon = 0$), as required by the stability criteria of Eqs. (4.15) and (4.16). One can also note that the DOGS generally becomes wider with increasing Δ^* as a consequence of the widening gaps between odd and even electron energy levels (see Fig. 4.1). The evolution of the DOGS with Δ^* can be understood more completely as follows.

At $\Delta^* = 0$, the array is equivalent to a granular normal metal. As a consequence, the curve $g_1^*(\varepsilon)$ at $\Delta^* = 0$ is identical to the one reported in Ref. [30]. The most salient feature of this curve is its "triptych" symmetry, with two identical peaks that are symmetric about their centers. As explained in Ref. [30], this symmetry is a result of the ES stability criterion of Eq. (4.15) in conjunction with the uniform spacing between electron energy levels (at $\Delta^* = 0$, $\varepsilon_i^{1+} - \varepsilon_i^{1-} = 2$ for all i, as shown in Fig. 4.1). Thus, the "soft" Coulomb gap at $\varepsilon = 0$ gets repeated identically at $\varepsilon = \pm 2$. On the other hand, the pair DOGS, $g_2^*(\varepsilon)$, at $\Delta^* = 0$ has a hard gap at the Fermi level with width 4. This hard gap can be understood by considering that at $\Delta^* = 0$, Eqs. (4.11) – (4.14)

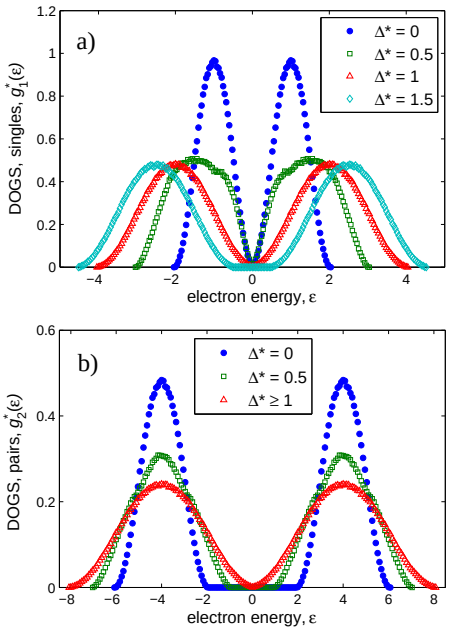

Figure 4.2: (Color online) Single electron and pair DOGS, $g_1^*(\varepsilon)$ and $g_2^*(\varepsilon)$, of a regular 2d array of monodisperse metallic grains as a function of the dimensionless electron energy $\varepsilon = E/E_c$ at different values of the superconducting gap $\Delta^* = \Delta/E_c$. At $\Delta^* < 1$, the single electron DOGS g_1^* has a soft Coulomb gap at $\varepsilon = 0$, while the pair DOGS g_2^* has a hard gap, and the situation is reversed for $\Delta^* > 1$. $\Delta^* = 1$ is a critical point at which both $g_{1,2}^*$ have a soft Coulomb gap. The three DOGS curves corresponding to $g_1^*(\varepsilon)$ at $\Delta^* = 0, 1$ and $g_2^*(\varepsilon)$ at $\Delta^* \geq 1$ constitute "Coulomb gap triptychs" and can be scaled onto each other by rescaling the electron charge, as discussed in Sec. 4.3. One can equivalently say that these three curves exhibit effective charges e, $\sqrt{2}e$, and $2e$, respectively.

imply that $\varepsilon_i^{2\pm} = 2\varepsilon_i^{1\pm} \pm 2$. Since $\varepsilon_i^{1-} < 0$ and $\varepsilon_i^{1+} > 0$ for all i, we have $|\varepsilon_i^{2\pm}| > 2$, and therefore there must be a hard gap of width 4. Physically, one can say that the gap arises in $g_2^*(\varepsilon)$ because the charging energy $4E_c$ associated with adding two electrons to a given grain is larger in magnitude than the random Coulomb potential, which is screened effectively by the rearrangement of single electrons. As a consequence of the relation between $\varepsilon_i^{2\pm}$ and $\varepsilon_i^{1\pm}$, at $\Delta^* = 0$ the two DOGS can be mapped onto each other via the relation $g_1(\varepsilon) = 2g_2[2\varepsilon + 2\,\mathrm{sgn}(\varepsilon)]$. A slightly different version of this relation was reported in Ref. [55].

When the pairing interaction is finite but small, $0 < \Delta^* < 1$, $g_1^*(\varepsilon)$ is unchanged very close to the Fermi level, but away from the Fermi level it becomes somewhat broadened due to the widening energy gaps between even and odd parity electron states (see Fig. 4.1). The pair DOGS, meanwhile, retains a hard gap near the Fermi level, but the width of this gap shrinks to $4(1 - \Delta^*)$.

In the opposite case, where the pairing interaction is strong enough that $\Delta^* > 1$, the situation is reversed. That is, the single-electron DOGS $g_1^*(\varepsilon)$ acquires a hard gap at the Fermi level while $g_2^*(\varepsilon)$ has only a soft Coulomb gap. This result can be understood by first noting that at $\Delta^* \geq 1$, all electrons are paired in the ground state. This is true because at $\Delta^* > 1$ any grain with an odd number of electrons can lower its energy by acquiring an electron from a distant grain with electron energy close to the Fermi level (or from the voltage source). Making use of Eqs. (4.11) – (4.14) for even-parity grains produces the relation $\varepsilon_i^{1\pm} = \frac{1}{2}\varepsilon_i^{2\pm} \pm (\Delta^* - 1)$. Since $\varepsilon_i^{2+} > 0$ and $\varepsilon_i^{2-} < 0$, it follows that all $|\varepsilon_i^{1\pm}| > \Delta^* - 1$ for all i, and thus there is a hard gap in $g_1^*(\varepsilon)$ of width $2(\Delta^* - 1)$. Physically, this hard gap arises because the pairing interaction is stronger than the disorder Coulomb potential, which is screened effectively by Cooper pairs. Thus, any excitation of single-electron hops requires a finite activation energy of at least $\Delta^* - 1$. The relations between $\varepsilon_i^{2\pm}$ and $\varepsilon_i^{1\pm}$ at $\Delta^* > 1$ imply a mapping between $g_1^*(\varepsilon)$ and $g_2^*(\varepsilon)$ that was also noticed by Ref. [55], namely $g_2^*(\varepsilon) = \frac{1}{2}g_1^*[\frac{1}{2}\varepsilon + \mathrm{sgn}(\varepsilon)(\Delta^* - 1)]$. At such large values of Δ^*, the fixed relation $\varepsilon_i^{2+} - \varepsilon_i^{2-} = 8$ implies that $g_2^*(\varepsilon)$ becomes saturated and has a fixed width for all $\Delta^* \geq 1$.

At the point where $\Delta^* = 1$ precisely, some remarkable features emerge in the DOGS. This might be expected by noticing the special role played by $\Delta^* = 1$ in the single-electron energy spectrum; this is the point where pairs of energy levels become degenerate (see Fig. 4.1, right). At $\Delta^* = 1$ neither $g_1^*(\varepsilon)$ nor $g_2^*(\varepsilon)$ has a hard gap, and in fact the two DOGS can be mapped onto each other via the simple relation $g_2^*(\varepsilon) = \frac{1}{2}g_1^*(\frac{1}{2}\varepsilon)$. In addition, there is a simple scaling relation between $g_1^*(\varepsilon)$ at $\Delta^* = 1$ and $g_1^*(\varepsilon)$ at $\Delta^* = 0$. Namely,

$$g_1^*(\varepsilon)\Big|_{\Delta^*=1} = \frac{1}{2}g_1^*(\varepsilon/2)\Big|_{\Delta^*=0} = 2g_2^*(2\varepsilon)\Big|_{\Delta^*\geq 1}. \tag{4.17}$$

The second equality in Eq. (4.17) can be understood in a straightforward way. Indeed, the second equality suggests that one can arrive at the pair DOGS at large Δ^*

by taking the single-electron DOGS at $\Delta^* = 0$ and rescaling the value of the electron charge by a factor of 2. Replacing e by an effective charge $e^* = 2e$ in the unit of energy E_c produces a factor 4 expansion of the x-axis and a factor 4 contraction of the y-axis, which is equivalent to the second equality in Eq. (4.17). This scaling can be expected, since for large pairing interaction $\Delta^* > 1$, all electrons are paired, and one can naturally think that only charge $2e$ objects exist in the problem. Thus, at such large Δ^* the problem of the arrangement of electron pairs in the disorder potential is equivalent to the problem of the arrangement of single electrons in a disorder potential, with rescaled units.

The first equality in Eq. (4.17), on the other hand, is unexpected, since it implies that $g_1^*(\varepsilon)\,\big|_{\Delta^*=1}$ can be determined from $g_1^*(\varepsilon)\,\big|_{\Delta^*=0}$ by replacing the electron charge with an effective charge $e^* = \sqrt{2}e$. This remarkable feature of the DOGS at $\Delta^* = 1$ was first pointed out by Ref. [55]. Those authors showed that the result $e^* = \sqrt{2}e$ is the natural consequence of single electrons hopping in a Coulomb landscape that is shaped predominantly by Cooper pairs. More formally, one can say that the pair stability criterion of Eq. (4.16) produces a stronger constraint on $g_1^*(\varepsilon)$ than the single-electron criterion of Eq. (4.15). This can be seen by substituting $\varepsilon_i^{2\pm} = 2\varepsilon_i^{1\pm}$, which is correct at $\Delta^* = 1$ (see Fig. 4.1), into Eq. (4.16). As a result, one finds that $\varepsilon_i^{1+} - \varepsilon_j^{1-} - 2/r_{ij}^* > 0$, or in dimensionfull units, $E_i^{1+} - E_j^{1-} - (\sqrt{2}e)^2/\kappa r_{ij} > 0$. Repeating the traditional derivation of the Coulomb gap [3] starting with this inequality leads to an effective charge $e^* = \sqrt{2}e$ in the DOGS.

In addition to its importance for the DOGS, the effective charge e^* plays a prominent role in the electron conductivity. Specifically, it enters the characteristic temperature $T_{\rm ES}$ in the ES law [Eq. (4.1)]. Since $T_{\rm ES} \propto e^2$ [see Eq. (4.2)], the arguments above suggest that if one defines the ES temperature $T_{\rm ES}^s(\Delta^*)$ for single-electron conductivity and $T_{\rm ES}^p(\Delta^*)$ for pair conductivity at a given value of Δ^*, then these should satisfy

$$T_{\rm ES}^p(\Delta^* \geq 1) = 2T_{\rm ES}^s(\Delta^* = 1) = 4T_{\rm ES}^s(\Delta^* = 0). \tag{4.18}$$

It should be noted that, for energies close to the Fermi level our results for $g_1(E)$ and $g_2(E)$ are similar to those of an earlier seminal work [55], which aimed to capture the effect of pairwise attraction of electrons on the Coulomb gap and VRH conductivity. The authors of Ref. [55] started from the canonical Efros model of the Coulomb glass [52]

with strong disorder and added the possibility of occupation of a site by two electrons with a finite (positive or negative) interaction energy U. They used this model to study how varying the on-site energy U affects $g_1(E)$, $g_2(E)$, and the hopping conductivity σ in the presence of large external disorder. In the present chapter we examine a model that is more realistic for granular superconductors, and we confirm a number of interesting observations made in Ref.[55].

In order to verify the prediction Eq. (4.18), we measured the single-electron resistivity $\ln \rho_1^*$ and the electron pair resistivity $\ln \rho_2^*$ at various values of Δ^* and over a range of temperatures using the resistor network approach described in Sec. 4.2. The result is plotted in Fig. 4.3 as $\ln \rho^*$ versus $(T^*)^{-1/2}$. As expected, at low temperature, $T^* \ll 1$, the conductivity is well described by the ES law in all cases. By making linear best fits to the data at low temperature, we find that the corresponding temperatures $T_{\rm ES}$ indeed satisfy Eq. (4.18). This can be seen from the dashed lines in Fig. 4.3, which show three fit lines with relative slopes $1 : \sqrt{2} : 2$, as predicted by the corresponding effective charges e^*. If the data in Fig. 4.3 are fitted with independent best fit lines, we find that $T^p_{\rm ES}(\Delta^* \geq 1) \approx 2.2 T^s_{\rm ES}(\Delta^* = 1) \approx 4.3 T^s_{\rm ES}(\Delta^* = 0)$, which is within our numerical uncertainty of the prediction in Eq. (4.18).

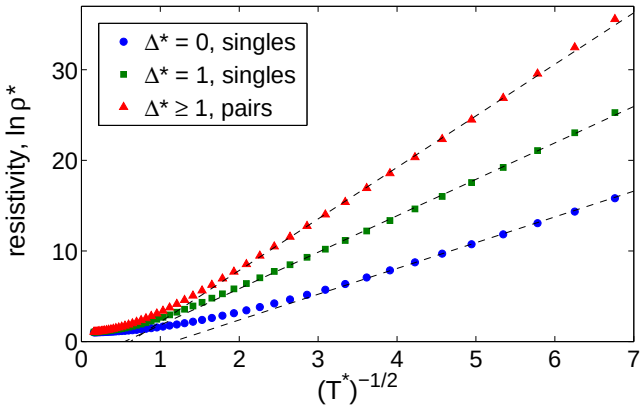

Figure 4.3: (Color online) The temperature dependence of the resistivity for single electron conduction at $\Delta^* = 0, 1$ and pair conduction at $\Delta^* \geq 1$. The dimensionless resistance $\ln \rho^*$ is plotted against $(T^*)^{-1/2}$ to illustrate that the resistivity follows the ES law [Eq. (4.1)] at low temperatures. The dashed lines are linear fits whose slopes have the ratio 1:$\sqrt{2}$:2.

The evolution of $T_{\rm ES}$ with Δ suggests an interesting mechanism for the magnetoresistance of the sample. Generally speaking, the pairing energy Δ in a superconducting material decreases monotonically [60] with the intensity of an applied magnetic field B. Thus, by applying a magnetic field one can tune the pairing energy and thereby alter the DOGS, the ES temperature $T_{\rm ES}$, and the resistivity. In the following discussion we assume that this tuning of Δ is the primary role of an applied magnetic field, and we ignore the effect of the magnetic field on hopping interference phenomena [61]. One could also imagine that the magnetic field is applied parallel to the array, so that all hopping trajectories encircle zero magnetic flux.

In order to investigate this mechanism for magnetoresistance, we consider first the case where all conduction is due to single electron hopping. This would be the case, for example, when $\xi_2/\xi_1 \ll 1$. In such a case the results of Figs. 4.2 and 4.3 imply a monotonic negative magnetoresistance. That is, as a magnetic field B is applied, the gap Δ decreases, leading to a larger DOGS near the Fermi level and thus to enhanced conductivity. More specifically, if the superconducting gap is large enough that at zero magnetic field $\Delta^* > 1$, then in the absence of a magnetic field the single-electron DOGS has a hard gap. This hard gap implies that at low temperatures $T^* \ll (\Delta^* - 1)$, the resistivity is very large and described by an Arrhenius-type activation law. When B is increased to the point that $\Delta^* = 1$, the resistivity becomes smaller and obeys the ES law with a characteristic temperature $T^s_{\rm ES}(1)$. As the magnetic field is increased even further, $T_{\rm ES}$ decreases and the resistivity declines. This decline continues until such large fields that $\Delta^* \ll 1$, when the resistivity plateaus and $T_{\rm ES} = T^s_{\rm ES}(0)$. According to the second equality in Eq. (4.18), at small temperatures one should expect that the large-B resistivity and the resistivity at $\Delta^* = 1$ are related by $[\ln \rho_1^*(\Delta^* = 1)]/[\ln \rho_1^*(\Delta^* = 0)] \simeq \sqrt{2}$.

This result is confirmed in Fig. 4.4, which shows the single-electron resistivity as a function of the superconducting gap Δ^* at various values of temperature. As expected, the resistivity indeed declines with decreasing gap (increasing B), and at very small temperatures (large $(T^*)^{-1/2}$) the relation $[\ln \rho_1^*(\Delta^* = 1)]/[\ln \rho_1^*(\Delta^* = 0)] = \sqrt{2}$ is nearly satisfied. This result provides an additional confirmation of the picture of an effective electron charge $\sqrt{2}e$ at $\Delta^* = 1$.

We would like to emphasize that this mechanism for negative magnetoresistance

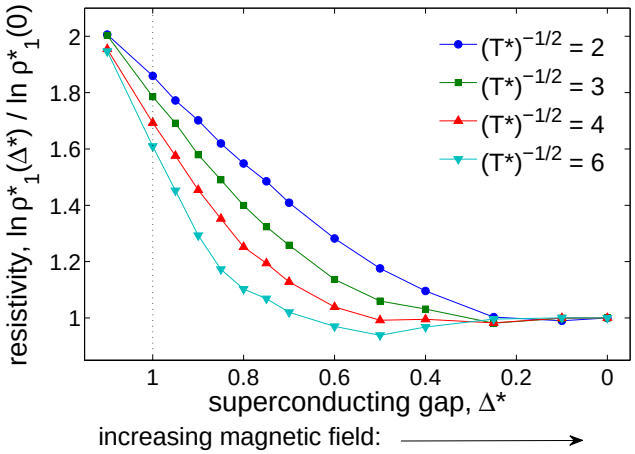

Figure 4.4: (Color online) Resistivity for single-electron hopping, $\ln \rho_1^*$, as a function of the superconducting gap Δ^* at different values of the temperature T^*. The resistivity is normalized by its value at $\Delta^* = 0$, and one can see that for small temperatures the ratio $[\ln \rho_1^*(\Delta^* = 1)]/[\ln \rho_1^*(\Delta^* = 0)]$ seems to approach $\sqrt{2}$. The declining resistivity with decreasing gap implies a negative magnetoresistance. The dotted vertical line indicates $\Delta^* = 1$, which can be thought of as the point where the resistivity crosses over from an activated dependence to the ES law with increasing magnetic field (at small temperature).

is quite unusual, and cannot be understood simply as a reduction of some activation energy due to weaker Cooper pairing. Rather, the negative magnetoresistance arises because decreased Δ^* leads to a DOGS $g_1^*(\varepsilon)$ that is less depleted by intimidation by Cooper pairs, and thus to enhanced electron conduction at low temperature.

The results of Fig. 4.4 focus on the case where conduction is provided by single electrons only, which is appropriate when $\xi_2/\xi_1 \ll 1$. On the other hand, when the localization lengths ξ_1 and ξ_2 are similar in magnitude, the conduction should be dominated by single-electron hopping at $\Delta^* \ll 1$ and by pair hopping at $\Delta^* \gg 1$. This is the case because at all $\Delta^* \neq 1$ one of the two DOGS has a hard gap. By increasing the magnetic field, then, one can apparently produce a transition between pair-dominated conduction and single-electron-dominated conduction, provided that $\Delta^* > 1$ in the absence of applied field. Such a transition may help to explain the giant magnetoresistance peak seen in experiments [6, 7, 8], as was proposed by Ref. [55].

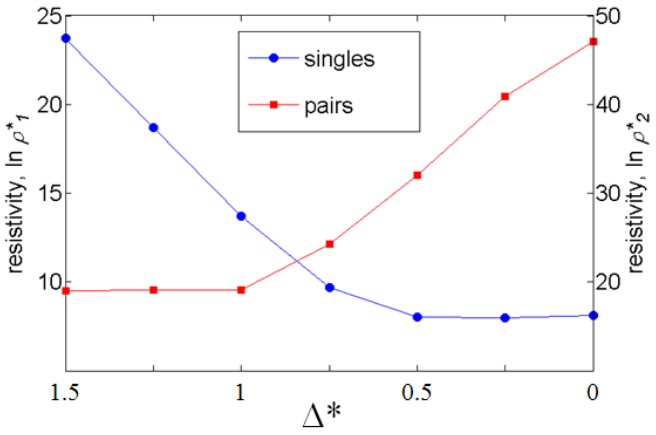

Figure 4.5: (Color online) Resistivity for both single-electron hopping (blue curve), $\ln \rho_1^*$, and electron pair hopping (red curve), $\ln \rho_2^*$, as a function of the superconducting gap Δ^* at a certain low temperature. At $\Delta^* > 1$, the ground state of the system is governed by electron pairs, so that pair DOGS has a soft gap at the Fermi level, while single-electron DOGS is gapped. As a result, resistivity for single-electron hopping is much larger than that of pair hopping. At $\Delta^* < 1$, the mechanisms for ground state and resistivity are just the opposite: pair DOGS is gapped and resistivity for pair hopping is exponentially large. The declining resistivity of single-electron hopping with decreasing gap implies a negative magnetoresistance, while the increasing resistivity of electron pair hopping with decreasing gap implies a positive magnetoresistance.

A comparison of field-dependence of hopping resistivity between single-electron and electron pairs is shown in Fig. 4.5. At $\Delta^* > 1$, the system is dominated by electron pairs. Therefore, pair DOGS has a soft (Coulomb) gap at the Fermi level, while single-electron DOGS has a hard gap. As a result, the resistivity associated with single-electron hopping is much larger than that with pair hopping. At $\Delta^* < 1$, however, the situation is reversed: pair DOGS is gapped, which leads to exponentially large resistivity. The declining resistivity of single-electron hopping with decreasing gap implies a negative magnetoresistance, while the increasing resistivity of electron pair hopping with decreasing gap implies a positive magnetoresistance.

To investigate this possibility, we performed simulations to measure the resistivity at different values of the localization lengths ξ_1, ξ_2 and the temperature T, using a resistor network that allows for mixed conductivity of singles and pairs. We find that if ξ_1, ξ_2, and T are chosen such that the resistivities are nearly equal at $\Delta^* \gg 1$ and

$\Delta^* = 0$, then one can indeed observe a moderate peak in the resistivity in the vicinity of $\Delta^* = 1$. One such result is shown in Fig. 4.6, and is qualitatively similar to a result obtained in Ref. [55] for an array in which the quantity $E_c - \Delta$ varies strongly between grains.

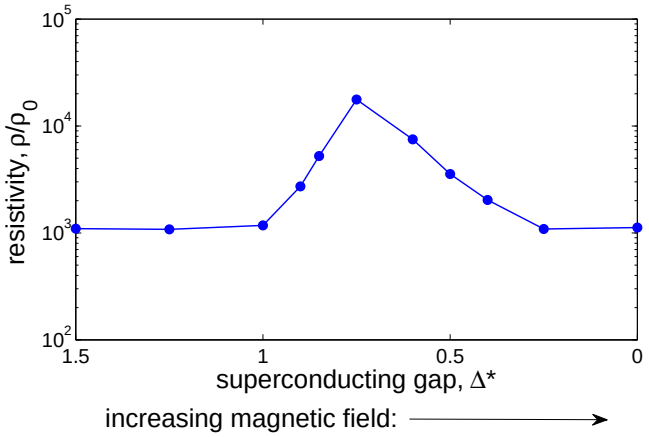

Figure 4.6: (Color online) The resistivity, ρ/ρ_0, as a function of the superconducting gap Δ^* for a 2d array with localization lengths $\xi_1 = D$ and $\xi_2 = 10D$ and temperature $T = 0.1E_c/k_B$ [so that $(T_1^*)^{-1/2} = 2.1$ and $(T_2^*)^{-1/2} = 6.7$]. The maximum in ρ/ρ_0 suggests a magnetoresistance peak associated with the transition from pair-dominated conduction (at large Δ^*, small magnetic field) to single electron-dominated conduction (at small Δ^*, large magnetic field).

While this result is promising, we caution that by itself it does not provide a satisfactory qualitative description of the magnetoresistance peak observed in experiment. For example, the peak in Fig. 4.6 arises out of the deeply insulating state, $\rho \sim 10^3\rho_0$. Since the constant ρ_0 is generally on the order of $h/e^2 \approx 26$ kΩ, this disagrees with experiment [6, 8, 7], where the magnetoresistance peak is seen to arise from a state with $\rho \sim h/e^2$. The appearance of a noticeable peak also apparently requires a large ratio ξ_2/ξ_1, which is likely to be possible only very close to the superconductor-insulator transition. Such large values of ξ_2 probably go beyond the limit of applicability of our model.

4.4 3d arrays

Thus far our presentation of results has focused on the case of 2d arrays. In this section we briefly report on simulations of the DOGS and resistivity in 3d arrays. Generally speaking, while some details of the shape of the DOGS and the magnitude of the resistivity are modified relative to the 2d case, the triptych structure of the DOGS and the values of the effective charges remain unchanged. All results in this section correspond to simulated 3d systems of $24 \times 24 \times 24$ lattice sites with open boundary conditions, averaged over 1000 realizations of the disorder.

When considering the DOGS, the most prominent difference between 2d and 3d systems is that in 3d the ES criterion [Eq. (4.15)] imposes a stronger constraint on $g_1^*(\varepsilon)$. Specifically, in d dimensions the ES criterion implies [32] that $g_1^*(\varepsilon) < k_d|\varepsilon|^{d-1}$, where k_d is a constant, so that in 3d the DOGS vanishes at least quadratically with energy near the Fermi level while in 2d it is constrained to vanish only linearly. Fig. 4.7 shows $g_1^*(\varepsilon)$ and $g_2^*(\varepsilon)$ for 3d arrays, and one can see that in cases where $g_1^*(\varepsilon)$ is ungapped it indeed vanishes as a higher power of ε near the Fermi level.

Nonetheless, the most important qualitative features of the DOGS from the 2d case remain in 3d as well. Specifically, the curves corresponding to $g_1^*(\varepsilon)$ at $\Delta^* = 0, 1$ and $g_2^*(\varepsilon)$ at $\Delta^* \geq 1$ have the "triptych" structure of two identical, symmetric peaks, and they can be scaled onto each other using the same scaling relations of Eq. (4.17). This implies that in 3d we have the same effective charges $e^* = 1e$, $e^* = \sqrt{2}e$, and $e^* = 2e$ for single electrons at $\Delta^* = 0, 1$ and for pairs at $\Delta^* \geq 1$, respectively.

Thus, the most important conclusion from our results in 2d remains for the 3d case as well. This is as expected, since, as explained in Sec. 4.3, the effective charges arise from the single-electron energy spectrum (Fig. 4.1), and are therefore independent of the system dimensionality.

One can also check that in 3d the effective charges have the same influence on the ES temperature as predicted by Eq. (4.18). By numerically evaluating the resistivity of these 3d systems, we indeed find that the ES temperatures $T_{\rm ES}$ obey Eq. (4.18). A plot of the dimensionless resistivity $\ln \rho^*$ against $(T^*)^{-1/2}$ in 3d is essentially identical to that of Fig. 4.3, with slight downward shifts in the magnitude of the resistivity relative to the 2d case. Making independent linear fits to the data gives $T_{\rm ES}^p(\Delta^* \geq 1) \approx 2.6 T_{\rm ES}^s(\Delta^* =$

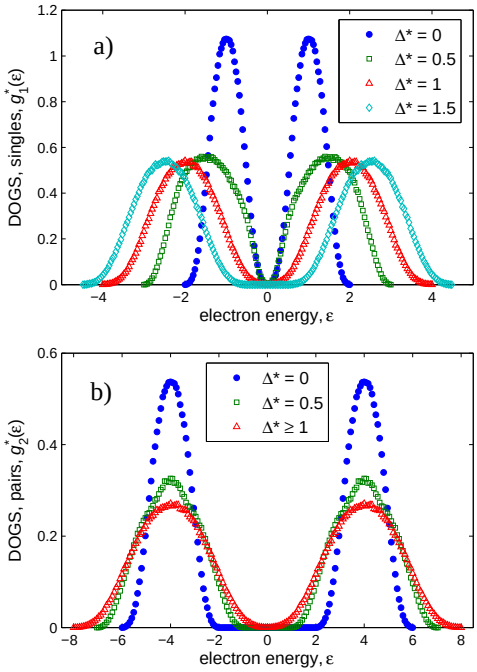

Figure 4.7: (Color online) Single electron and pair DOGS, $g_1^*(\varepsilon)$ and $g_2^*(\varepsilon)$, of a 3d array of monodisperse metallic grains. The DOGS curves obey the same scaling relations as in 2d, [see Eq. (4.17)], indicating the presence of the same effective charges $1e$, $\sqrt{2}e$, and $2e$ and $\Delta^* = 0$, $\Delta^* = 1$, and $\Delta^* > 1$, respectively.

1) $\approx 5.1 T_{\rm ES}^s(\Delta^* = 0)$, which agrees with Eq. (4.18) to within our numerical uncertainty.

4.5 Tunneling experiments

In the previous sections we presented results for the DOGS and we showed that these results have important consequences for the characteristic temperature $T_{\rm ES}$ and for the magnetoresistance. In this section we discuss how the DOGS can be observed directly from tunneling experiments.

Tunneling experiments have previously been used to directly observe the Coulomb gap in lightly-doped semiconductors [62, 53], and have also measured the superconducting gap in isolated superconducting grains [54] and in disordered films [10]. It is therefore natural to think that the single-electron DOGS $g_1(E)$ predicted here can also

be measured via tunneling. In the problem we are considering, however, the energy scales E_c and Δ are similar in magnitude, and thus the tunneling conductance reflects a convolution of the DOGS $g_1(E)$ with the density of states $f(E)$ within each grain. As a result, we consider it worthwhile to explicitly state our predictions for the tunneling conductance $G(\Delta, V)$, where V is the applied voltage, at different values of the gap Δ.

For simplicity, in this section we ignore the potential effects of spin polarization on the tunneling rates. This is equivalent to assuming that any applied magnetic field modifies the superconducting gap Δ primarily through orbital effects rather than the Zeeman effect, so that the electron energy levels shown in Fig. 4.1 are not labeled by spin.

Since the spacing δ between discrete electron energy levels within the grain satisfies $\delta \ll E_c$, as explained in the Introduction, we can take the density of states $f(E)$ within each grain to be a continuous function. For metallic grains with $\Delta = 0$, $f(E)$ can be considered a constant, $f(E) = f_0$, as long as $|(E-\mu)/\mu| \ll 1$. On the other hand, when Δ is finite, coherence peaks arise in the density of states [60], so that at $|E| > \Delta$

$$\frac{f(E)}{f_0} = \frac{E}{\sqrt{E^2 - \Delta^2}}, \tag{4.19}$$

where in this expression E is measured relative to the center of the superconducting gap. [Eq. (4.19) ignores the potential effect of thermal broadening of the coherence peaks.]

The expression of Eq. (4.19) indicates that the conductance into a single grain is greatly enhanced when the voltage is aligned with the edge of the superconducting gap. For an array of grains, the total conductance is the integrated conductance of all the individual grains, each of which has a different relative alignment with the voltage. Thus, the differential conductance satisfies

$$G(\Delta, V) = G_0 A D^{1+d} \int_0^{eV} g_1(E) f(eV - E + \Delta) dE, \tag{4.20}$$

where G_0 is a constant and A is the area of the tunnel barrier. [The term $+\Delta$ in the argument of f in Eq. (4.20) accounts for the fact that the function $f(E)$ in Eq. (4.19) is defined relative to the center of the superconducting gap while the ground state energies described by $g_1(E)$ include the gap energy Δ.]

Given our results for $g_1(E)$, one can use Eq. (4.20) to numerically evaluate the conductance $G(\Delta, V)$. For the limiting case $\Delta = 0$, where the density of states $f(E)$ is constant, Eq. (4.20) becomes simply $G(\Delta = 0, V) \propto \int_0^{eV} g_1(E)dE$, or in other words $g_1(eV) \propto dG(0, V)/dV$. For small but finite Δ, on the other hand, such that $0 < \Delta^* < 1$, the conductance $G(\Delta, V)$ is enhanced at small V relative to $G(0, V)$ as a result of the coherence peaks. At large $\Delta^* > 1$, a gap opens in $g_1(E)$, and $G(\Delta, V)$ remains at zero for $|eV| < (\Delta^* - 1)E_c$.

This result is shown in Fig. 4.8 for the case of tunneling into a 2d array. Here the conductance $G(\Delta, V)$ is plotted normalized to the value $G(0, V)$ as a function of dimensionless voltage eV/E_c for different values of Δ^*. One can think that these different curves correspond to different magnetic field, since, as explained above, an increased magnetic field reduces the gap Δ. Thus, Fig. 4.8 suggests that if one starts with a sample for which $\Delta^* > 1$ and increases the magnetic field, a dramatic change occurs in the quantity $G(\Delta, V)/G(0, V)$. Namely, $G(\Delta, V)/G(0, V)$ first remains at zero for small V, since the single-electron DOGS is gapped. As the magnetic field is increased, the width of this gap decreases, until the point where $\Delta^* = 1$ and it disappears. Once $\Delta^* \leq 1$, the value of $G(\Delta, V)/G(0, V)$ undergoes an abrupt change such that it becomes divergently large at small voltage. This divergence can be seen as the result of the coherence peaks, which greatly increase the tunneling at small voltage relative to the case where there is no Cooper pairing (high magnetic field). Increasing the magnetic field also has the effect of lowering the conductance peak at larger voltage, $eV/E_c \sim 2 + \Delta^*$.

It should be noted that the prediction of Fig. 4.8 is dependent on the existence of *unscreened*, long-range Coulomb interactions between electrons, which create the Coulomb gap in $g_1(E)$. If such long-range interactions are screened by the presence of a nearby metal electrode, which creates an image charge for each charged grain and truncates the $1/r$ interaction, then the Coulomb gap will not be preserved and the predictions of this chapter will be modified. For 2d arrays, it is therefore likely that macroscopic tunneling experiments will not be effective in identifying a Coulomb gap. The behavior of Fig. 4.8 may nevertheless still be identified if one uses a scanning tunneling tip to measure the conductance through individual grains and takes an ensemble average (as in, e.g., Ref. [63]). Alternatively, one can measure the conductance into a 2d face of a thick, 3d array, as was done in Ref. [53]. While Fig. 4.8 plots the conductance assuming

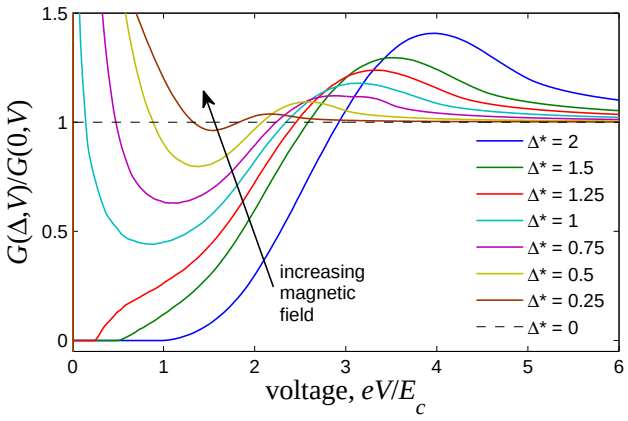

Figure 4.8: (Color online) Tunneling conductance $G(\Delta, V)$ into a 2d array of superconducting grains as a function of voltage V and for different values of the superconducting gap Δ^*, plotted as a ratio of the conductance at $\Delta = 0$. The voltage V is plotted in the dimensionless form eV/E_c. As the magnetic field is increased, driving down the value of Δ, the ratio $G(\Delta, V)/G(0, V)$ at small voltage changes from zero to a divergently large value as Δ^* is made smaller than 1.

tunneling into a 2d array, if one assumes that $g_1^*(\varepsilon)$ is identical to that of a 3d system (Fig. 4.7), the results are qualitatively very similar.

4.6 Disordered Indium Oxide thin films

In this section, a specific material of granular superconductors is discussed: InO_x (InO). InO thin films is one of the materials in which the disorder-driven superconductor-insulator transition (SIT), a quantum phase transition, has been discovered [64, 65]. Compared to other materials such as amorphous Bi [66] and TiN_x [67] that also host SIT, amorphous InO is of particular interest for its giant magnetoresistance (MR) peak in the insulating regime, a puzzle that has long drawn great attention in the physics community both theoretically and experimentally [65, 68, 69]. Beside the transition, direct evidence of Cooper pairs, both above the transition temperature and in the insulating regime, has also been reported [70].

Traditionally, disorder in InO is tuned by varing its stoichiometric oxygen concentration during the fabrication process. This method, however, can introduce unavoidable

complexities to the system such as the conflation of variations of carrier concentration and levels of disorder, and therefore cannot account for the intrinsic variations over different samples. In contrast to the method of chemical doping, electrostatic tuning of SIT offers the advantage of modulating the carrier concentration without altering its disorder. In a recent work Ref. [71], a field effect transistor (FET) configuration was used to electrostatically tune the SIT in InO thin films. In this experimental study, many interesting phenomena were observed, such as variable range hopping in the insulating regime and the broadening of superconducting fluctuations near the SIT. As the charge carrier density in the thin film was tuned, the size and location of the MR peak in the insulating regime changed as well. In this section, we will apply our transport theory for superconducting grains illustrated above to the case of InO thin films, and try to explain the evolution mechanism of MR peaks with charge carrier concentration found in [71].

The details of sample growth and fabrication and the approach of electrostatic tuning are explained in Refs. [[30, 55]]. Fig. 3 in Ref. [71] shows the MR measurements of two InO thin film samples at different gate voltages. Both samples exhibited SIT tuned by carrier modulation, which is clearer in the case of sample B. The most significant feature of the data for sample A [Fig. 3(a1)-(a3)] is the transition from negative MR to positive MR followed by downward slope of R_s upon further increase of H, all taken at fixed T, over the range of 0.5 K to 1 K. Strong MR Peak is also found in insulating regime for both samples.

In a disorder-driven SIT, the spatial inhomogeneity of the pairing energy Δ can be very important. In the insulating regime, in some models, the system may break up into superconducting islands. Near the SI transition, it has been suggested that the MR peaks in disordered systems arise because magnetic fields affect the concentration and size of superconducting islands, so that as these islands shrink with increasing field there is a transition from Cooper pair-dominated to single electron-dominated transport.

On the other hand, reduction of the superconducting pairing energy within islands can itself lead to a tradeoff between conduction by Cooper pairs and conduction by unpaired electrons, and thus (potentially) to a MR peak, even when the concentration and the size of the superconducting islands are fixed. Recent theoretical works [30, 55] studied a model with fixed size and concentration of superconducting grains, and they

showed how a MR peak deep in the insulating state can arise as a result of the reduction of the superconducting gap with increased magnetic field H. This predicts that near the MR peak and at low temperature, the conduction should be described by ES VRH, as shown in Fig. 1(a2) and Fig. 1(b2) in Ref. [71]. Both approaches lead to an insulator in which Cooper pairs with nonzero Δ are formed in the insulating regime of the system and are responsible for the MR peak.

The shift of the MR peak to higher magnetic fields with increasing carrier concentration, as shown in Figs. 3 in Ref. [71], can be explained qualitatively within the context of the theory of Refs. [30, 55, 72]. Increasing the carrier density presumably increases the density of states at the Fermi level within the superconducting grains, thereby driving up the zero-field superconducting gap Δ_0. A larger Δ_0 implies that a larger H is required in order to reduce Δ to the value of the grain charging energy E_c, so that the MR peak shifts to higher H. In this way the transition from negative MR [as in Fig. 3(a1)] to a peak at an intermediate H [Fig. 3(a2)] to a peak at a larger H [Fig. 3(a3)] can be understood.

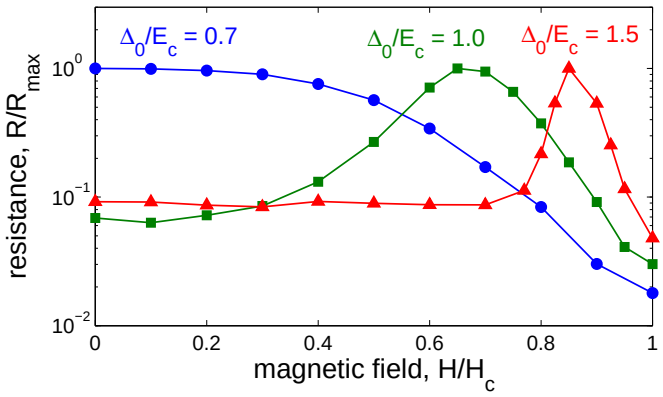

Figure 4.9: (Color online) Simulation of log resistivity of a 2D array of identical superconducting grains deep in the insulating state as a function of H. Different curves are labeled with their corresponding values of Δ_0/E_0. As Δ_0 is increased, which presumably corresponds to larger carrier density, a MR peak develops that shifts to larger magnetic field, in qualitative agreement with what is seen in Ref. [71]. Here all curves correspond to a temperature such that $K_BT = 0.1E_c$ and have localization lengths ξ_1 and ξ_2 for single-electron and pair conductivity, respectively, satisfying $\xi_1/\xi_2 = 8$.

As an example, Fig. 4.9 shows values of the resistance of a simulated 2D array of

regularly-spaced, monodispersed superconducting grains (or islands) as a function of H, calculated using the method described in [30]. At small Δ_0/E_c, the conductivity is primarily due to hopping of unpaired electrons, and there is a monotonic negative MR [as seen, for example, in Fig. 3(a1) in Ref. [71]]. At larger Δ_0/E_c, which ostensibly corresponds to larger carrier density, the MR develops a peak associated with a trade-off between conductivity by single electrons and conductivity by Cooper pairs. This peak moves to larger H as Δ_0/E_c is increased [as in Fig. 3(a1) in Ref. [71]]. For the simulation of Fig. 4.9 we have assumed a conventional BCS-like dependence of Δ on the field H: $\Delta = \Delta_0\sqrt{1-(H/H_c)^2}$. In this way the data shown in Figs. 3 in Ref. [71] is consistent with the concept of tuning the local superconducting gap by modulating the carrier density. Moreover within this picture, the global transition from insulating state to superconducting state can be understood as the increasing carrier density drives zero Δ regions to non-zero Δ, therefore connecting each superconducting grains otherwise disconnected. Unfortunately, the simulation method used to generate Fig. 4.9 cannot be used for a quantitative determination of the relationship $\Delta(n)$, since this requires a knowledge of the H-dependence of the gap as well as the relative localization lengths ξ_1 and ξ_2 for unpaired and paired electron hopping. We also caution that the simulation technique is applicable only for the heavily-insulating limit, and in this sense our comparison between Figs. 3 in Ref. [71] and 4.9 is only qualitative. It should also be noted that within this simple model a strong MR peak develops only at relatively large ξ_2/ξ_1. A final caveat is the possibility that other models may give similar results.

4.7 Conclusion

In this chapter we have proposed a model of a disordered granular superconductor and evaluated the DOGS and resistivity at different values of the superconducting gap Δ. Our primary result is the DOGS for single electrons and electron pairs shown in Figs. 4.2 and 4.7. We also have considered the implications of the DOGS for the conductivity of the system (Figs. 4.3), and explained a mechanism for negative magnetoresistance (Fig. 4.4). Our predictions for the tunneling conductance are given in Fig. 4.8.

Perhaps the most remarkable result is the existence of effective charges $1e$, $2e$, and $\sqrt{2}e$ at $\Delta^* = 0$, $\Delta^* > 1$, and $\Delta^* = 1$, respectively, which was first reported by Ref.

[55]. These effective charges codify exact scaling relations between different results for the DOGS [Eq. (4.17)] and for the conductivity at low temperature [Eq. (4.18)], and can be understood in a fairly intuitive way. At $\Delta^* = 0$, electrons are unpaired and electronic conduction is performed by single electrons. At $\Delta^* > 1$, electrons become bound in Cooper pairs and these pairs are the primary players both in the conductivity and in determining the DOGS. At the point $\Delta^* = 1$, single electrons hop in a disorder potential that is shaped primarily by Cooper pairs, and the single-electron DOGS and conductivity can be described by an effective charge $e^* = \sqrt{2}e$.

It is perhaps worth emphasizing that this effective charge $\sqrt{2}e$ does not represent a real quasiparticle in the traditional sense. For example, unlike the charges $1e$ and $2e$, the charge $\sqrt{2}e$ is unlikely to appear in the shot noise of the current (or the Fano factor), since the actual hopping is performed by single electrons. Rather, the appearance of the charge $\sqrt{2}e$ in $g_1(E)$ and T_{ES} is the result of a degeneracy in the electronic spectrum, which results in electrons being paired in the ground state. These paired electrons rearrange in the presence of a disorder potential and determine the properties of the ground state, while transport is carried by singles. It is this combination of intimidation by pairs and conduction by singles that produces the appearance of a $\sqrt{2}$ charge.

More generally, this view represents something of a novel paradigm in hopping transport. Namely, that a system can be simultaneously populated by two or more charged species (here, singles and pairs), one of which determines the Coulomb landscape while the other is responsible for transport. Exploring this kind of physics in other classes of disordered systems remains a promising topic for future study.

Chapter 5

Topological insulator and strongly compensated semiconductor

5.1 Completely compensated topological insulator

5.1.1 Introduction

The three-dimensional (3D) topological insulator (TI) [12, 13, 14, 15, 16] has gapless surface states, which host a spectrum of quantum transport phenomena [73, 74]. In Fig. 5.1(a), the band structure of an undoped Bi_2Se_3, a typical 3D TI, measured by ARPES is shown. While the bulk is a normal band insulator, the surface states are gapless and has a dirac-cone structure, with the dirac point inside the band gap of the bulk.

While a number of crystals have been identified to be 3D TIs, most of them are poor insulators and the bulk of TI crystals of substantial size (> 10 μm) shunts the surface conductivity. The current literature [18, 19, 20, 21, 22, 23, 24, 25, 26]broadly discusses how one can achieve a bulk-insulating state.

Typically as-grown TI crystals such as Bi_2Se_3 are heavily doped n-type semiconductors. (It is believed that Bi_2Se_3 is doped by Se vacancies.) To make them insulating, these TIs are compensated by acceptors. The compensation process is illustrated in Fig. 5.1(b). With increasing compensation $K = N_A/N_D$, where N_D and N_A are the concentrations of monovalent donors and acceptors, the Fermi level shifts from the conduction band to inside the gap and then into the valence band at $K > 1$. When compensation

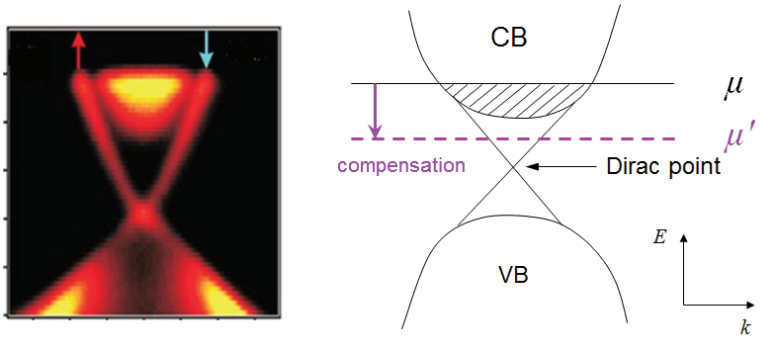

Figure 5.1: (a) Energy band structure of undoped Bi_2Se_3 measured by ARPES. The top and bottom are the conduction and valence band of the bulk, respectively; in the middle are the gapless surface states that have a dirac-cone like band structure. (b) Schematic drawing of energy band structure of 3D TI in k-space. The large concentration of intrinsic dopants puts the Fermi level μ high in the conduction band. To achieve a bulk insulating state, the (shallow) intrinsic dopants must be compensated by (shallow) acceptors. As a result, the original Fermi level moves from the conduction band down into the band gap.

of donors is complete, $K = 1$, the Fermi level is in the middle of the gap and the most insulating state of TI is achieved, as shown in Fig. 5.2. For a TI with a gap $E_g \sim 0.3$ eV the resistivity is expected to obey the activation law

$$\rho = \rho_0 \exp(\Delta / k_B T) \tag{5.1}$$

with activation energy $\Delta = E_g/2 \sim 0.15$ eV, so that the TI is a good insulator at room temperatures and below.

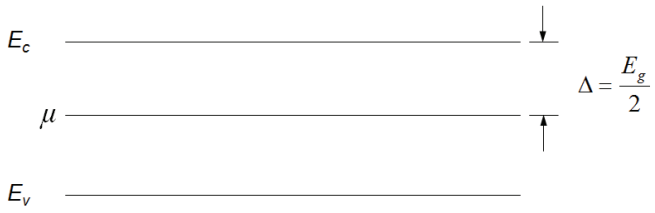

Figure 5.2: Energy diagram of a completely compensated TI with band gap E_g assumed in the flat bands picture. While the compensation is complete, the Fermi level lies in the middle of the gap, and the corresponding resistivity is thermally activated with activation energy to be half of the band gap.

However, the current experimental situation near $K = 1$ is frustrating [25]. In the

temperature range from 100 and 300 K, although resistivity is activated, the activation energy $\Delta \sim 50$ meV, which is three times smaller than expected. At $T \sim 100$ K the activated transport crosses over to variable range hopping (VRH), characterized by $\rho \propto \exp[(T_0/T)^x]$ with $x < 1$, and the resistivity grows even more slowly with decreasing T. In Ref. [25] the authors show that Mott VRH ($x = 1/4$) provides a reasonable fit to their data at 50 K $\lesssim T \lesssim$ 100 K. When temperature is further decreased, resistivity grows even more slowly and below 50 K, resistivity saturates around $\rho(T) < 10$ Ωcm. This means that in spite of complete compensation, even at helium temperatures conductance of TI samples thicker than 10 μm is dominated by the bulk.

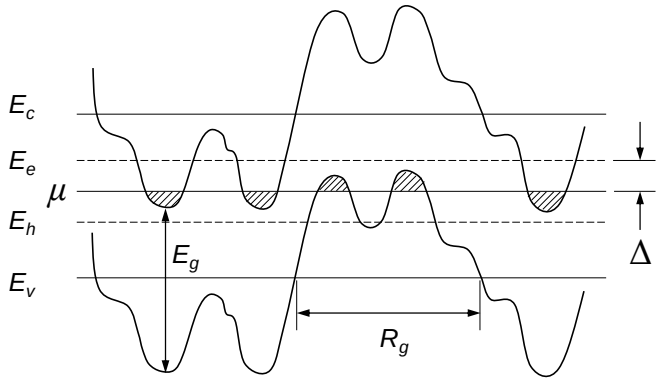

Figure 5.3: Energy diagram of a completely compensated TI with band gap E_g. The upper and the lower straight lines (E_c and E_v) indicate the unperturbed positions of the bottom of the conduction band and the ceiling of the valence band; the middle line (μ) corresponds to the Fermi level. Meandering lines represent the band edges, which are modulated by the fluctuating potential of charged impurities; R_g is the characteristic size of these potential fluctuations. The percolation levels for electrons, E_e, and holes, E_h, are shown by dashed lines; the activation energy Δ corresponds to the difference $E_e - \mu$ (or $\mu - E_h$). Puddles occupied by carriers are shaded. Shallow impurity levels are not shown because they merge with the band edges.

In Sec. 5.1, we suggest an explanation for the unexpectedly small bulk resistivity of completely compensated TIs ($K = 1$). We assume that both donors and acceptors are shallow and we use the theory of completely compensated semiconductors (CCS) [75, 32]. This theory is based on the idea that near $K = 1$, when almost all donors and acceptors are charged, random fluctuations in the local concentration of impurities result in large fluctuations of charge. The resulting Coulomb potential is poorly screened because

of the vanishing average concentration $n = N_D - N_A$ of screening electrons. Huge fluctuations in the random potential bend the conduction and valence bands edges and in some places bring them to the Fermi level, thereby creating electron and hole puddles that non-linearly screen the random potential. Thus, the amplitude of fluctuations is limited only by the semiconductor gap E_g. As a result the ground state of a CCS, shown in Fig. 5.3, is similar to a network of p-n junctions [75, 32]. The characteristic size of these p-n junctions, also called the nonlinear screening radius, is given by

$$R_g = \frac{E_g^2 \kappa^2}{8\pi N e^4}, \tag{5.2}$$

where κ is the dielectric constant, e is the electron charge, and $N = N_D = N_A$. For $N = 10^{19}$ cm^{-3} and $\kappa = 20$, $R_g \approx 70$ nm $\gg N^{-1/3} \approx 4.6$ nm, so that we deal with a very long range potential. As a result, the resistivity can be dramatically different from the expectation outlined above, which assumed flat bands. First, at relatively high temperatures conduction is due to electrons and holes being activated from the Fermi level to their corresponding classical percolation levels (classical mobility edges), E_e and E_h, in the conduction and the valence bands. These may be substantially closer to the Fermi level μ than $E_g/2$, but so far the resulting value of Δ has not been studied theoretically. Second, at sufficiently low temperatures electrons and holes can hop (tunnel) between distant puddles, so that variable range hopping replaces activated transport. In the low temperature limit $\rho(T)$ should obey the Efros-Shklovskii (ES) law of VRH [3],

$$\rho = \rho_0 \exp\left[(T_{\rm ES}/T)^{1/2}\right], \tag{5.3}$$

where $T_{\rm ES} = Ce^2/\kappa\xi$, ξ is the localization length of states with energy close to the Fermi level, and C is a numerical coefficient. So far the magnitude of $T_{\rm ES}$ and the nature of the crossover between activated and VRH conduction have not been studied.

In this section, motivated by the TI resistivity puzzle, we return to CCS and model numerically the $K = 1$ case. In Sec. 5.1.2 the theoretical model for completely compensated TI is defined, and our computer simulation methods for numerically calculating the DOGS and resistivity are introduced. Results are presented and discussed in Sec. 5.1.3.

Our assumption of random distribution of impurities is crucial for this theory. Usually, for samples made by cooling from melt, the distribution of impurities in space is a

snapshot of the distribution the impurities have at higher temperature when the diffusion of impurities practically freezes. In semiconductors with a narrow enough gap at this temperature, there is a concentration of intrinsic carriers larger than the concentration of impurities. Intrinsic carriers screen the Coulomb interaction between impurities, so that impurities remain randomly distributed in space. At lower temperatures, when intrinsic carriers recombine, impurities are left in random positions [76, 32]. If diffusion freezes at $T \sim 1000K$, it is reasonable to assume that impurities are randomly positioned in a semiconductor with $E_g \leq 0.3\ eV$. This justifies the use of this theory for typical TIs. Our results are applicable to other narrow gap semiconductors, for example, InSb. (Historically, large effort was made to make InSb insulating via strong compensation. The goal was to improve characteristics of InSb based photo-detectors. Results were again frustrating: the dark resistivity was too small. Our results are in reasonable agreement with transport experiment data for InSb [77, 78].)

For moderately large T we find that $\Delta = 0.15E_g$. For a TI with $E_g = 0.3$ eV this implies $\Delta = 45$ meV, in agreement with observed values [25]. We also find that the single-particle DOS has a Coulomb gap at the Fermi level [3]. We show from our simulation that the resistivity is described by Eq. (5.3) at low temperatures and crosses over to Eq. (5.1) at higher T. We present a crude estimate of the localization length ξ which suggests that $T_{\rm ES} \sim 900$ K and that the crossover between activation and ES VRH occurs at $T \sim 40$ K. Together our results for the activated and VRH resistivity establish a universal upper limit for the resistivity $\rho(T)$ that one can achieve for a 3D TI compensated by shallow inpurities.

5.1.2 The model, pseudoground state, and density of states

In order to model the CCS numerically, we simulate a cube filled by an equal number of randomly positioned donors and acceptors (20000 of each). We numerate all donors and acceptors by the index i and we define $n_i = 0, 1$ as the number of electrons residing at impurity i and the variable f_i to discriminate between donors ($f_i = 1$) and acceptors ($f_i = -1$). The resulting Hamiltonian is

$$H = \frac{E_g}{2} \sum_i f_i n_i + \sum_{\langle ij \rangle} V(r_{ij}) q_i q_j, \tag{5.4}$$

where $q_i = (f_i + 1)/2 - n_i$ is the net charge of site i and all energies are defined relative to the Fermi level. The first term contains the energies of shallow donors and acceptors, which is very close to the semiconductor gap E_g. The second term of H is the sum of interaction energies of charged impurities. If two impurities are at distance $r >> a_B$, where a_B is the Bohr radius of impurity states, one can use the Coulomb interaction $V(r) = e^2/\kappa r$. For a pair of empty donors, one donor shifts down the energy of the electron on the other by an energy $V(r) = -e^2/\kappa r$. This classical form for $V(r)$ is good for a lightly doped SCS. But in a heavily doped SCS, where $a_B > N_D^{-1/3}$, most impurities have at least one neighbor at distance $r < a_B$ and quantum-mechanical averaging over electron wave function becomes important. (This is why an uncompensated heavily doped semiconductor is a good metal). For example, such a pair of donors cannot create a state deeper than that of the helium-like ion with a binding energy $4E_B$, where $E_B = e^2/2\kappa a_B$ is the binding energy of the shallow donor state. Here, we deal with heavily doped SCS, where $(E_c - \mu) > 4E_B$ and quantum effects limit the role of short-range potential. To model such a case, we continue to use the classical Hamiltonian Eq. (5.4), but truncate the Coulomb potential to $V(r) = e^2/\kappa(r^2 + a_B^2)^{1/2}$. Note that Eq. (5.4) does not include the kinetic energy of electrons and holes in conduction and valence bands and, therefore, aims only at description of the low temperature ($k_B T \ll E_g$) physics of SCS.

In all results below we use dimensionless units for r, a_B, ξ, H, E_g, and $k_B T$, measuring all distances in units of $N^{-1/3}$ and all energies in units of $e^2 N^{1/3}/\kappa$. Thus, Eq. (5.4) can be understood as dimensionless, with $E_g \gg 1$ and $V(r) = (r^2 + a_B^2)^{-1/2}$. For a TI with $E_g = 0.3$ eV, $\kappa = 20$ and $N = 10^{19}$ cm^{-3}, the unit of energy $e^2 N^{1/3}/\kappa \approx 15$ meV, so that the dimensionless gap $E_g \approx 20$. We were unable to directly model $E_g = 20$, since in this case the very large $R_g \approx 16$ leads to large size effects. Instead, we present results for the more modest $E_g = 10$, where $R_g \approx 4$ and size effects are negligible, and for $E_g = 15$, where $R_g \approx 9$ and size effects can be treated using extrapolation. Unless otherwise stated, results below use $a_B = 2$ and are averaged over 100 random initializations of the donor and acceptor positions.

In our simulation, we first search for the set of electron occupation numbers $\{n_i\}$ that minimizes H. We start by assuming that all donors are empty ($n_i = 0$, $q_i = 1$) and that all acceptors are filled ($n_i = 1$, $q_i = -1$). These charged donors and acceptors

create a random Coulomb potential whose magnitude exceeds E_g. We then sequentially choose pairs consisting of one filled site and one empty site and attempt to transfer an electron from the filled site to the empty site. If the proposed move lowers the total system energy H, it is accepted, otherwise it is rejected. To describe the change in H resulting from such a transfer it is convenient to introduce the single-electron energy state, ε_i, at a given impurity i:

$$\varepsilon_i = \frac{E_g}{2} f_i - \sum_{j \neq i} V(r_{ij}) q_j. \tag{5.5}$$

The process of transferring electrons concludes when all pairs i, j with $n_i = 1$ and $n_j = 0$ satisfy the ES stability criterion:

$$\varepsilon_j - \varepsilon_i - V(r_{ij}) > 0. \tag{5.6}$$

This final arrangement of electrons can be called a pseudo-ground state, since higher stability criteria of the ground state (involving multiple simultaneous electron transfers) are not checked. Such pseudo-ground states are known to accurately describe the properties of the real ground state at all but extremely small energies [32, 45, 46]. The resulting DOS of impurties in the pseudo-ground states $g^*(\varepsilon)$ is calculated by making a histogram of the single-electron energies ε_i.

Once the energies $\{\varepsilon_i\}$ are calculated, we evaluate the resistivity using the approach of the Miller-Abrahams resistor network [32]. Namely, each pair of impurities i, j is said to be connected by the resistance $R_{ij} = R_0 \exp[2r_{ij}/\xi + \varepsilon_{ij}/k_B T]$, where the activation energy ε_{ij} is defined [32] as follows:

$$\varepsilon_{ij} = \begin{cases} |\varepsilon_j - \varepsilon_i| - V(r_{ij}), & \varepsilon_j \varepsilon_i < 0 \\ \max\left[|\varepsilon_i|, |\varepsilon_j|\right], & \varepsilon_j \varepsilon_i > 0. \end{cases} \tag{5.7}$$

The resistivity of the system as a whole is found using a percolation approach. Specifically, we find the minimum value R_c such that if all resistances R_{ij} with $R_{ij} < R_c$ are left intact, while others are eliminated (replaced with $R = \infty$), then there exists a percolation pathway connecting opposite faces of the simulation volume. The system resistivity $\rho(T)$ is taken to be proportional to R_c, which captures the exponential term while details of the prefactor are ignored [32].

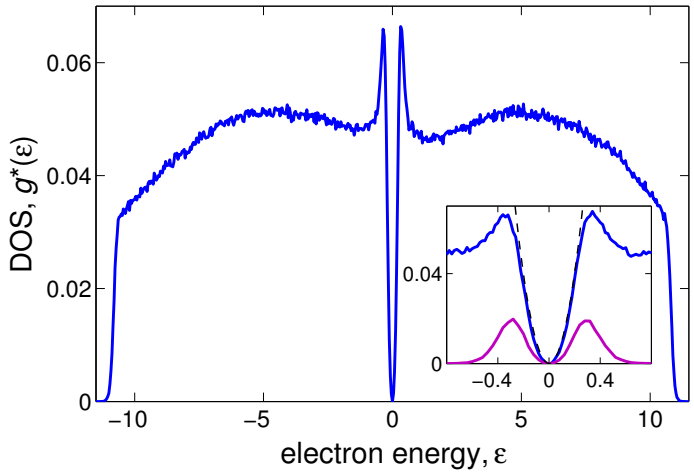

Figure 5.4: (Color online) Dimensionless single-electron DOS $g^*(\varepsilon) = g(\varepsilon)/[2N/(e^2N^{1/3}/\kappa)]$ for a completely-compensated semiconductor with $a_B = 2$ and $E_g = 10$. The inset shows the DOS near the Fermi level $\varepsilon = 0$ (upper curve, blue). For comparison, the quadratic Coulomb gap $g(\varepsilon) = (3/\pi)\varepsilon^2$ is shown by the dashed line [3, 52]. The lower (magenta) line shows separately the DOS of rare filled donors and empty acceptors.

5.1.3 Results and discussion

The result is shown in Fig. 5.4, with the DOS in units of $[2N_D/(e^2N_D^{1/3}/\kappa)]$, so that the total area is equal to unity. Occupied and empty states are separated by the Fermi level at $\varepsilon = 0$, which is defined as a half distance between minimum empty and maximum occupied energy ε. At $K = 1$, the almost constant symmetric DOS between $-E_g = -15$ and $E_g = 15$ reflects a practically uniform distribution of random potential from $-E_g/2$ to $E_g/2$, and a corresponding uniform distribution of band edges E_c between 0 and E_g and E_v between 0 and $-E_g$ [see Fig. 5.3(a)]. Near the Fermi level one sees the Coulomb gap as a consequence of ES stability criterion [3]. (For comparison, the quadratic Coulomb gap $g(\varepsilon) = (3/\pi)\varepsilon^2$ is shown by the dashline. The DOS of rare filled donors and empty acceptors is shown by magenta line in the inset of Fig. 5.4.)

In Fig. 5.5 we plot the computed resistivity as a function of temperature, using the dimensionless logarithm of the resistance $(\ln\rho)^* = (\xi/2)\ln(R_c/R_0)$ and the dimensionless temperature $T^* = 2k_BT/\xi$. These notations are introduced to exclude any explicit dependence on ξ. Fig. 5.5(a) shows $(\ln\rho)^*$ versus $(T^*)^{-1/2}$ over the huge range

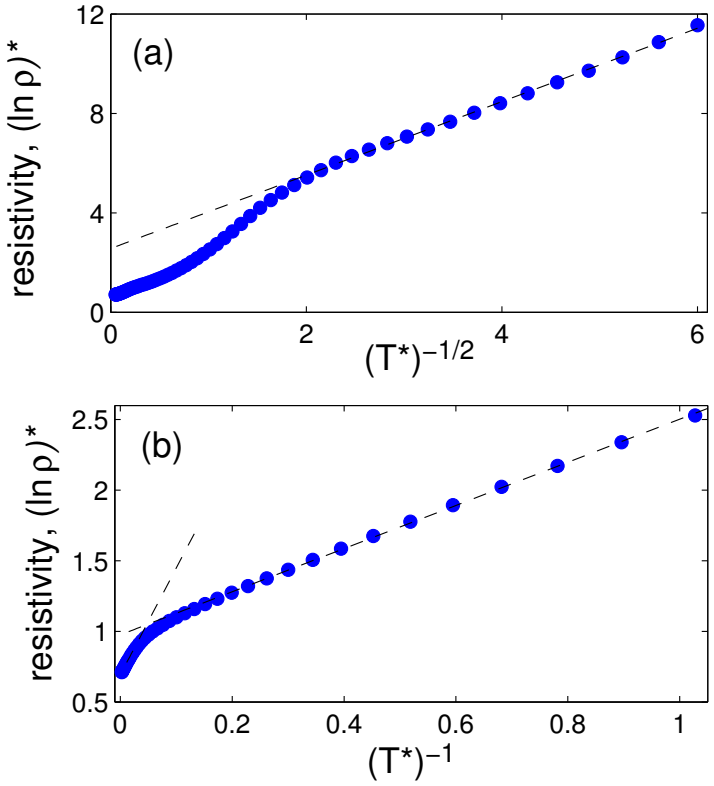

Figure 5.5: (Color online) The temperature dependence of the resistivity for $E_g = 10$ (blue dots). The dimensionless resistivity $(\ln \rho)^*$ is plotted in (a) against $(T^*)^{-1/2}$ to illustrate that the resistivity follows the ES law at low temperatures, and in (b) against $(T^*)^{-1}$ to show that the resistivity is activated at larger T^*, with two distinct activation energies. The dashed lines (black) are linear best fits.

of temperatures $0.03 < T^* < 200$. One can see that at low temperatures $T^* < 0.3$ the resistivity is well described by the ES law, Eq. (5.3), with $C \approx 4.4$. The higher temperature range $1 < T^* < 200$ is plotted separately as a function of $1/T^*$ in Fig. 5.5(b). Here we find two activated regimes of hopping conductivity. At extremely high temperatures $T^* > 50$ we see the large activation energy $E_a \sim 0.75 E_g$ while in the intermediate range $1 < T^* < 10$ we see an activation energy $\Delta = (0.15 \pm 0.01) E_g$. We repeated this analysis for the larger band gap $E_g = 15$ using systems of 10000, 20000 and 30000 donors and by extrapolating to infinite size we find $\Delta = (0.15 \pm 0.02) E_g$. These results for Δ remain unchanged, within our statistical uncertainty, if we use $a_B = 1$ instead of $a_B = 2$.

It should be noted that the large activation energy $E_a \sim 0.75E_g$ observed at $T^* > 50$ does not have any physical meaning for a real CCS, since at such large temperatures the conduction is not due to hopping but rather to free, "hot" carriers far from the conduction and valence band edges. Nonetheless, for our model Hamiltonian this result is consistent with established theories which say that at such large temperatures $E_a = \langle \varepsilon_{ij} \rangle$, where $\langle ... \rangle$ denotes averaging over all pairs i, j (see Ch. 8 of Ref. [32]).

On the other hand, the second activation energy $\Delta = 0.15E_g$ makes full physics sense and should be seen in experiment. At $T \ll E_g$ electrons optimize their conductivity by hopping among impurities that are energetically close to the Fermi level. The activation energy Δ can be understood as the resulting percolation level for hopping between nearest-neighboring sites. In other words, if electrons are activated only to those sites with $|\varepsilon| < \varepsilon_p$, then precisely at $\varepsilon_p \geq \Delta = 0.15E_g$ there exists an infinite conduction pathway for electrons comprised of hops of length $\sim N^{-1/3}$ or shorter.

In a heavily doped semiconductor this energy is equivalent to the activation energy of electrons from the Fermi level to the conduction band mobility edge E_e. (Of course, holes are activated from the Fermi level to their percolation level E_h as well.) For a typical TI $E_g = 0.3$ eV, so that we get $\Delta = 45$ meV, in good agreement with typical experimental data [25]. (We note, however, that recent experiments on Sn-doped Bi_2Te_2Se have achieved $\Delta \sim 125$ meV [26]. Such large activation energies may be associated with deep donor impurity levels, which go beyond our model.)

This activation to the percolation level persists until much smaller temperatures, where Δ becomes prohibitively large compared to the thermal energy. At such small T^* conduction proceeds by VRH among electron/hole puddles at the Fermi level and the resistivity is given by Eq. (5.3).

One can interpret the relatively small numerical factor 0.15 above by recalling that in a typical 3D continuous random potential, $\sim 17\%$ of space has a potential smaller than the percolation level [32]. As we demonstrated above the energy of the conduction band bottom is roughly uniformly distributed in the interval $(0, E_g)$. This means that the percolation level E_e should be close to $0.17E_g$ and makes our result $\Delta = 0.15E_g$ quite reasonable.

So far we have emphasized results that do not explicitly depend on the localization

length ξ. In fact, knowledge of ξ is necessary to predict $T_{\rm ES}$ and the transition temperature T_t between Eq. (5.1) and Eq. (5.3) in real temperature units. (According to Fig. 5.5a, the transition happens at $T^* \approx 1/2$, or $T_t \approx \xi/4$). We argue now that in a TI ξ is quite large, leading to a prominent role for VRH. To see this, consider that if an electron with energy close to the Fermi level is assumed to tunnel from one electron puddle to another distant puddle along the straight line connecting them, then the tunneling path passes through regions where the conduction band bottom is quite high above Fermi level. This implies a small tunneling amplitude, or $\xi \ll a_B$. In fact, however, a tunneling electron can use the same geometrical path as a classical percolating electron with energy Δ above the Fermi level. In order to roughly estimate ξ, we assume that along such a classical percolation path the tunneling barriers V are uniformly distributed in the range $0 \leq V \leq \Delta$ and we neglect the curvature of this path. Integrating the action along this path then gives $\xi \sim \hbar/(m\Delta)^{1/2} = a_B\sqrt{e^2/a_B\Delta}$. For a TI with $E_g = 20$ and $a_B = 2$ this gives $\xi \simeq 0.8$. This crude estimate leads to $T_{\rm ES} \sim 900$ K and $T_t \sim 40$ K, which is similar in magnitude to the experimentally observed $T_t \sim 100$ K where the resistivity crosses over from activated to VRH behavior [25].

We note that if one plots our result for $(\ln \rho)^*$ against $(T^*)^{-1/4}$ in the relatively narrow crossover range 50 K $< T <$ 100 K, one gets a mostly straight line, as seen in Ref. [25]. However, our results suggest that at low temperatures the bulk resistivity follows the ES law of VRH with temperature exponent $x = 1/2$, which should become apparent if the bulk resistivity can be probed to very low temperature. Such measurements are presumably possible in samples that are much thicker than those studied in Ref. [25] ($\sim$ 100 μm). For such thick samples conduction through the bulk of the TI crystal dominates over the surface transport until much smaller temperatures.

5.2 Strongly compensated semiconductor

5.2.1 Introduction

In the previous section we suggest an explanation of anomalously large bulk conductivity of TI at $K = 1$. We assume that both donors and acceptors are shallow and randomly positioned in space and the theory of completely compensated semiconductor (CCS) [32, 75] is adopted. According to our numerical simulation, at $K = 1$ the activation energy

$\Delta \simeq 0.15E_g$, in good agreement with the experimental value. This is because E_e and E_h are substantially closer to the Fermi level μ than the unperturbed by a random potential bottom of the conduction band E_c and ceiling of the valence band E_ν [see Fig. 5.3]. At low enough temperatures, electrons and holes can hop (tunnel) between puddles so that VRH replaces activated transport.

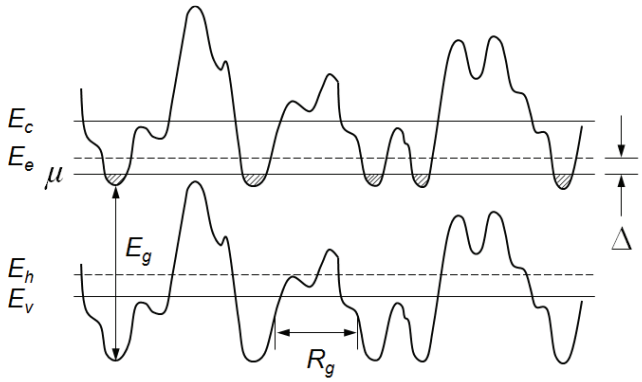

Figure 5.6: Energy diagram of a strongly compensated semiconductor ($1 - K \ll 1$) with gap E_g. The upper and the lower straight lines indicate the unperturbed positions of bottom of the conduction band, E_c, and ceiling of the valence band E_ν; the middle straight line corresponds to the Fermi level μ. Meandering lines represent the band edges, which are modulated by the fluctuating potential of charged impurities. R_g is the characteristic size of potential fluctuations. Percolation levels E_e for electrons and E_h for holes are shown by dashed lines. Puddles occupied by carriers are shaded. Shallow impurities levels are not shown because they practically merge with band edges.

In the present section, we change our focus from a possible maximum bulk resistivity of a completely compensated semiconductor at $K = 1$ to the more practical question of the dependence of bulk resistivity of a strongly compensated semiconductor (SCS) on K at $0 < 1 - K \ll 1$. Indeed, with existing methods of growth of TI samples one can not get $K = 1$ exactly. It is important to know how stable the resistivity results at $K = 1$ are for the case of $1 - K \ll 1$. For example, one can ask at which $1 - K$ the activation energy Δ is twice smaller than at $K = 1$. For definiteness, we consider n-type SCS, where the concentration of electrons $n = N_D - N_A \ll N_D$ and $1 - K \ll 1$. We model numerically the ground state of such SCS and its resistivity using algorithms similar to Sec. 5.1. We find that in agreement with the analytic theory [32], when $1 - K$ grows, the screening of the random potential improves and its correlation length R decreases.

The amplitude of the random potential decreases as well. As a result, hole puddles shrink and eventually vanish and the chemical potential μ moves up, so that $E_c - \mu$ decreases. One can say that with increasing $1 - K$, the screening due to bending of the conduction band occurs only while all acceptors remain occupied by electrons and negatively charged. All these changes are illustrated by transition from Fig. 5.3 to Fig. 5.6.

As a result of these changes, the activation energy Δ decreases with growing $1 - K$. We find that the relation $\Delta = 0.3(E_c - \mu)$ obtained in Ref. [31] for $K = 1$ remains valid for $1 - K \ll 1$ (see Fig. 5.12 below) as well. [In p-type semiconductor where $K = N_D/N_A$, a similar relationship $\Delta = 0.3(\mu - E_v)$ takes place.] By $K = 0.97$ the activation energy Δ is about two times smaller than at $K = 1$. This result shows that achieving maximum resistivity with $\Delta = 0.15E_g$ is problematic. It also explains the origin of large scatter of magnitude of Δ among TI samples [25].

In principle, our prediction that $\Delta = 0.3(E_c - \mu)$ can be directly compared with experiments in TIs. Indeed, for each K, the position of the Fermi level can be found via measurements of the surface concentration of electrons in the gapless surface state using Shubnikov-de-Haas oscillations. On the other hand, at low temperatures, we find numerically a direct cross-over from activation to ES VRH. We also find how $T_{\rm ES}$ being correlated with Δ decreases with $1 - K$.

The plan of sec. 5.2 is as follows. In Sec. 5.2.2, we formulate the model, explain the algorithm of numerical simulation of the pseudoground state and resistivity. In Sec. 5.2.3, we present our results for DOS and resistivity, and arrive at a small activation energy for conduction band resistivity $\Delta = 0.3(E_c - \mu)$. We also evaluate the localization length of states with energy close to Fermi energy and estimate the characteristic temperature of ES law $T_{\rm ES}$. In Sec. 5.2.4, we estimate the thermopower of strongly compensated semiconductor and show that the Peltier energy (heat) is $\Pi \simeq \Delta/2 = 0.15(E_c - \mu)$, in qualitative agreement with a recent experimental paper.

5.2.2 The model, pseudoground states, and the density of states

To model a heavily doped SCS, we create a cube filled with 20000 donors and $20000K$ acceptors that are randomly positioned in space. We numerate all donors and acceptors by index i and use $n_i = 0$ or 1 for the number of electrons residing on a donor or an

acceptor. In addition, we use a variable f_i to discriminate between donors ($f_i = 1$) and acceptors ($f_i = -1$). The Hamiltonian of our system is defined the same way as Eq. (5.4).

We use dimensionless units for r, a_B, H, E_g, and k_BT as defined in Sec. 5.1.2. Thus Eq. (5.4) now can be understood as dimensionless, where $E_g \gg 1$ and $V(r) = (r^2 + a_B^2)^{-1/2}$. For TI with $E_g = 0.3$ eV, $\kappa = 30$, and $N_D = 10^{19}$ cm^{-3}, we have $N_D^{-1/3} = 4.6$ nm and $e^2 N_D^{1/3}/\kappa \simeq 10$ meV, so that the dimensionless gap $E_g = 30$. We could not model $E_g = 30$, because in this case, the very large correlation length of long-range potential, R_g, leads to large size effect. Instead, we run more modest $E_g = 15$, for which the size effect requires extrapolation only at $K = 1$ [31]. Our goal is to find the activation energy Δ and estmate $T_{\rm ES}$ as a function of K or μ.

We search for the set $\{n_i, f_i\}$ that minimizes H and use such a set to calculate the DOS and the conductivity. We start from the neutral system of all populated by electrons (negatively charged) acceptors ($n_i = 1, q_i = -1$), of equal number of randomly chosen $20000K$ empty (positively charged) donors ($n_i = 0, q_i = 1$), and of $20000(1-K)$ filled (neutral) donors ($n_i = 1, q_i = 0$). Charged donors and acceptors create a random potential whose magnitude exceeds E_g. In order to screen the Coulomb potential fluctuations, some electrons leave acceptors for donors. At any stage of this process, there are two types of occupied states – neutral donors and negatively charged acceptors, and two types of empty states – positively charged donors and neutral acceptors, respectively. Electrons may hop from an occupied impurity to an empty one. If the proposed move lowers the total system energy H, then it is accepted, otherwise it is rejected. To check whether H goes down, for a given set of electron occupation numbers $\{n_i, f_i\}$, it is convenient to introduce the single-electron energy state, ε_i at a given impurity i as in Eq. (5.5). For all i, j with $n_i = 1$ and $n_j = 0$, we check that ES pseudoground state stability criterion Eq. (5.6) is satisfied.

If this criterion is not satisfied, we move the electron from impurity i to j and recalculate all ε_i. This process is done by looping all possible pairs of impurities i, j with $n_i = 1$ and $n_j = 0$ and is continued until no single-electron transfers can be made to lower H. The final arrangement of electrons can be called a pseudoground state, because the higher stability criteria of ground state are not checked. Once the

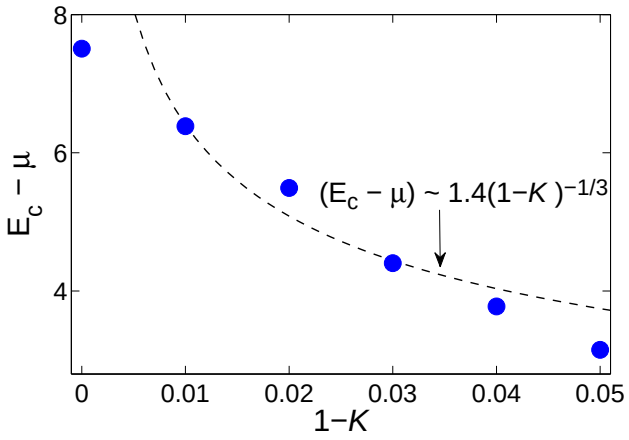

Figure 5.7: (Color online) Fermi level μ as a function of $1-K$ for $a_B = 1$ and $E_g = 15$. The size of dots characterizes the uncertainty.

energies $\{\varepsilon_i\}$ are known, we evaluate the resistivity using the approach of the Miller-Abrahams resistor network [32]. The results below are obtained at $E_g = 15$, $a_B = 1$ for $K = 1, 0.99, 0.98, 0.97, 0.96$, and 0.95 (averaged over 100 realizations of impurities coordinates).

5.2.3 Results and discussion

For a pseudoground state, we find the Fermi energy μ as a half distance between the minimum empty and maximum occupied energy ε. Fig. 5.7 shows how the Fermi level $\mu(K)$ shifts from the middle of the gap towards the conduction band bottom with growing $1-K$. At $1-K > 0.01$, this dependence is in reasonable agreement with the prediction of single-band theory (the theory that ignores valence band and acceptors) [32] that $E_c - \mu = A(1-K)^{-1/3}$. However, note that for heavily doped SCS, the coefficient $A_h \simeq 1.4$ is twice smaller than the coefficient $A_l \simeq 2.8$ obtained in Ref. [32] for a lightly doped SCS, where $a_B \ll 1$. In this case, the short-range Coulomb interaction at distance $r \ll N_D^{-1/3}$ leads to an additional contribution to μ of the same order of magnitude.

To confirm our understanding of results for $1-K > 0.01$, we obtained the same results for the position of Fermi level μ (and DOS of donors and conductivity, see below) using a simplified one-band model where all acceptors are assumed to be negative. Such

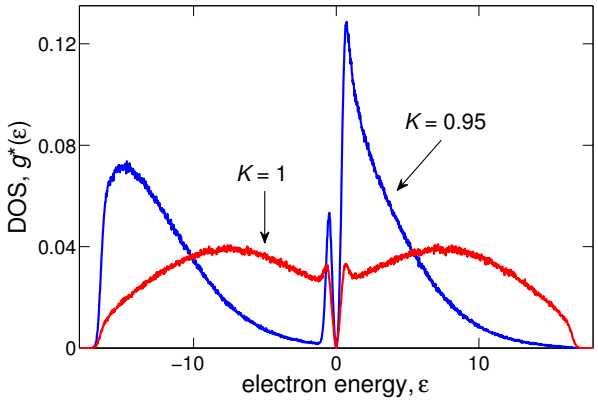

Figure 5.8: (Color online) Dimensionless single-electron DOS $g^*(\varepsilon)$ in units of $[(1+K)N_D/(e^2N_D^{1/3}/\kappa)]$ as a function of ε calculated from the Fermi level for $a_B = 1$ and $E_g = 15$ at $K = 0.95$ (blue) and 1 (red). Impurity states with $\varepsilon < 0$ are occupied and with $\varepsilon > 0$ are empty. At $K = 1$, the total DOS of impurities has donor-acceptor symmetry, which is lost with growing $1 - K$.

program is similar to the classical impurity band program used in Chapter 14 of Ref. [32], but uses the redefined $V(r)$.

The resulting DOS of impurities is shown in Fig. 5.8 for $K = 1$ and $K = 0.95$. At $K = 1$, the almost constant symmetric DOS between $-E_g = -15$ and $E_g = 15$ reflects a practically uniform distribution of random potential from $-E_g/2$ to $E_g/2$, and a corresponding uniform distribution of band edges E_c between 0 and E_g and E_ν between 0 and $-E_g$ [see Fig. 5.3]. In the middle (at the Fermi level) one sees the ES Coulomb gap [3].

At $K < 1$, the DOS of impurities loses the donor-acceptor symmetry it has at $K = 1$. As mentioned in Sec. 5.2.1 (see Fig. 5.6), with growing $1 - K$, acceptors become all filled and disengaged from screening. Acceptor DOS (leftmost peak) splits from the donor one, which in turn has two peaks separated by the Fermi level. The large right peak belongs to empty donors, while the small and narrow left peak belongs to occupied donors. The donor peaks are separated by the ES Coulomb gap.

Growing with $1-K$ the disengagement of acceptors from screening is also illustrated in Fig. 5.9, where we show the DOS $g^*(\varepsilon)$ for neutral donors and acceptors. If at $K = 1$, the total number of electrons and holes in puddles are equal, with growing $1 - K$, the

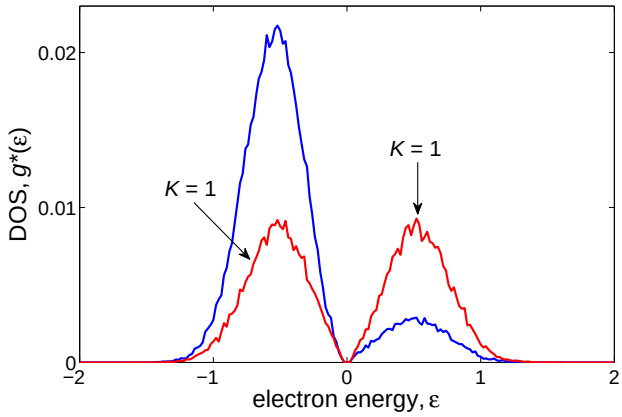

Figure 5.9: (Color online) Dimensionless DOS $g^*(\varepsilon)$ for neutral (occupied by electrons) donors with $\varepsilon < 0$ and neutral (empty) acceptors with $\varepsilon > 0$ for $a_B = 1$ and $E_g = 15$ at $K = 0.98$ (blue) and 1 (red).

total number of electrons in electron paddles grows, while the total number of holes in hole puddles decreases. Thus, at $1 - K \geq 0.02$, valence band practically plays no role in screening.

For $K = 0.95$, 0.97, 0.98, and 1 at $a_B = 1$ and $E_g = 15$, the computed dependence of $(\ln \rho)^* = (\xi/2) \ln(R_c/R_0)$ is shown as a function of $(T^*)^{-1/2}$ in the huge range of temperatures $0.03 < T^* < 200$ in Fig. 5.10. Here, $T^* = 2k_BT/\xi$ is yet another dimensionless temperature. These notations are introduced to exclude any explicit dependence on ξ. One can see at low temperatures $0.03 < T^* < 0.3$ the resistivity is well described by ES law Eq. (5.3) (with $C \simeq 4.4$ at $K = 1$). The higher temperature range $1 < T^* < 200$ is plotted separately as a function of $1/T^*$ in Fig. 5.11. We find two activated regimes of hopping conductivity. At high temperatures $50 < T^* < 200$, we see the large activation energy $E_a \sim E_c - \mu$, while in the range of intermediate temperatures $1 < T^* < E_g$, we see much smaller activation energy $\Delta = 0.3(E_c - \mu)$.

The first activation energy E_a does not have any physical meaning for a real SCS, because at $k_BT > E_g$ conductance of SCS is actually not due to hopping but free carriers with high energy, which are not taken into account by energy Eq. (5.4) (see Ref. [31]). In contrary to E_a, the second activation energy $\Delta = 0.3(E_c - \mu)$ makes full physical sense and should be seen in real experiment. The origin of this activation energy for the hopping transport is also explained in Chapter 8 of Ref.[32]. At $T \ll E_g$,

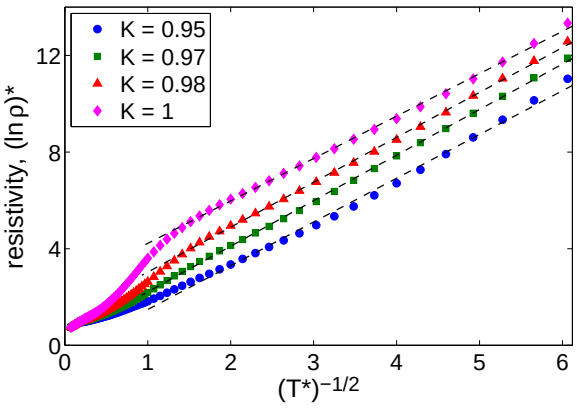

Figure 5.10: (Color online) The temperature dependence of the resistivity in the whole temperature range $0.03 < T^* < 200$. The dimensionless resistance $(\ln \rho)^*$ is plotted against $(T^*)^{-1/2}$ to illustrate that the resistivity follows the ES law at low temperatures. The dashed lines are the best linear fits.

electrons optimize their conductivity by using for hopping impurities energetically close to the Fermi level. Eventually at very low temperatures, such opitmization leads to ES conductivity. However, when donor energies are slowly modulated by the long-range potential, there are large areas that do not have donors with energies close to the Fermi level and the tunneling through them is slow. Therefore, there is a range of temperatures where electrons use only nearest-neighbor donors for hopping, while activating to donors is located at the percolation level of nearest-neighbor percolation. We then find the activation energy from the Fermi level to the nearest-neighbor percolation level by studying the hopping activation energy Δ. In a heavily doped semiconductor, this energy is indistinguishable from the activation energy of electrons from the Fermi level to the conduction band percolation level E_e. [Of course, holes are activated from the Fermi level to their percolation E_h as well so that $\Delta = 0.3(\mu - E_h)$].

We verified that hopping conduction modeling correctly predicts the activation energy of the band transport by direct calculation of the percolation level E_e. For this purpose, we created a cubic lattice with a small lattice constant $N_D^{-1/3}/3$. At every site of this lattice, we calculated the potential of all charged impurities and then found lowest energy E_e at which percolation over this lattice takes place. The activation energy of the band transport was again close to $\Delta = 0.3(E_c - \mu)$. This result is also close to

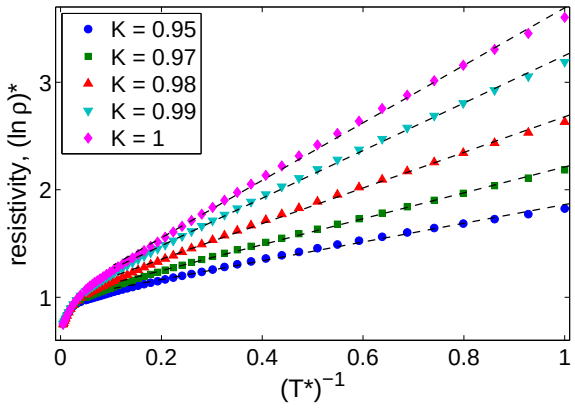

Figure 5.11: (Color online) The temperature dependence of the resistivity in the high temperature range $1 < T^* < 200$. $(\ln \rho)^*$ is plotted against $(T^*)^{-1}$ to illustrate that the resistivity is activated at high temperatures. The dashed lines are the best linear fits.

what was obtained in Ref. [79] based on an estimate of percolation level for a generic long-range random potential [32].

In Fig.5.12, we plot Δ as a function of $E_c - \mu$ for all the values $\mu(K)$ obtained at $K = 1, 0.99, 0.98, 0.97, 0.96$, and 0.95. We see that the relation $\Delta \simeq 0.3(E_c - \mu)$ holds well for all K in this interval.

So far, we emphasized the results that do not explicitly depend on ξ. Actually, a magnitude of ξ is necessary to calculate T_{ES}. We argue now that in a TI ξ is quite large leading to the prominent role of VRH. If an electron with an energy close to the Fermi level were tunneling from an electron puddle to a distant one along the straight line, it would tunnel through high barriers and its wave function would decay with $\xi \ll a_B$. Actually, a tunneling electron can use the same geometrical path as a classical percolating electron with energy Δ above the Fermi level that avoids large barriers. We assume that along such a path tunneling barriers V are uniformly distributed in the range $0 \leq V \leq \Delta$ and neglect contribution of curvature of this path into action. Integration over V then gives (here we return to normal units) $\xi = \hbar/(8m\Delta/9)^{1/2}$ and $k_B T_{ES} = 4.2(e^2/\kappa\hbar)(m\Delta)^{1/2}$. For a TI with $a_B = N_D^{-1/3}$, we get $T_{ES} = 4.2[(e^2 N_D^{1/3}/\kappa)\Delta]^{1/2}$. For Δ varying between 1 and $2.5e^2 N_D^{1/3}/\kappa$ as shown in Fig. 5.12, T_{ES} changes from 4.2 to $6.6e^2 N_D^{1/3}/\kappa$. For $\kappa = 30$, $N_D = 10^{19} cm^{-3}$, and $e^2 N_D^{1/3}/\kappa k_B \simeq 100$ K, T_{ES} varies from 420 to 660 K. In order to study VRH in TI samples experimentally, one has to deal with large enough

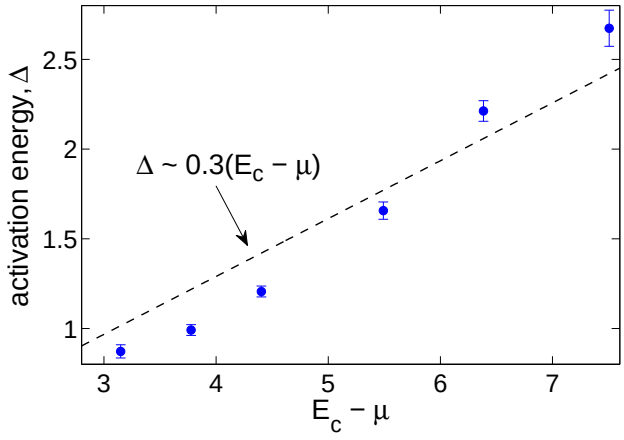

Figure 5.12: (Color online) The activation energy Δ at $K = 1, 0.99, 0.98, 0.97, 0.96$, and 0.95 (from right to left). The dashed line is the best linear fit $\Delta \simeq 0.3(E_c - \mu)$.

.

samples, where surface conductance is smaller than the bulk one. [1]

5.2.4 Thermopower

In a recent paper, the authors studied activation energy of the bulk resistivity of series of samples of $Bi_2Te_{3-x}Se_x$ with different x and thereby different positions of the Fermi level in the TI gap. They found that when the Fermi level sinks into the gap, the activation energy of resistivity Δ grows and reaches a maximum at 40 meV and then decreases. The increase of the activation energy Δ on both sides of the maximum is accompanied by the increase of the absolute value of the thermopower S. However, near the maximum of Δ, the thermopower abruptly changes its sign. These findings are in agreement with what one can expect when a semiconductor goes through the point of complete compensation. Here, we would like to concentrate on the maximum absolute value of the thermopower, for example, at n-type side of the maximum.

It is known that for flat bands n-type semiconductor with the Fermi level μ inside its gap the thermopower $S = \Delta/eT$, where the activation energy $\Delta = E_c - \mu$. For

[1] Historically VRH between puddles was studied in Ref. [80]. This paper was written before Ref. [3] and claimed Mott VRH. Now it is clear that resistivity obeys Eq. (5.3). The theory [80] of the transition from activated transport to ES law is to be modified as well, but we are not dwelling on this transition range, because it is difficult to study details of such a transition in experiment.

bended bands of a strongly compensated n-type semiconductor, one could think that $S = \Delta/eT$, where the activation energy $\Delta = E_e - \mu$ is determined by the activation to percolation level E_e. Actually, it was argued [81, 82, 83] that the Peltier energy (heat) $\Pi = eTS$ is determined by the average potential energy of electrons E (conduction band bottom) along most conducting one-dimensional percolation paths, $\Pi =< E-\mu >$. (We call a percolation path any line where the potential energy of electron is smaller than E_e and we call a set of the least resistive of these paths, which carry most of the current, the most conducting percolation paths.) The thermopower of an open circuit following an individual percolation path can be obtained by integrating $E - \mu$ along this path. Among two parallel paths connecting points A and B, the more resistive one has a somewhat larger open circuit thermopower and, therefore, drives circular current back through the least resistive one. This current reduces thermopower of the resistive path so that the voltage between A and B is determined by the more conducting path.

If the probability distribution of potential energy E on most conducting paths is the same as for the unconditional probability distribution of E, which we call DOS $g^*(E)$ above, we can use $g^*(E)$ to calculate Π and S. For example, in the case of a constant $g^*(E)$ for $\mu < E < E_e$, we get $E_S =< E - \mu >= \Delta/2 = (E_e - \mu)/2$. This conclusion was confirmed by the numerical experiment [81] for the case of a constant $g^*(E)$.

In a strongly compensated semiconductor, one can use the real $g^*(E)$ found above. For example, at $K = 0.95$ one can use Fig. 5.12 to find that $\Delta = E_e - \mu \simeq 1$. Then using DOS shown in Fig. 5.8 one can check that the average energy in the range of $0 < E < 1$ is $< E - \mu > \simeq \Delta/2 = 0.5$. Thus our simple approximate prediction is that the largest achievable $\Pi \simeq \Delta/2$. This conclusion is valid for all $K \leq 0.98$ we studied.

For the data of the paper, our prediction means that at $T = 100$ K the largest thermopower $S = \Pi/eT$ observed should be of the order 25 mV/100 K = 0.25 mV/K in resonable agreement with the observed value $S = 0.4$ mV/K.

Here, we are not considering the additional contribution to thermopower of activated electrons from phonon drag [84, 85]. This effect becomes significant only at temperature $T \leq T_D/3$, where T_D is the Debye temperature, because at larger temperatures, the low-energy phonons interacting with electrons are strongly scattered by thermal phonons, which in turn are strongly interacting with imperfections of the crystal. In Bi_2Se_3, $T_D \sim 150$ K, so that phonon drag should get important only below 50 K (where electron

transport is already via hopping), while the activated transport we are interested in happens at $T \geq 100$ K.

In order to go beyond the above approximation that the distribution of energies on paths contributing to Π is given by the density of states $g(E)$, we calculate currents I_{ij} in every Miller-Abrahams resistor R_{ij} and the total current $I(U)$ for a small applied voltage U by solving Kirchhoff equations for the ground state of impurities obtained by our algorithm. Following Ref. [86], we then calculate the energy flux through a cross-section of the sample $Q(U)$ as a sum of energy fluxes carried by resistors $q_{ij} = (E_i + E_j)I_{ij}/2e$ and found $\Pi = Qe/I$. We simplify the implementation of this procedure by modifying our algorithm in the following way: instead of dealing with completely randomly positioned donors and acceptors, we randomly position them on all sites that are appropriate to their number cubic lattice. To find the energies E_i, we use a simple Coulomb potential. (There is no need in truncation at small distances via finite a_B.) We concentrate on the range of relatively high temperatures, where the conductivity is characterized by activated behavior. We checked that the conductance I/U has the same activation energy Δ as obtained by the percolation algorithm. We found that in the range of $0.95 \leq K \leq 0.98$, where the asymmetry of the density of states is large and donors dominate the transport, Peltier energy $\Pi/\Delta \simeq 0.40 \pm 0.05$, not too far from the simplified theories and the experimental data. For $K > 0.98$, growing donor-acceptor symmetry reduces Π and brings it to zero at $K = 1$, in agreement with the data of the paper.

5.3 Conclusion

In this chapter, we apply the model of strongly compensated semiconductor to a bulk TI with narrow gap. For a completely compensated TI, at moderately large T we find that $\Delta = 0.15E_g$, in agreement with observed values [25]. We also find that the single-particle DOS has a Coulomb gap at the Fermi level [3], and the resistivity is described by Eq. (5.3) at low temperatures and crosses over to Eq. (5.1) at higher T. A crude estimate of the localization length ξ is presented, which suggests that $T_{\rm ES} \sim 900$ K and that the crossover between activation and ES VRH occurs at $T \sim 40$ K. Together our results for the activated and VRH resistivity establish a universal upper limit for the

resistivity $\rho(T)$ that one can achieve for a 3D TI compensated by shallow inpurities.

We then use the same model to the case of finite compensation. We calculate the activation energy of the bulk resistivity Δ and showe that it grows as $\Delta = 0.3(E_c - \mu)$, when the compensation degree $K \to 1$ and the Fermi level sinks into the gap. If one of the two carriers still dominates and the thermopwer is still monopolar the Peltier energy is $\Pi \simeq \Delta/2$. Both predictions seem to agree with most of the TI data.

We would like to mention that the same model is able to interpret measurements of the Hall Effect obtained for the same samples. The Hall constant R_H is expected to grow exponentially with decreasing temperature with the same activation energy Δ as the resistivity [87, 88, 81]. The reason for such growth is that R_H is dominated by nodes of percolation path network that occur at energy close to the percolation level. Such nodes are relatively rare at low temperatures. Therefore $R_H(T) = \rho(T)u(T)/c$ grows with decreasing T, where mobility $u(T) \propto T^m$ and $m \geq 2$. The observed behavior of $R_H(T)$ does not contradict this prediction [25]. Indeed, the largest activation energy of R_H was found to be on average ~ 15 meV larger than the largest $\Delta \sim 50$ meV. This difference is of the order of $1.5k_BT$ at the characteristic measurement temperature of activation law $T = 100K$ and, therefore, the experimental data is compatible with a power law $u(T)$. In future work, we plan to narrow the range of theoretical predictions by a numerical evaluation of R_H for the simulated above potential of our model.

Chapter 6

Conclusions and Discussion

In this thesis we have studied charge transport in two disorder systems, NC assemblies and 3D TIs, in which disorder effects play a significant role. In these systems, at relatively low temperatue electron states are strongly localized, and electronic conduction proceeds primarily by hopping of electrons between grains through the insulating gaps which separate them. Although in different materials the disorder mechanisms are different, they are all shown to have great impact on the ground state electron energy distribution and charge transport of the system.

In arrays of semiconductor NCs, disorder mainly originates from the fluctuations in number of donors from one NC to another. We show that, when the NC size is sufficiently small, because of the competition between quantum energy gaps and charging energy, this disorder becomes the driving force for charging of some of the NCs. These charged NCs produce long-range, random Coulomb potential that smears the charging (hard) energy gap in the DOGS, which eventually leads to VRH rather than activated transport at low temperatures. The condition for activated transport and VRH is summarized in Fig. 2.8, and is confirmed by a computer simulation.

For metallic and superconducting grains, disorder is provided by donors and acceptors that are randomly situated in the interstitial spaces between grains. As explained in Ch. 3 and 4, this disorder results in two rather striking features of the DOGS which are unseen in conventional Coulomb glass. First, there is not one but three identical adjacent Coulomb gaps, which together form a structure that we call a "Coulomb gap triptych." Second, the DOGS has a fixed width in the limit of large disorder. These two

features are found in the DOGS for both metallic and superconducting grains, as seen in Fig. 3.2 and Fig. 4.2 and 4.7. Electron transport is calculated based on the DOGS. In metallic grains, the system is governed by VRH at relatively low temperatures. For superconducting grains, the conduction mechanism is determined by two important energy scales, charging energy E_c and superconducting gap Δ within a grain. As the ratio of these two energies is increased, the system goes from the regime of single-electron hopping to that of electron pair hopping, as seen in Fig. 4.4. The evolution mechanism of DOGS and conductivity is also applied to explain the origin of the giant MR peak in the deeply insulating regime that has been found in some of the superconducting thin films, in particular, amorphous InO.

The rest of the thesis discusses 3D TIs and strongly compensated seminconductor, in which disorder is assumed to be due to the largely-fluctuating, random Coulomb potential created by a large number of charged impurities present in the bulk [as seen in Fig. 5.3 and 5.6]. We show that, the band bending by poorly screened fluctuations in the random Coulomb potential results in an anomalously small bulk resistivity and thermopower as found in recent transport experiments on 3D TIs. Using numerical simulations of strongly compensated TI, we find that the bulk resistivity has an activation energy and thermopower with values in good agreement with experimental data (Fig. 5.12). The conductivity of the system has two major regimes: at higher temperature it is thermally activated through nearest hopping among impurity states; at lower temperatures activated transport crosses over to variable range hopping with a relatively large localization length.

In summary, this thesis provides some new insight into the disorder effects on charge transport in systems that are promising candidates for new photovaltaic and spintronics devices. In particular, we aim to use the theories developed here to address some of the experimental puzzles such as the coeistence of different conduction mechanisms in NC assemblies and the anomalously small resistivity in 3D TIs. Using the combined theoretical and computational approach described above, we hope to further the microscopic understanding of charge conduction in NC arrays and 3D TIs, and thereby aid in the development of crucial new technologies.

References

[1] N.F. Mott. Introductory talk; conduction in non-crystalline materials. *Journal of Non-Crystalline Solids*, 810(0):1 – 18, 1972.

[2] N.F. Mott. Conduction in glasses containing transition metal ions. *Journal of Non-Crystalline Solids*, 1(1):1 – 17, 1968.

[3] A L Efros and B I Shklovskii. Coulomb gap and low temperature conductivity of disordered systems. *J. Phys. C: Solid State Phys.*, 8:L49, 1975.

[4] Heng Liu, Alexandre Pourret, and Philippe Guyot-Sionnest. Mott and efros-shklovskii variable range hopping in cdse quantum dots films. *ACS Nano*, 4(9):5211–5216, 2010.

[5] I. S. Beloborodov, A. V. Lopatin, V. M. Vinokur, and K. B. Efetov. Granular electronic systems. *Rev. Mod. Phys.*, 79:469–518, Apr 2007.

[6] Myles Steiner and Aharon Kapitulnik. Superconductivity in the insulating phase above the field-tuned superconductorinsulator transition in disordered indium oxide films. *Physica C: Superconductivity*, 422(1 - 2):16 – 26, 2005.

[7] T. Baturina, A. Mironov, V. Vinokur, M. Baklanov, and C. Strunk. Hyperactivated resistance in tin films on the insulating side of the disorder-driven superconductor-insulator transition. *JETP Letters*, 88:752–757, 2008. 10.1134/S0021364008230112.

[8] Yen-Hsiang Lin and A. M. Goldman. Magnetic-field-tuned quantum phase transition in the insulating regime of ultrathin amorphous bi films. *Phys. Rev. Lett.*, 106:127003, Mar 2011.

[9] A. Gerber, A. Milner, G. Deutscher, M. Karpovsky, and A. Gladkikh. Insulator-superconductor transition in 3d granular al-ge films. *Phys. Rev. Lett.*, 78:4277–4280, Jun 1997.

[10] D. Sherman, G. Kopnov, D. Shahar, and A. Frydman. Measurement of a superconducting energy gap in a homogeneously amorphous insulator. *Phys. Rev. Lett.*, 108:177006, Apr 2012.

[11] R. P. Barber, L. M. Merchant, A. La Porta, and R. C. Dynes. Tunneling into granular pb films in the superconducting and insulating regimes. *Phys. Rev. B*, 49:3409–3412, Feb 1994.

[12] Liang Fu, C. L. Kane, and E. J. Mele. Topological insulators in three dimensions. *Phys. Rev. Lett.*, 98:106803, Mar 2007.

[13] J. E. Moore and L. Balents. Topological invariants of time-reversal-invariant band structures. *Phys. Rev. B*, 75:121306, Mar 2007.

[14] Liang Fu and C. L. Kane. Topological insulators with inversion symmetry. *Phys. Rev. B*, 76:045302, Jul 2007.

[15] Xiao-Liang Qi, Taylor L. Hughes, and Shou-Cheng Zhang. Topological field theory of time-reversal invariant insulators. *Phys. Rev. B*, 78:195424, Nov 2008.

[16] Rahul Roy. Topological phases and the quantum spin hall effect in three dimensions. *Phys. Rev. B*, 79:195322, May 2009.

[17] Y. L. Chen, J.-H. Chu, J. G. Analytis, Z. K. Liu, K. Igarashi, H.-H. Kuo, X. L. Qi, S. K. Mo, R. G. Moore, D. H. Lu, M. Hashimoto, T. Sasagawa, S. C. Zhang, I. R. Fisher, Z. Hussain, and Z. X. Shen. Massive dirac fermion on the surface of a magnetically doped topological insulator. *Science*, 329(5992):659–662, 2010, http://www.sciencemag.org/content/329/5992/659.full.pdf.

[18] Dong-Xia Qu, Y. S. Hor, Jun Xiong, R. J. Cava, and N. P. Ong. Quantum oscillations and hall anomaly of surface states in the topological insulator bi2te3. *Science*, 329(5993):821–824, 2010.

[19] James G. Analytis, Ross D. McDonald, Scott C. Riggs, Jiun-Haw Chu, G. S. Boebinger, and Ian R. Fisher. Two-dimensional surface state in the quantum limit of a topological insulator. *Nat. Phys.*, 6(12):960–964, December 2010.

[20] J. G. Checkelsky, Y. S. Hor, M.-H. Liu, D.-X. Qu, R. J. Cava, and N. P. Ong. Quantum interference in macroscopic crystals of nonmetallic bi_2se_3. *Phys. Rev. Lett.*, 103:246601, Dec 2009.

[21] N. P. Butch, K. Kirshenbaum, P. Syers, A. B. Sushkov, G. S. Jenkins, H. D. Drew, and J. Paglione. Strong surface scattering in ultrahigh-mobility bi_2se_3 topological insulator crystals. *Phys. Rev. B*, 81:241301, Jun 2010.

[22] James G. Analytis, Jiun-Haw Chu, Yulin Chen, Felipe Corredor, Ross D. McDonald, Z. X. Shen, and Ian R. Fisher. Bulk fermi surface coexistence with dirac surface state in bi_2se_3: A comparison of photoemission and shubnikov˘de haas measurements. *Phys. Rev. B*, 81:205407, May 2010.

[23] Kazuma Eto, Zhi Ren, A. A. Taskin, Kouji Segawa, and Yoichi Ando. Angular-dependent oscillations of the magnetoresistance in bi_2se_3 due to the three-dimensional bulk fermi surface. *Phys. Rev. B*, 81:195309, May 2010.

[24] Zhi Ren, A. A. Taskin, Satoshi Sasaki, Kouji Segawa, and Yoichi Ando. Observations of two-dimensional quantum oscillations and ambipolar transport in the topological insulator bi_2se_3 achieved by cd doping. *Phys. Rev. B*, 84:075316, Aug 2011.

[25] Zhi Ren, A. A. Taskin, Satoshi Sasaki, Kouji Segawa, and Yoichi Ando. Optimizing $\mathbf{bi}_{2-x}\mathbf{sb}_x\mathbf{te}_{3-y}\mathbf{se}_y$ solid solutions to approach the intrinsic topological insulator regime. *Phys. Rev. B*, 84:165311, Oct 2011.

[26] Zhi Ren, A. A. Taskin, Satoshi Sasaki, Kouji Segawa, and Yoichi Ando. Fermi level tuning and a large activation gap achieved in the topological insulator bi_2te_2se by sn doping. *Phys. Rev. B*, 85:155301, Apr 2012.

[27] David Jurbergs, Elena Rogojina, Lorenzo Mangolini, and Uwe Kortshagen. Silicon nanocrystals with ensemble quantum yields exceeding 60%. *Applied Physics Letters*, 88(23):233116, 2006.

[28] Dmitri V. Talapin, Jong-Soo Lee, Maksym V. Kovalenko, and Elena V. Shevchenko. Prospects of colloidal nanocrystals for electronic and optoelectronic applications. *Chemical Reviews*, 110(1):389–458, 2010.

[29] Jingshan Zhang and Boris I. Shklovskii. Density of states and conductivity of a granular metal or an array of quantum dots. *Phys. Rev. B*, 70:115317, Sep 2004.

[30] Tianran Chen, Brian Skinner, and B. I. Shklovskii. Coulomb gap triptychs, $\sqrt{2}$ effective charge, and hopping transport in periodic arrays of superconductor grains. *Phys. Rev. B*, 86:045135, Jul 2012.

[31] Brian Skinner, Tianran Chen, and B. I. Shklovskii. Why is the bulk resistivity of topological insulators so small? *Phys. Rev. Lett.*, 109:176801, Oct 2012.

[32] A. L. Efros and B. I. Shklovskii. *Electronic Properties of Doped Semiconductors*. Springer-Verlag, New York, 1984. Available from http://www.tpi.umn.edu/shklovskii.

[33] M. A. Rafiq, Y. Tsuchiya, H. Mizuta, S. Oda, Shigeyasu Uno, Z. A. K. Durrani, and W. I. Milne. Hopping conduction in size-controlled si nanocrystals. *Journal of Applied Physics*, 100(1):014303, 2006.

[34] H. Moreira, Q. Yu, B. Nadal, B. Bresson, M. Rosticher, N. Lequeux, A. Zimmers, and H. Aubin. Electron cotunneling transport in gold nanocrystal arrays. *Phys. Rev. Lett.*, 107:176803, Oct 2011.

[35] Dong Yu, Congjun Wang, and Philippe Guyot-Sionnest. n-type conducting cdse nanocrystal solids. *Science*, 300(5623):1277–1280, 2003.

[36] David J. Norris, Alexander L. Efros, and Steven C. Erwin. Doped nanocrystals. *Science*, 319(5871):1776–1779, 2008.

[37] Cherie Kagan. The role of surface ligands in electronic charge transport in semiconductor nanocrystal arrays. APS March Meeting, 2012.

[38] Hugo E. Romero and Marija Drndic. Coulomb blockade and hopping conduction in pbse quantum dots. *Phys. Rev. Lett.*, 95:156801, Oct 2005.

[39] L. R. Wienkes, C. Blackwell, and J. Kakalios. Electronic transport in doped mixed-phase hydrogenated amorphous/nanocrystalline silicon thin films. *Applied Physics Letters*, 100(7):072105, 2012.

[40] A.I. Ekimov, I.A. Kudryavtsev, M.G. Ivanov, and Al.L. Efros. Spectra and decay kinetics of radiative recombination in cds microcrystals. *Journal of Luminescence*, 46(2):83 – 95, 1990.

[41] Al. L. Efros and M. Rosen. The electronic structure of semiconductor nanocrystals1. *Annual Review of Materials Science*, 30(1):475–521, 2000.

[42] Yigal Meir, Ned S. Wingreen, and Patrick A. Lee. Transport through a strongly interacting electron system: Theory of periodic conductance oscillations. *Phys. Rev. Lett.*, 66:3048–3051, Jun 1991.

[43] J C Maxwell. *A Treatise on Electricity and Magnetism*, volume 2. Clarendon, Oxford, 3 edition, 1891.

[44] William T. Doyle. The clausius-mossotti problem for cubic arrays of spheres. *Journal of Applied Physics*, 49(2):795 –797, feb 1978.

[45] A. Möbius, M. Richter, and B. Drittler. Coulomb gap in two- and three-dimensional systems: Simulation results for large samples. *Phys. Rev. B*, 45:11568–11579, May 1992.

[46] A. L. Efros, Brian Skinner, and B. I. Shklovskii. Coulomb gap in the one-particle density of states in three-dimensional systems with localized electrons. *Phys. Rev. B*, 84:064204, Aug 2011.

[47] Allen Miller and Elihu Abrahams. Impurity conduction at low concentrations. *Phys. Rev.*, 120:745–755, Nov 1960.

[48] A I Larkin and D E Khmelnitskii. Activation conductivity in disordered systems with large localization length. *Sov. Phys. JETP*, 56:647, 1982.

[49] A G Zabrodskii. *Sov. Phys. Semicond.*, 11:345, 1977.

[50] Tianran Chen, Brian Skinner, and B. I. Shklovskii. Cooperative charging in a nanocrystal assembly gated by ionic liquid. *Phys. Rev. B*, 84:245304, Dec 2011.

[51] Brian Skinner, Tianran Chen, and B. I. Shklovskii. Theory of hopping conduction in arrays of doped semiconductor nanocrystals. *Phys. Rev. B*, 85:205316, May 2012.

[52] A L Efros. Coulomb gap in disordered systems. *J. Phys. C: Solid State Phys.*, 9(11):2021, 1976.

[53] J. G. Massey and Mark Lee. Direct observation of the coulomb correlation gap in a nonmetallic semiconductor, si: B. *Phys. Rev. Lett.*, 75:4266–4269, Dec 1995.

[54] C. T. Black, D. C. Ralph, and M. Tinkham. Spectroscopy of the superconducting gap in individual nanometer-scale aluminum particles. *Phys. Rev. Lett.*, 76:688–691, Jan 1996.

[55] Joe Mitchell, Anirban Gangopadhyay, Victor Galitski, and Markus Müller. Two-component coulomb glass in insulators with a local attraction. *Phys. Rev. B*, 85:195141, May 2012.

[56] D. V. Averin and Yu. V. Nazarov. Single-electron charging of a superconducting island. *Phys. Rev. Lett.*, 69:1993–1996, Sep 1992.

[57] K. A. Matveev and A. I. Larkin. Parity effect in ground state energies of ultrasmall superconducting grains. *Phys. Rev. Lett.*, 78:3749–3752, May 1997.

[58] M. T. Tuominen, J. M. Hergenrother, T. S. Tighe, and M. Tinkham. Experimental evidence for parity-based 2 e periodicity in a superconducting single-electron tunneling transistor. *Phys. Rev. Lett.*, 69:1997–2000, Sep 1992.

[59] M. T. Tuominen, J. M. Hergenrother, T. S. Tighe, and M. Tinkham. Even-odd electron number effects in a small superconducting island: Magnetic-field dependence. *Phys. Rev. B*, 47:11599–11602, May 1993.

[60] Michael Tinkham. *Introduction to Superconductivity*. McGraw-Hill, 2 edition, 1996.

[61] B. I. Shklovskii and B. Z. Spivak. Scattering and interference effects in variable range hopping conduction. In M. Pollak and B. I. Shklovskii, editors, *Hopping Transport in Solids*, pages 271 – 348. North Holland, Amsterdam, 1991.

[62] Mark Lee, J. G. Massey, V. L. Nguyen, and B. I. Shklovskii. Coulomb gap in a doped semiconductor near the metal-insulator transition: Tunneling experiment and scaling ansatz. *Phys. Rev. B*, 60:1582–1591, Jul 1999.

[63] Benjamin Sacepe, Thomas Dubouchet, Claude Chapelier, Marc Sanquer, Maoz Ovadia, Dan Shahar, Mikhail Feigel/'man, and Lev Ioffe. Localization of preformed cooper pairs in disordered superconductors. *Nat Phys*, 7:239–244, 2011.

[64] D. Shahar and Z. Ovadyahu. Superconductivity near the mobility edge. *Phys. Rev. B*, 46:10917–10922, Nov 1992.

[65] G. Sambandamurthy, L. W. Engel, A. Johansson, and D. Shahar. Superconductivity-related insulating behavior. *Phys. Rev. Lett.*, 92:107005, Mar 2004.

[66] D. B. Haviland, Y. Liu, and A. M. Goldman. Onset of superconductivity in the two-dimensional limit. *Phys. Rev. Lett.*, 62:2180–2183, May 1989.

[67] T. I. Baturina, A. Yu. Mironov, V. M. Vinokur, M. R. Baklanov, and C. Strunk. Localized superconductivity in the quantum-critical region of the disorder-driven superconductor-insulator transition in tin thin films. *Phys. Rev. Lett.*, 99:257003, Dec 2007.

[68] M. A. Paalanen, A. F. Hebard, and R. R. Ruel. Low-temperature insulating phases of uniformly disordered two-dimensional superconductors. *Phys. Rev. Lett.*, 69:1604–1607, Sep 1992.

[69] I. Shammass, O. Cohen, M. Ovadia, I. Gutman, and D. Shahar. Superconducting correlations in thin films of amorphous indium oxide on the insulating side of the disorder-tuned superconductor-insulator transition. *Phys. Rev. B*, 85:140507, Apr 2012.

[70] D. Sherman, G. Kopnov, D. Shahar, and A. Frydman. Measurement of a superconducting energy gap in a homogeneously amorphous insulator. *Phys. Rev. Lett.*, 108:177006, Apr 2012.

[71] Yeonbae Lee, Aviad Frydman, Tianran Chen, Brian Skinner, and A. M. Goldman. Electrostatic tuning of the properties of disordered indium-oxide films near the superconductor-insulator transition. *Phys. Rev. B*, 88:024509, Jul 2013.

[72] A. V. Lopatin and V. M. Vinokur. Hopping transport in granular superconductors. *Phys. Rev. B*, 75:092201, Mar 2007.

[73] M. Z. Hasan and C. L. Kane. *Colloquium* : Topological insulators. *Rev. Mod. Phys.*, 82:3045–3067, Nov 2010.

[74] Xiao-Liang Qi and Shou-Cheng Zhang. Topological insulators and superconductors. *Rev. Mod. Phys.*, 83:1057–1110, Oct 2011.

[75] B I Shklovskii and A L Efros. Completely compensated crystalline semiconductor as a model of an amorphous semiconductor. *Sov. Phys.-JETP*, 35:610, 1972.

[76] Yu S Gal'perin and A L Efros. A. *Sov. Phys. - Semicond.*, 6:941, 1972.

[77] E M Gershenzon, I N Kurilenko V A Il'in, and L B litvak Gorskaya. B. *Sov. Phys. - Semicond.*, 9:874, 1975.

[78] N G Yaremenko. F. *Sov. Phys. - Semicond*, 9:554, 1975.

[79] V. F. Mitin. Preparation and properties of heavily doped and strongly compensated ge films on gaas. *Journal of Applied Physics*, 107(3):033720, 2010.

[80] B I Shklovskii. E. *Sov. Phys. - Semicond*, 7:77, 1973.

[81] H Overhof and W Beyer. D. *Philos. Mag. B*, 43:433, 1981.

[82] D. Quicker and J. Kakalios. Influence of deposition conditions on long-range electronic disorder in n -type doped hydrogenated amorphous silicon. *Phys. Rev. B*, 60:2449–2455, Jul 1999.

[83] H. Overhof and M. Schmidtke. Effect of long-range random potentials on the electronic transport properties of disordered semiconductors: A numerical study. *Phys. Rev. B*, 61:12977–12981, May 2000.

[84] L. Gurevich. G. *J. Phys. (U.S.S.R)*, 9, 10:477, 67, 1945, 1946.

[85] Conyers Herring. Theory of the thermoelectric power of semiconductors. *Phys. Rev.*, 96:1163–1187, Dec 1954.

[86] I.P.Zvyagin. On the theory of hopping transport in disordered semiconductors. *Phys. Stat. Sol. (b)*, 58:443, 1973.

[87] V G Karpov, A Y Shik, and B I Shklovskii. C. *Sov. Phys. - Semicond*, 16:901, 1982.

[88] A Y Shik. *Electronic Properties of Inhomogeneous Semiconductors.* Gordon and Breach, 1995.

Appendix A

Glossary and Acronyms

Care has been taken in this thesis to minimize the use of jargon and acronyms, but this cannot always be achieved. This appendix defines jargon terms in a glossary, and contains a table of acronyms and their meaning.

A.1 Acronyms

Table A.1: Acronyms

Acronym	Meaning
nanocrystal	NC
topological insulator	TI
variable range hopping	VRH
density of ground states	DOGS
density of states	DOS